Glycopolymers with Diverse Applications: From Common Polymer Brushes to Novel Lab-on-a-Chip Devices

Von der Fakultät für Mathematik, Informatik, und Naturwissenschaften der RWTH Aachen University zur Erlangung des akademischen Grades einer Doktorin der Naturwissenschaften genehmigte Dissertation

vorgelegt von

Master of Science

Hyunji Park

aus Daegu / Republik Korea

Berichter: Universitätsprofessor Dr. rer. nat. Alexander Böker
Universitätsprofessor Dr. rer. nat. Lothar Elling

Tag der mündlichen Prüfung: 29. Juni 2015

Contents

List of Figures

List of Schemes

List of Abbreviations

AFM atomic force microscopy

APTS 8-aminopyrene-1,3,6-trisulfonic acid

ATRP atom transfer radical polymerization

BisBIBED bis[2-(2'-bromoisobutyryloxy)ethyl]disulfide

BisBIBUD bis[2-(2'-bromoisobutyryloxy)undecyl]disulfide

bpy 2,2'-bipyridine

BSA bovine serum albumin

CA contact angle

CLRP controlled/living free-radical polymerization

CRD carbohydrate-recognition domain

Cryo-SEM cryo-scanning electron microscopy

DLS dynamic light scattering

EBiB ethyl α-bromoisobutyrate

ECL *Erythrina cristagalli* lectin

EIS electrochemical impedance spectroscopy

ELISA enzyme-linked immunosorbent assay

ELLA enzyme-linked lectin assay

FCS fluorescence correlation spectroscopy

FESEM field emission scanning electron microscopy

FITC fluorescein isothiocyanate

FLLA fluorescence-linked lectin assay

GlcNAcEMA 2-O-(*N*-acetyl-β-D-glucosamine)ethyl methacrylate

GlcNAc *N*-Acetylglucosamine

GS-II *Griffonia simplicifolia* lectin

HEMA 2-hydroxyethyl methacrylate

HEPES 4-(2-hydroxyethyl)-1-piperazineethanesulfonic acid

IDT interdigital transducer

IGB impedimetric glyco-biosensor

IUPAC international union of pure and applied chemistry

LacNAc *N*-acetyllactosamine

MEK methyl ethyl ketone

NP nanoparticle

PCB printed circuit board

PDMS polydimethylsiloxane

PFGB plasmonic flow-through glyco-biosensor

PGlcNAcEMA poly(2-O-(*N*-acetyl-β-D-glucosamine)ethyl methacrylate)

PHEMA poly(2-hydroxyethyl methacrylate)

QCM quartz crystal microbalance

RAFT reversible addition-fragmentation chain transfer

RIU refractive index units

RI refractive index

SAM self-assembled monolayer

SAW surface acoustic wave

SI-ATRP surface-initiated ATRP

SIP surface-initiated polymerization

SPR surface plasmon resonance

TEM transmission electron microscopy

TEOS tetraethyl orthosilicate

UDP-Gal uridinediphospho-α-D-galactose

1 Introduction

Saccharides, a synonym of carbohydrates, are the most abundant bio-organic compounds in the biological world. They play an essential role in living organisms as a major source of metabolic energy, as structural compounds, or as recognition sites on cell surfaces.[1] Moreover, cell-surface oligo- and polysaccharides are known to be involved in cell adhesion, signal transduction and regulation as well as bacterial and viral infections.[2] These molecular recognition processes are based on specific and noncovalent carbohydrate-protein interactions.[3] Carbohydrate-binding proteins are generally called “lectins”. The International Union of Pure and Applied Chemistry (IUPAC) defines lectins as "(glyco)proteins isolated from plants but recently found also in animals and micro-organisms that react specifically with terminal glycosidic residues of other molecules (e.g. cell wall polysaccharides); some causing cells to agglutinate".[4] Lectins are found in organisms ranging from viruses and plants to humans.[5] Lectins have often been categorized according to their mono- or, sometimes, disaccharide binding specificity. The interaction between a monosaccharide and one protein is often assessed by physical methods and inhibition assays. In general, the binding is weak with an association constant beyond 106 M^{-1}. Hence, an affinity enhancement is required to attain biologically relevant strength and can be achieved by multivalent binding sites.[6, 7] For example, the application of lectins with clustered sugar binding sites or ligands presenting multivalent sugars results in a significantly strong “glycoside cluster effect”.[8] A wide range of multivalent saccharide ligands have been reported and polymers containing pendant carbohydrate moieties, so-called “glycopolymers”, recently attracted considerable attention.[9, 10]

1.1 Lectins

Lectins generally comprise a structurally diverse class of proteins characterized by their ability to bind carbohydrates with considerable specificity. They are responsible for cell surface recognition processes in bacteria, plants and animals.[11] The structural basis for selective saccharide recognition by different lectin types has been investigated by X-ray crystallography. The recognition mechanisms of carbohydrates are varied in types of lectins, but share some key features. First, the low binding affinity for monosaccharides results from shallow indentation on protein surfaces. Second, high selectivity is achieved

through a combination of different binding forces such as hydrogen bonding and van der Waals forces as well as by extending binding sites through additional direct and water-mediated contacts between sugars and lectins. Finally, the sugar binding affinity can be increased dramatically by clustering of simple binding sites of saccharides in the lectin polypeptides. This multivalent formation of carbohydrates helps lectins to distinguish surface arrays of sugars or to crosslink glycoconjugates. In addition, the organizations of the various types of lectins have two similar aspects. First, the sugar-binding activity can be usually ascribed to a single protein module within the lectin polypeptide. Such a module is referred to a globular carbohydrate-recognition domain (CRD) of less than 200 amino acids. Second, a CRD shares certain degree of sequence identity and structural similarity. For instance, all of the structurally characterized bacterial toxins which use carbohydrates as cellular receptors display common structural features. Plant lectins have two major categories. One of them includes lectins isolated from the seeds of legumes and they have homologous sequences. The other one is derived from the seeds of cereals. Figure 1.1 illustrates the structure of plant lectins for example *Griffonia simplicifolia* lectin-I and *Erythrina cristagalli*. The animal lectins can be categorized in five major types: Ca^{2+}-dependent C-type lectins, P-type Man 6-phosphate receptors, I-type lectins including sialoadhesins and other immunoglobulin-like sugar-binding proteins, Gal-binding galectins (Figure 1.2), and pentraxins. However, recent findings point to the existence of additional new groups of animal lectins.[12, 13, 14]

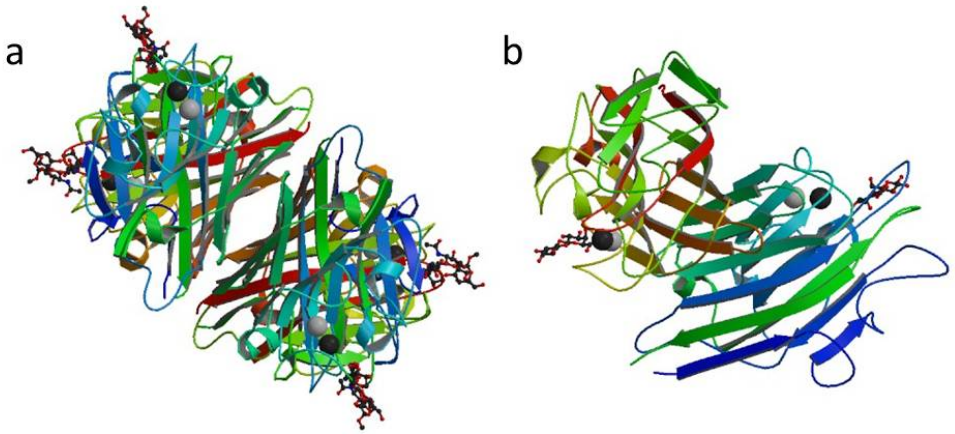

Figure 1.1: Structure of plant lectins. A: *Griffonia simplicifolia* lectin-I in complex with xenograft antigen (PDB rendering based on 1HQL).[15] B: *Erythrina cristagalli* lectin with bound *N*-linked oligosaccharide and lactose (PDB rendering based on 1V00).[16] Protein chains are colored using spectral gradient from the N-terminal to the C-terminal.

Cooperative hydrogen bonding is a characteristic of the interaction between sugar binding proteins and sugar hydroxyls. Selective binding to epimeric hydroxyls is an important aspect of differential binding of sugars. The majority of hydrogen-bond donors and ac-

ceptors are composed with charged or polar planar groups of lectins. The hydroxyl group can act simultaneously as an acceptor of two hydrogen bonds and as a donor of a single hydrogen bond. Generally, one acidic side chain is used as a hydrogen bond acceptor from one or two sugar hydroxyls. Hydrogen-bond donors come primarily from main-chain amid groups and the side-chain amid group of asparagine and, less frequently, glutamine. Charged side-chain donors also occur with some frequency. Protein hydroxyls from tyrosine, serine, and threonine are much less common as either donors or acceptors of hydrogen bonds with sugar hydroxyls. Normally, lectins undergo few changes in conformation upon saccharide binding. In addition, unliganded lectins can form hydrogen bonds with ordered water molecules. These water molecules mimic a pattern of the hydrogen-bonding by sugar hydroxyls. Besides of the hydrogen bonding, the van der Waals forces between sugars and proteins often play an important roll in packing interactions with aromatic amino acid side chains. Particularly these packing reactions are common for the Gal-specific sites. In case of hydrophobic interactions and hydrogen bondings between lectins and substituents on hexose rings of sugars provide further selectivity for specific groups of saccharide ligands. Acetamido groups in *N*-Acetylglucosamine (GlcNAc), GalNAc, and NeuNAc can be the representative examples of such substituents.[17]

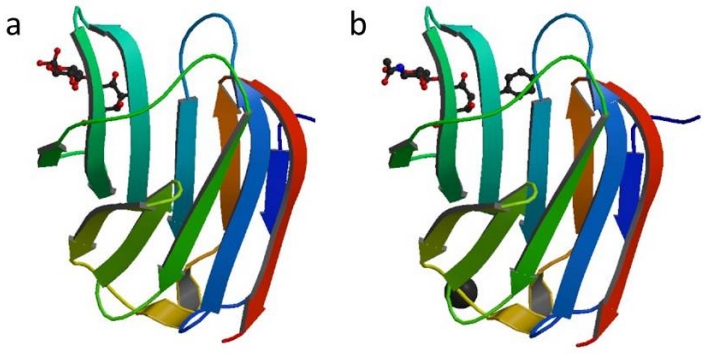

Figure 1.2: Structure of human lectins. A: Galectin-3 in complex with lactose (PDB rendering based on 3ZSJ).[18] B: Galectin-3 with bound a benzamido-*N*-acetyllactosamine inhibitor (PDB rendering based on 2XG3).[19] Protein chains are colored using spectral gradient from the N-terminal to the C-terminal.

1.2 Glycopolymers

Glycopolymers are synthetic polymers possessing non-carbohydrate main chains but carrying pendant and/or terminal saccharide groups.[20] They have been developed as alternative structures to oligosaccharides.[21] Their multivalent presentation of carbohydrates increases the binding affinity of lectins dramatically and this affinity enhancement is considerably larger than the effect of the increased glycan concentration.[7] Due to their

carbohydrate functionalities, glycopolymers are expected to mimic the functions of natural carbohydrates.[22] Some reports describe the imitation of the reversible and specific carbohydrate-lectin binding, where the binding intensity could be regulated by external stimulus.[23] The interaction between glycopolymers and lectins can be greatly influenced by various factors such as the rigidity, the molecular weight and the architecture of the polymer, the density of sugar molecules and other parameters.[21] The diverse architectures of glycopolymers have been published by several research groups [Okada, Haddleton, Miura, Stenzel, Fukuda etc.]. They include linear glycopolymers, glycodendrimers, spherical glycopolymers in the form of micelles, vesicles and micro/nano particles and surface grafted glycopolymers.[10] Synthetic glycopolymers can be prepared by two different strategies: (i) the direct polymerization of carbohydrate-containing monomers, glycomonomers, or (ii) the post glycosylation of synthetic polymers.[24, 25] The development of controlled/living free-radical polymerization (CLRP) techniques has rendered it possible to polymerize the glycomonomers (protected or not). The CLRP techniques include nitroxide mediated controlled free-radical polymerization[26, 27, 28, 29], atom transfer radical polymerization (ATRP)[20, 30, 22, 31, 32], and reversible addition-fragmentation chain transfer (RAFT) polymerization[33, 34, 35, 36, 37].

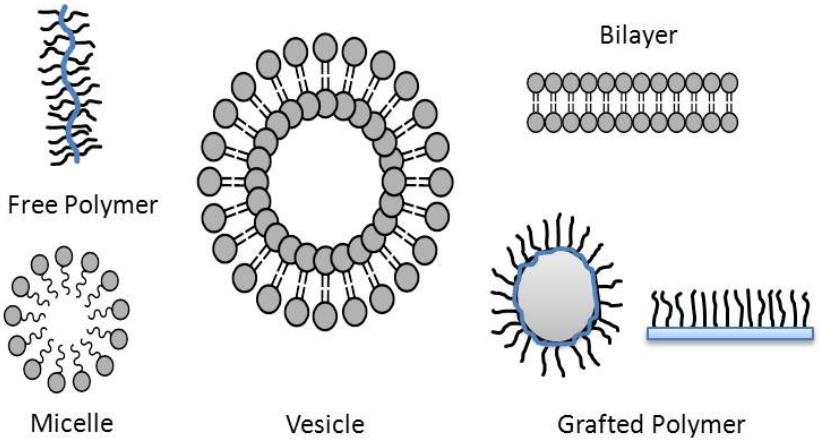

Figure 1.3: Diverse architectures of glycopolymer [10, 9].

Using CLRP methods, polymer brushes are most frequently prepared by one of the three routes: “grafting through”, “grafting to” and “grafting from”. Grafting through methods involve the incorporation of macromonomers with polymerizable end groups into a backbone prepared by CLRP. “Grafting through” enables the attachment of side chains to every backbone unit. However, the polymerization degree of the backbone is usually low because it is dependent on the macromonomer length and type.[38, 39, 40] “Grafting to” methods include the covalent binding of a preformed polymer to the surface via reaction with co-reactive groups. This approach is beneficial for the characterization of the backbone and side chains due to the individual synthesis of polymers. However, the dense grafting is limited because the attachment of polymers onto the surface becomes more difficult with increasing conversion due to the steric congestion.[41] “Grafting from”

methods involve the growth of the polymer from a predetermined number of initiating sites. Owing to the fast initiation step and simultaneous growth of all polymer chains, the grafting from methods lead to the formation of well-defined polymer brushes with high grafting density and low dispersity of backbone and side chains.[42]

1.2.1 ATRP Techniques

The ATRP technique is one of the recently developed CLRP methods. It has a "living" characteristic which can be described as the continuous growth of the formed macromolecular chains if some extra amount of monomer is added to the polymerization system. This polymerization method was developed independently by the research groups headed by Sawamoto[43] and Matyjaszewski[44] in 1995. To date, ATRP is the most widely used polymerization technique among the several CLRP methods. The reason for this can be its tolerance to protic compounds such as water and a high reaction rate. Moreover, ATRP methods are known to be tolerant towards many functional groups like allyl, amino, epoxy, hydroxy, and vinyl groups which present in either the monomer or the initiator. Furthermore, this technique is also advantageous due to the ease of preparation, commercially available and favorable catalysts (e.g. copper complexes), pyridine based ligands and initiators (e.g. alkyl halides).[45] A general mechanism for ATRP is shown in Figure 1.4.

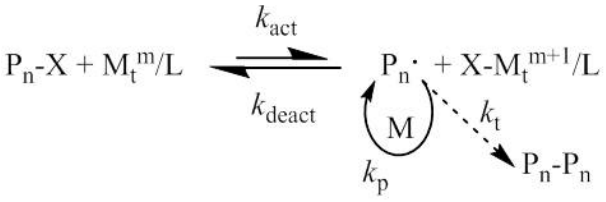

Figure 1.4: Scheme of Transition-Model-Catalyzed ATRP (adapted from [45]).

The radicals (P_n·) or active species are generated through a reversible redox process catalyzed by a transition metal complex. Here, M_t^m represents the transition metal species in oxidation state m, L a ligand, and M a monomer. The dormant species periodically react with transition metal complexes with the rate constant of activation (k_{act}). The transition metal complex undergoes an one electron oxidation with concomitant abstraction of a (pseudo)halogen atom, X, from a dormant species, P_n-X. For the reformation of the dormant species and the activator (M_t^m/L), the transition metal complex in higher oxidation state reacts with the propagating radical in a reverse reaction (k_{deact}). Polymer chains grow by the addition of the intermediate radicals to monomers with the rate constant of propagation (k_p). The manner of the polymer growth is similar to a conventional radical polymerization. Termination reactions (k_t) occur mainly through radical coupling and disproportionation. However, in a well-controlled ATRP, no more than a few percent

of the polymer chains undergo termination. In ideal case, the polydispersity index of a polymer prepared by ATRP is related to different parameters and can be summarized as in Eq. 1.1. Thus, for the same monomer, a catalyst that deactivates the growing chains faster will produce polymers with a lower polydispersity index and a narrower MW distribution. The polydispersity index can be further reduced by increasing the deactivator concentration.[46]

$$\frac{M_W}{M_n} = 1 + \frac{1}{DP_n} + \left(\frac{k_p[P_nX]}{k_{deact}[X - Cu^{II}/L]}\right)\left(\frac{2}{p} - 1\right) \tag{1.1}$$

ATRP consists of a monomer, an initiator with a transferable (pseudo)halogen, a transition metal salt and a ligand which form the active catalyst complex. Sometimes an additive can be used for a successful ATRP. There are also some factors, such as solvent and temperature, which must be taken into consideration to the polymerization. Various monomers have been successfully polymerized using ATRP: styrene, (meth)acrylate, dienes, and other monomers which contain substituents that stabilize the propagating radicals.[47, 48] 2-Hydroxyethyl methacrylate (HEMA) is the most commonly used monomer in numerous applications. This monomer is commercially available and can be easily polymerized similar to the majority of methacrylic derivatives. HEMA is water soluble and possesses a hydrophilic pendant group. Due to this hydrophilic pendant group, HEMA can form a hydrogel after polymerization. For this reason, it is widely used in the manufacture of soft contact lenses.[49, 50, 51] HEMA has a primary alcohol function. Hence, a number of nucleophilic substitution reactions can be performed and the modified monomer can be polymerized. The low toxicity of this monomer is widely accepted, although numerous clinical trials have found minimal irritant reactions. Therefore, poly(2-hydroxyethyl methacrylate) (PHEMA) is known as an appropriate biomaterial for biomedical application because of its biocompatibility and high resistance to degradation.[52]

In ATRP, the amount of the initiator determines the number of growing polymer chains. When initiation is fast and chain transfer or termination is negligible, the number of growing chains is constant and equal to the initial concentration of the initiator. Typically, alkyl halides (P_n-X) are used as ATRP initiator and the polymerization rate is first order with respect to the concentration of P_n-X. X is usually either bromine or chlorine and can migrate between the growing chain and the transition metal complex. This rapid and selective migration process allows to form well-defined polymers. ATRP is a catalytic process and thus the catalyst plays the key roll in addition to the initiator. The catalyst determines the equilibrium state of the atom transfer and the transition dynamics between the dormant and active species. It can be mediated by many redox-active transition metal complexes. Generally, Cu^{I}/L and X-Cu^{II}/L are used as transition metal complex, but other metal sources such as Ru, Fe, Mo and Os have been also reported.[53] The ATRP ligand solubilizes the

transition metal salt in the organic media and adjusts the redox potential of the metal center for appropriate reactivity and dynamics for the atom transfer. Therefore, steric effects around the Cu center are very important.[54, 55] The kinetically optimum ratio of ligand to catalyst in the polymerization can vary with regard to changes in the monomer, counterion, ligand, temperature, and other factors.[56, 57] In general, bridged cyclam including tris(2-dimethylaminoethyl)-amine (so-called Me_6TREN) and tris(2-pyridylmethyl)amine is the most active ligand for Cu complexes, whereas pyridineimine and 2,2'-bipyridine are the least active.[58] Activation rate constants increase with elevating temperature due to the increase of both the radical propagation rate constant (k_p) and the atom transfer equilibrium constant (K_{eq}). As temperature increases, the ratio of k_p/k_t also increases and it hence delivers better control of the polymerization and better solubility of the catalyst.[59]

1.2.2 Glycopolymer Synthesis via ATRP Techniques

Recently, a range of carbohydrates is commercially available and thereby provides the accessibility of a wide array of different glycomonomers. However, the type of vinyl-functionalized sugars is still less accessible. Furthermore, it is necessary to synthesize vinyl-functionalized sugars for the free radical polymerization. In an early article, Wulff and co-workers highlighted the synthesis of polymerizable vinyl sugars.[60] They introduced two natures of the vinyl sugars: protected and unprotected carbohydrates. For the decision between both carbohydrates, there are some considerable factors which can impact on the whole procedure. For example, those factors include the ease of stereospecific functionalization of the sugar, the solubility of the monomer and polymer, the potential incompleteness of the removal of the protective group, and the ease of purification. The most common synthetic approaches are already outlined and described in detail by Stenzel and co-workers.[61]

The first report about glycopolymers was completed in 1961 when Kimura et al.[62] and Whistler et al.[63, 64] introduced the free radical homo- and copolymerization of glycomonomers. Then, in 1998 Fukuda et al. first reported the glycopolymer synthesis by ATRP method.[65] They have shown that the ATRP technique could provide low polydispersity, high-molecular weight glycopolymers as well as an amphiphilic block copolymer with glycopolymer chains. Up to now, a number of glycopolymers have been introduced to prepare well-defined glycopolymers with narrow molecular weight distribution using the grafting from approach via copper-mediated ATRP. ATRP technique is a recently developed CLRP method and most widely employed in industrial- and laboratory-scale processes for polymer synthesis among the several CLRP methods. This polymerization technique tolerates impurity of the reactants and solvents as well as protic compounds such as water. It allows the synthesis of a variety of well-defined polymers under mild reac-

tion conditions. Furthermore, ATRP can be applied for the grafting approaches requiring well-defined structures.[66, 67, 68]

Müller and co-workers synthesized hyperbranched glycopolymers via self-condensing vinyl copolymerization of an acrylic acid with a glucofuranoside via ATRP and introduced a strategy for generating water-soluble hyperbranched glycopolymers.[69] Vázquez-Dorbatt and Maynard have published biotinylated glycopolymers by ATRP techniques. They polymerized both a protected and unprotected glycomonomer, GlcNAc side chain methacrylate. The unprotected monomer performed slightly better control of polymerization. Researchers also investigated biological interactions between biotinylated glycopolymers and a streptavidin-coated surface. In addition they showed that the polymers with GlcNAc side chains may be employed to investigate biological interactions involving GlcNAc.[32] Armes and co-workers have reported the synthesis of sugar side chain poly(methacrylate) homo and block copolymers by ATRP and studied the self-assembly of the block copolymers in solution.[70] Many other groups have investigated further applications of glycopolymers including macromolecular drugs and drug delivery systems, biocatalytic and biosensitive hydrogels, matrices for controlled cell culture, stationary phases for chromatographic purposes, surface modifiers, and the use as models of biological systems.[24]

1.2.3 Surface Grafted Glycopolymer Brushes via surface-initiated ATRP Techniques

In recent decades, interest in new ways for surface modification of solid substrates has been aroused with their increasing application possibilities. Surface grafting of glycopolymers has gained great interest because the prepared surface is not only highly biocompatible, but can also mimic the extracellular matrix. Additionally, surface properties can be widely changed by graft-polymerization methods due to the variety of functional monomers. Surface-initiated ATRP (SI-ATRP) is an effective method for achieving a high density of polymer brushes which are covalently linked to a surface. In general, the concentration of the initiator in SI-ATRP is not high enough to generate sufficient Cu^{II} at the beginning of the polymerization by reaction with the Cu^{I} catalyst species. Therefore, alternative routes are required to achieve this purpose in order to boost the deactivator concentration. As the first approach, sacrificial initiator can be added to the reaction mixture and hence enables to proceed polymerization both in solution and from the surface. This approach has a great advantage such as the production of free polymer which can be often used to analyze the grafted polymer. However, there are still some considerable problems such as the adsorption of the free polymer chains on the substrate or the interference of the grafting process and the unexpected consumption of the monomer in solution instead of at the surface. As the second approach, Cu^{II} can be added to the initial polymerization mixture to ensure sufficient deactivator at the start of the polymerization.[61]

Fukuda and co-workers prepared glucose containing homopolymers and block copolymers by ATRP in solution and from a surface-immobilized initiator. They have shown a successful polymerization of glycomonomers by using the SI-ATRP techniques for the first time.[71] Then, many reports have published the synthesis of glycopolymer brushes on solid substrates. Huck und Gunkel prepared antifouling polymer surfaces using poly(oligoethylene glycol) methacrylate, poly(sulfobetaine methacrylate), and poly(2-hydroxyethyl methacrylate) by ATRP and determined which proteins from blood plasma foul protein-resistant surface by gel electrophoresis and mass spectrometry.[66] Yu and Kizhakkedathu have synthesized homoglycopolymer brushes containing mannose, galactose and glucose by SI-ATRP and exhibited the anti-fouling properties of the prepared surfaces against bovine serum albumin (BSA) and fibrinogen. Besides, they showed specific protein interaction of grafted glycopolymer brushes with concanavalin A.[67] Although there have been major developments in synthesizing glycopolymers, the synthesis of glycopolymers capable of mimicking oligosaccharides in selective binding to lectins still remains a challenging task.[21]

1.3 Microfluidic Biosensors

In recent years, the area of nanoscience and nanotechnology has become increasingly important. Since the size of nanomaterials is comparable to that of biomolecules, there is great potential to understand and modify biological systems. This allows to enable early diagnosis, to identify the molecular origins of diseases, to develop more selective therapeutics and biocompatible medicines. In spite of a lot of technical challenges, the integration of artificial nanomaterial with natural biological systems has accomplished significantly. Most fabricated nanodevices have been used for biological, medical, and clinical applications. Additionally, they have been also applied in other fields such as environmental monitoring as well as food industry.[72]

Biosensors are devices or materials typically used for the detection of biological targets such as proteins, enzymes or nucleic acids. According to IUPAC, a biosensor is "a device that uses specific biochemical reactions mediated by isolated enzymes, immunosystems, tissues, organelles or whole cells to detect chemical compounds usually by electrical, thermal or optical signals".[4] Generally, a biosensor includes two components, a biological probe (or an analyte) and a physicochemical transducer. Biosensors response selectively to the target molecules and the biological recognition event convert into a sensing signal by a transducer. The selectivity of a biosensor often depends on the specificity of the measuring probe to the biosensor. The sensitivity and the detection limit of biosensors strongly rely on the physicochemical properties of the transducer. Conventionally, biosensors have been developed in two broad categories: (1) microarray type and (2) microfluidic and nanofluidic

sensors. In case of microarray type biosensors, they usually include cantilever or field-effect devices. The main transduction mechanism is the adsorption of target analytes to sensing elements. In the latter case, the measurement mechanisms are usually based on manipulations of small fluidic volumes (microliters to nanoliters) following to an optical detection method.[73]

Over the last two decades, there has been significant advancements in the miniaturized anayltical systems and hence developments of integrated biosensors comprising several unit operations on a single platform. These biosensors have several advantages such as reduced reagent consumption, short analysis time, a small-sized scale, low cost, and high sensitivity. In general, biosensors are expected to extract analytical information of given samples without pretreatment. Furthermore, bioassays can be beneficial to automatic sequential chemical synthesis that are linked to the detection part of a miniaturized analytical system. These so-called lab-on-a-chip can be potentially applied to many fields of medicine, biotechnology, and pharmacology.

There are several types of the detection principles for biosensors integrated on microfluidic chips. As examples, there are (1) optical, (2) electrochemical, and (3) mass-sensitive methods. Usually, optical detection methods for biosensors are based on ultra-violet (UV) absorption spectroscopy, emission spectroscopic measurement of fluorescence and luminescence, and Raman spectroscopy. Moreover, surface plasmon resonance (SPR) spectroscopy is able to analyze the given sample quickly without a labeling technique.[74, 75, 76] Most electrochemical detection methods have been regarded as particularly appropriate strategy for microfluidic chip systems because of their high sensitivity, low detection limits, reusability, long-time stability, simple and cost-effectivity.[77]

Electoanalytical detection principles are developed in three categories: potentiometry, amperometry, and conductometry (or impedometry). For example, conductometry is used to measure the electrical conductance in solution. When an AC electrical field is applied between two electrodes, the output data such as amplitude and phase angle are changed. The conductometer or impedance analyzer acquires the changed data. Hereby, amplitude change gives serial resistance value in equivalent circuit. Phase angle shift handles capative and inductive components in the electrochemical interface between the electrode surface and the solution. When DC input is provided, the output data include pure resistance changes. Therefore, it is favorable for miniaturized systems. However, DC input is normally avoided, because the applied potential difference is not focused on the solution instead of on the electric double layer on the electrode surface. This method has some challenging problems such as insufficient selectivity or specificity resulting in intrinsic limitation of electrochemical detection.[78, 79]

Mass-sensitive sensors include piezoelectric effects and surface acoustic waves. Piezoelec-

tricity means the electric charge that accumulates in some materials such as crystals, ceramics, biological matter like bone, DNA, and various proteins in response to mechanical stress. The piezoelectric effect has been mainly applied for immunosensors and nucleic sensors due to relatively large mass charge of antigen-antibody association and DNA hybridization. There have been a number of reports about quartz resonators: electrochemical quartz crystal microbalance, surface acoustic waves (SAW), thickness shear mode, flexural plate wave, and shear-horizontal acoustic plate mode. In case of quartz crystal microbalance (QCM) sensors, they are composed of a thin quartz disk and two electrodes and measure a mass per unit area by monitoring the change in frequency of a quartz crystal resonator. SAWs can be efficiently transferred in microfluidic platforms and hence can be applied to immunoassays and the detection of DNA, bacteria, and small molecules.[80, 81]

To manufacture a microfluidic-based biosensor, there are some essential steps such as sample pretreatment, surface modification and components like micropumps (with valve) and micromixers. Particularly, surface modification is crucial to improve the sensitivity of biosensors and to minimize nonspecific binding. For the surface modification, chemical and physical methods have been often utilized. Chemical modification immobilizes functional molecules on the surface to get desired properties. On the other hand, the surface properties can be changed by physical modification such as altering of the surface roughness, grain size, and grain boundary by exposure to lasers, plasmas, shear and polishing.[82] Biofouling of the surface has been one of the major problems in biological analysis. Several variables such as wettability, biocompatibility, and nonspecific adsorption were suggested to overcome this problem.[83, 84, 85] In conclusion, microfluidic-based biosensors have greatly advanced in various fields over the last few decades.[86, 87, 88] However, there are still challenges like technical problems such as miniaturization or integration on a chip. Microfluidic biosensors seem to possess great advantages such as high efficiency, convenience, cost-effectiveness, and compatibility. Particularly, their label-free technology deserves special attentions.

1.4 Structure of This Thesis

This work contains the research achievements concerning the synthesis of glycopolymers and glycopolymer brushes, their characterization, and the potential application as diagnostics or biosensors. This research was involved in several joint projects with the aim of fabricating a novel multivalent glycopolymer platform for specific protein binding. The projects were performed as cooperative works combining different scientific fields. The chemical synthesis and characterization of glycopolymers and glycopolymer brushes were performed at DWI - Leibniz Institute for Interactive Materials. The biological modification

and investigation of the glycopolymers were done at Lehr- Forschungsgebiet Biomaterialen und Helmholz-Institut für Biomedizinische Technik at RWTH Aachen University. The electochemical investigation of glyco-biosensors was carried out at Institut für Werkstoffe der Elektrotechnik. This thesis is structured as follows:

- Chapter 2 describes the used materials and the various characterization methods for the synthesis of polymers and polymer brushes, and diverse microfluidic chips.

- Chapter 3 includes the detailed description of the synthesis of glycopolymer brushes on silicon wafers and the surface characterization using various optical measurement techniques, ellipsometry as well as water contact angle measurements.

- New multivalent glycochips with gradient such as polymer molecular weight or grafting density will be fabricated and their characteristics discussed in Chapter 4. The prepared gradient glycopolymer brushes will be investigated in detail by AFM and fluorescence microscopy using lectin binding proteins.

- In Chapter 5, one of the possible glycochip applications as biosensors will be introduced. Hereby, we will focus on electrochemical measurement techniques. The impedimetric glyco-biosensor using microfluidic system will also be investigated by optical microscopies.

- As next, Chapter 6 focusses on additional application possibilities of surface grafted polymers for the microfluidic systems. At first, plasmonic flow-through glycochips will be synthesized and their potential as biosensors introduced. Then, a mass-sensitive detection method will be introduced. The biosensor integrated on a microfluidic chip will be monitored by the surface acoustic wave measurement technique. A potential automation of polymerization processes will be described.

- Glycopolymers can be also applied for the synthesis of core-shell microspheres. In Chapter 7, the synthesis of silica particle based glycopolymers and the characterization of these core-shell microspheres by several analytical methods will be reported.

- Chapter 8 describes super micelle structures of glycopolymers in water. For this, a synthetic diblock glycopolymer is introduced and its properties are investigated by several analytic methods.

- To summarize the results, Chapter 9 will give a short overview about the whole work.

2 Materials and Methods

2.1 Materials

GlcNAc (98%) and sodium methoxide (98%) produced by Alfa Aesar (Karlsruhe, Germany) have been used. Copper(I) chloride (CuCl, 97%) was purified by stirring with acetic acid overnight. After filtration, they were washed with ethanol followed by diethyl ether and then dried in vacuum. Copper(I) chloride (CuBr, 98%), copper(II) bromide ($CuBr_2$, 99%), 2,2‘-bipyridine (bpy), ethyl α-bromoisobutyrate (EBiB, 98%), silver perchlorate monohydrate (99.999%), acetyl chloride and silica gel 60 have been purchased from Sigma-Aldrich (Steinheim, Germany) and used as received. Celite® 545, silver carbonate (99%), and 2-hydroxyethyl methacrylate (HEMA, 97%) were provided by VWR (Darmstadt, Germany). The ATRP initiator 3-(trimethoxysilylpropyl)-2-bromo-2-methylpropionate (95%) was received from ABCR (Karlsruhe, Germany). All other solvents were purchased from Sigma-Aldrich or VWR and used as received unless otherwise noted. Deoxygenation of the solvents was accomplished by bubbling with nitrogen. The materials for enzymatic modification such as $MgCl_2$, $MnCl_2$, 4-(2-hydroxyethyl)-1-piperazineethanesulfonic acid (HEPES)-NaOH buffer and α-picoline borane were purchased from Sigma-Aldrich (Steinheim, Germany). Uridinediphospho-α-D-Galactose (UDP-Gal) and UDP-GlcNAc were purchased from Carbosynth Limited (Berkshire, UK). 8-aminopyrene-1,3,6-trisulfonic acid (APTS) was purchased from Beckman Coulter (Krefeld, Germany). All buffer and lectin solutions were provided by Lehr- Forschungsgebiet Biomaterialen und Helmholz-Institut für Biomedizinische Technik at RWTH Aachen University and used as received unless otherwise noted.

2.1.1 Synthesis of Glycomonomer 2-O-(N-acetyl-β-D-glucosamine)ethyl methacrylate (GlcNAcEMA 4)

The preparation of GlcNAc containing glycopolymers was started with the synthesis of glycomonomer 2-O-(N-acetyl-β-D-glucosamine)ethyl methacrylate (GlcNAcEMA **4**). The synthetic route is shown in Scheme 2.1. The acetylated GlcNAc chloride **2** was synthesized from GlcNAc **1** by the use of a similar procedure reported in the literature.[89] For the

synthesis of glycomonomer **3**, a modified König-Knorr reaction was performed according to literature.[89, 90] Compound **3** (4.8 g, 13.32 mmol) was dissolved in anhydrous methanol. Then, sodium methoxide (100 mg*cdot*mL^{-1}) was added and the reaction mixture was stirred at room temperature for 25 min. After that, the mixture was neutralized using DOWEX MAC-3® ion exchange resins (Sigma-Aldrich). Methanol was evaporated under reduced pressure and then water was added. Glycomonomer GlcNAcEMA **4** (2.5 g, 7.50 mmol, 52%) was obtained by lyophilization of the aqueous solution.

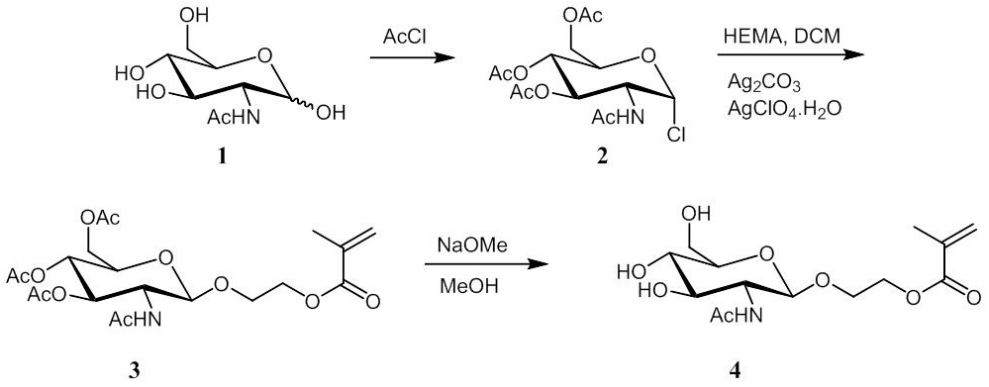

Scheme 2.1: Synthesis of the glycomonomer GlcNAcEMA **4** from GlcNAc.

NMR spectroscopic data of 2,3,4,6-α-D-tetraacetylglucosamine chloride (**2**):
^{1}H NMR (400 MHz, $CDCl_3$, δ): 6.20 (s, 1H; H1), 5.90 (d, J = 8 Hz, 1H; NH), 5.35 (t, J = 10 Hz, 1H; H3), 5.20 (t, J = 10 Hz, 1H; H4), 4.67-4.39 (m, 1H; H2), 4.39-4.20 (m, 2H; H5 and H6), 4.16 (d, J = 11 Hz, 1H; H6), 2.19 (s, 3H; COCH3), 2.06 (s, 6H; COCH3), 1.90 (s, 3H; NHCH3) ppm.
^{13}C NMR (100 MHz, $CDCl_3$, δ): 170.05-167.89 (4C; COCH3), 92.5 (C1), 69.6 (C5), 68.8 (C3), 65.9 (C4), 59.9 (C6), 52.1 (C2), 21.7 (NHCH3), 19.3 (3C; COCH3) ppm.

NMR spectroscopic data of 2-O-(2,3,4,6-β-D-tetraacetylglucosamine)ethyl methacrylate (**3**):
^{1}H NMR (400 MHz, $CDCl_3$, δ): 6.13 (s, 1H; C=CH2), 5.80 (d, J = 72 Hz, 1H; NH), 5.60 (s, 1H; C=CH2), 5.30 (t, J = 76 Hz, 1H; H3), 5.08 (t, J = 80 Hz, 1H; H4), 4.78 (d, J = 8.2 Hz, 1H; H1), 4.48-3.98 (m, 1H; CH2OCO), 4.25 (dd, J = 8.2 and 20.4 Hz, 2H; H6a, CH2OCO), 4.13 (d, J = 11.9 Hz, 1H; H6b), 4.09-3.98 (m, 1H; H5), 3.87 (dd, J = 7.3 and 16.3 Hz, 2H; OCH2), 3.73 (d, J = 7.1 Hz, 1H; H2), 2.09-2.03 (m, 9H; COCH3), 1.95 (s, 3H; NHCH3), 1.92 (s, 3H; CCH3) ppm.
^{13}C NMR (100 MHz, $CDCl_3$, δ): 170.7-170.2 (3C; COCH3), 169.3 (NHCH3), 167.2 (C9), 136.0 (C11), 125.9 (C10), 100.0 (C1), 72.3 (C3), 71.8 (C5), 68.5 (C4), 66.9 (C7), 63.0 (C6), 62.0 (C2), 54.4 (C8), 23.2 (CH3NH), 20.7-20.3 (3C; COCH3), 18.2 (C12) ppm.

NMR spectroscopic data of 2-O-(N-acetyl-β-D-glucosamine)ethyl methacrylate (GlcNAcEMA; **4**):

^{1}H (400 MHz, D_2O, δ): 6.15 (s, 1H; C=CH2), 5.74 (d, 1H; C=CH2), 5.15 (d, J = 3.38 Hz, 1H; H1), 4.56 (d, J = 8.5 Hz, 2H; CH2OCO), 4.46-4.22 (m, 1H; OCH2), 4.22-4.04 (m, 2H; OCH2, H6), 4.04-3.81 (m, 2H; H6, H2), 3.81-3.60 (m, 1H; H5), 3.61-3.33 (m, 2H; H3, H4), 2.06 (s, 3H; HCOCH3), 1.92 (s, 3H; CCH3) ppm.
^{13}C NMR (100 MHz, D_2O, δ): 174.6 (NHCH3), 169.5 (C9), 135.7 (C11), 127.1 (C10), 101.1 (C1), 75.8 (C3), 73.8 (C5), 69.9 (C4), 67.7 (C7), 64.0 (C6), 60.6 (C2), 55.5 (C8), 22.1 (CH3NH), 17.4 (C12) ppm.

2.1.2 Deposition of the Polymerization Initiator

Silicon (Si; 100) wafer, cut into 1×1 cm^2 pieces, was cleaned with absolute toluene and dried in a nitrogen stream. Subsequently, the surface of the wafer was oxidized for 5 min in air plasma (0.2 mbar, 18W, PDC-32 G, Harrick). The schematic illustration of the surface modification with an ATRP initiator and the polymerization process is shown in Scheme 2.2. For the modification of silicon wafer, the freshly cleaned wafer was directly immersed in a mixture containing 200 µL 3-(trimethoxysilylpropyl)-2-bromo-2-methylpropionate, 2.1 mL ammonia (29 %) and 25 mL ethanol. The reaction was left at room temperature overnight and then boiled for 1 h to ensure covalent binding.[91, 92] The wafer was removed from the solution, rinsed repeatedly with toluene, ethanol and milli-Q water and dried in a nitrogen stream.

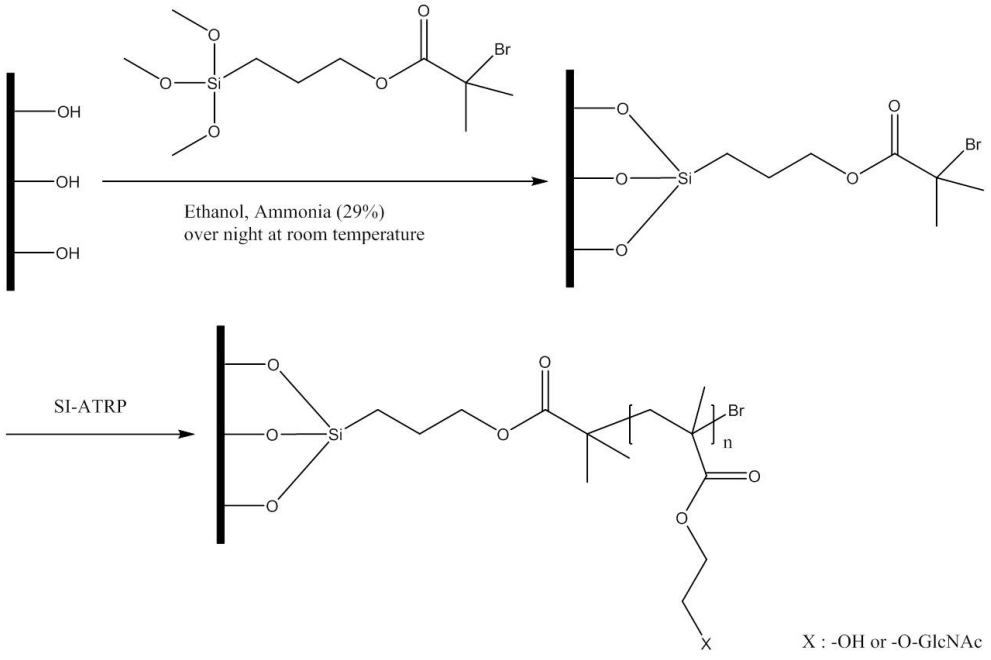

Scheme 2.2: Scheme of surface modification of silicon wafer with initiator and the polymerization of HEMA or GlcNAcEMA **4** by SI-ATRP

2.1.3 Synthesis of poly(2-O-(N-acetyl-β-D-glucosamine)ethyl methacrylate) (PGlcNAcEMA) Brushes by SI-ATRP

A representative procedure was as follows: The initiator modified wafer was placed on the holder of the reaction flask and then the flask was purged with nitrogen. 1.1 g (3.15 mmol) glycomonomer 4 was placed into a reaction flask and stirred in 10 mL methanol/water = 1/1 (v/v) until complete dissolution. The solution was degassed with nitrogen for 20 min. Then, 25.0 mg (0.25 mmol) CuCl, 14.1 mg (0.06 mmol) $CuBr_2$ and 98.4 mg (0.63 mmol) bpy were added and stirred under a nitrogen stream until a homogeneous dark brown solution was formed. The reactor was degassed with nitrogen for 20 min and then transferred into the flask containing the wafer. Soluble free initiator, 9.3 μL (0.06 mmol) EBiB in 1 mL methanol/water = 1/1 (v/v), was added immediately to the reaction mixture. The polymerization was allowed to proceed at room temperature for a defined reaction time. Then the wafer was thoroughly rinsed with water and N,N-dimethylformamide and dried in a nitrogen stream. After that, the wafer was cleaned by stirring in dimethyl sulfoxide overnight and again dried in a nitrogen stream. The soluble polymer was collected by passing through a column packed with silica to remove the remained catalysts. The polymer was diluted with methanol/water = 1/1 (v/v) and precipitated from diethyl ether. After filtration, the purified white polymers were dried in vacuum and analyzed using NMR spectroscopy and GPC.

2.1.4 Enzymatic Synthesis

β4GalT-1[93] and β3GlcNAcT[94] were expressed recombinantly and purified as described previously.[95] Except that the β4GalT-1 was expressed in E.coli Shuffle T7 Express (New England Biolabs, Frankfurt am Main, Germany) to enhance the activity. For investigating the kinetics of the galactosyl-transfer to **4**, a reaction cascade was used as described elsewhere.[93] The conversion at different concentrations of **4** was detected photometrically by following the NADH-formation. Enzymatic conversions were performed on the silicon wafer coated with PGlcNAcEMA. For galactosylation, the wafers were incubated at 30 °C for 24 h in a solution containing 100 mM HEPES-NaOH (pH=7.2), 25 mM KCl, 2.0 mM $MnCl_2$, 6.25 mM UDP-Gal, 1 U alkaline phosphatase and 200 mU β4GalT-1. The wafers were rinsed with water and PBS (50 mM Na_2HPO_4, 150 mM NaCl, pH=7.4) buffer for several times. Transfer of GlcNAc to galactosylated wafers was performed again at 30 °C for 24 h. The wafers were submerged in a solution containing 25 mM HEPES-NaOH (pH=7.2), 6.25 mM KCl, 0.25 mM DTT, 2.0 mM $MgCl_2$ and 200 mU β3GlcNAcT. Oxidation at C6-Position of terminal Gal was performed with a galactose oxidase from *Dactylium dendroides* (Worthington, NJ; US). The schematic illustration describing sequential reaction cascade of sugar units is shown in Scheme 2.3. The wafers were incubated at 22 °C

for 17 h in a solution of 25 mM MES-NaOH (pH=6.0), 15.5 U galactose oxidase and 322 U peroxidase (Merck, Darmstadt, Germany). After washing with water for several times, reductive amination was carried out with APTS (3 μmol) in the presence of α-picoline borane (2 eq.) and acidic acid (2 eq.) in methanol at 60 °C for 2 h. After incubation, the wafers were again cleaned with water and PBS buffer for several times. The whole procedures of the enzymatic synthesis were performed by the co-workers (R. R. Rosencrantz et al.) from Lehr- Forschungsgebiet Biomaterialen und Helmholz-Institut für Biomedizinische Technik at RWTH Aachen University.

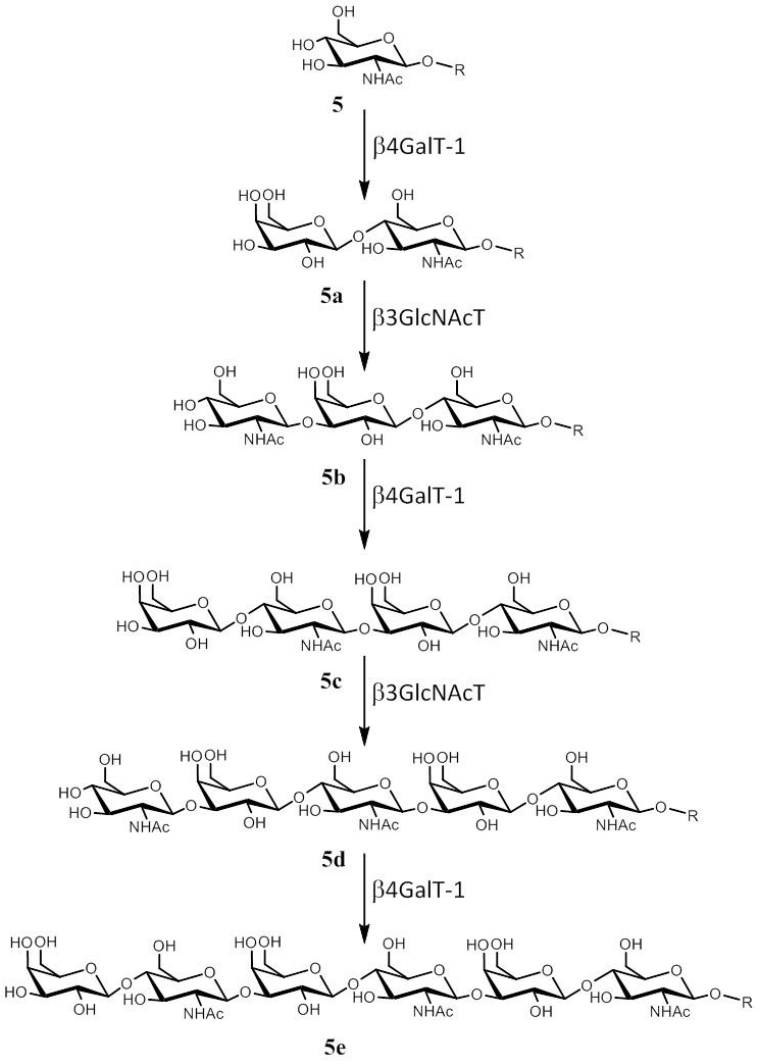

Scheme 2.3: Sequential reactions cascade for the production of oligo-*N*-acetyllactosamine (LacNAc) (**5a-5e**) structures on the PGlcNAcEMA **5** brushes utilizing two recombinant glycosyltransferases.[96]

2.1.5 Fluorescence-Linked Lectin Assay (FLLA)

Lectins *Griffonia (bandeiraea) simplicifolia* (GS-II) and *Erythrina cristagalli* lectin (ECL) were purchased as fluorescein isothiocyanate (FITC) conjugates from Vector Laboratories (Burlingame, CA, USA). For quantitative binding studies, the wafers were incubated in 24-well microtiter-plate with 1 mL 5 % (w/v) BSA for 15 min. After several washing steps with PBS and LBP (10 mM HEPES-NaOH (pH=7.5), 150 mM NaCl, 0.1 mM $CaCl_2$) 20 $\mu g \cdot mL^{-1}$ lectin in LBP was added and the wafers kept for 30 min at room temperature in the dark. Finally, the surfaces were washed with PBS containing 0.05 % (v/v) TWEEN-20 and the fluorescence signal was detected using a BioTek device. After measurement the wafers were washed with water, ethanol, DMSO and acetone. After drying the next lectin was applied. If the fluorescence signals did not reach the minimum threshold, the washing procedures were repeated as often as necessary. For binding studies focused on fluorescence imaging, the wafers were treated as mentioned above except for the blocking-step with BSA. Images were taken with a Zeiss Axioplan microscope.

2.2 Characterization Methods

2.2.1 Characterization by Microscopic Techniques

After synthesis of glycopolymer brushes in solution as well as on the solid substrate, they were analyzed by various microscopic methods. In this chapter, the concepts of the three mainly used microscopic techniques are introduced.

Atomic Force Microscopy (AFM)

AFM was first introduced by Binning, Quate and Gerber in 1986[97]. AFM has evolved into a multifunctional tool due to its pico-newton force sensitivity and nanometer positional accuracy in materials and biological sciences. This microscopic technique allows not only to present the surface topography with atomic or near-atomic resolution, but also to quantify surface roughness and feature size such as height. The basic parts of the AFM are the spring cantilever with integrated tips, the sample stage and the optical deflection system consisting of a laser diode and a photodetector (Figure 2.1). AFM works by scanning (in the x and y directions) a sharp tip along the sample surface and by probing the interaction forces between the tip and the surface with piconewton sensitivity. The cantilever is moved over the sample by a piezoelectric scanner which ensures three-dimensional positioning with subnanometer resolution. Any interaction between the tip and the sample leads to

a bending of the cantilever. The vertical bending (deflection) of the cantilever is directly proportional to the interaction force. It is detected by a laser beam focused on the end of the cantilever. The reflection of the laser beam is focused on a photodiode. The photodiode measures any minimal deformation of the cantilever and thus, the interaction between the tip and the sample.[98, 99]

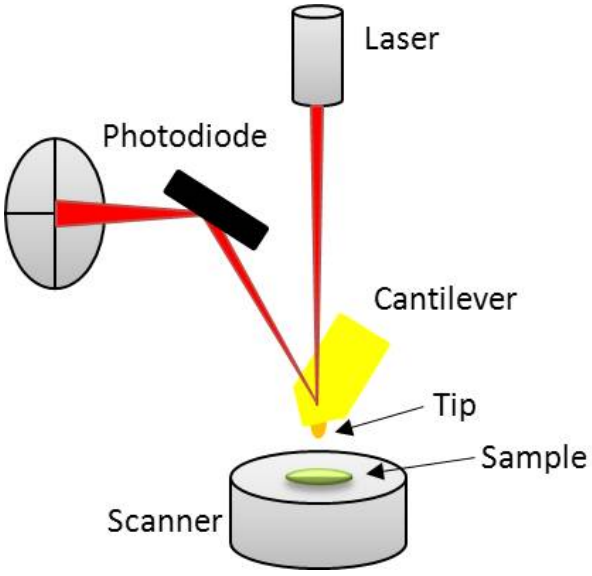

Figure 2.1: Schematic illustration of atomic force microscopy (AFM).

Imaging can be usually accomplished with either contact mode or tapping mode and both modes can be used in either air or fluid.[100] Contact mode imaging is carried out by simply keeping the contact of the tip with the sample surface constant. Then, the small (angular) movement of the lever is measured by the laser beam. Therefore this mode allows reasonably easy operation. However, the contact mode has the inherent drawback of the quite high lateral force exerted on the sample. This can cause sample damage or the movement of relatively loosely attached objects (Figure 2.2a). In tapping mode the cantilever vibrates at or near its resonance frequency. Upon approaching the sample, the tip briefly touches or taps the surface, which results in a decrease in oscillation amplitude. In tapping mode AFM, the lateral forces between the cantilever and surface can be reduced and consequently the damage can be avoided in soft samples (Figure 2.2b). Therefore, in most studies, the tapping mode leads to higher resolution images.[101]

AFM images were obtained in TappingMode® in air using Dimension^{TM} ICON® AFM of Bruker AXS (former Veeco Instruments Inc.). Bruker OTESPA probes with spring constants of approximately 42 N/m were used for all measurements. In addition, the measurements were performed using the resonance frequency in the range of 280 - 360 kHz and the moderate tapping at a ratio of oscillating amplitude to excited amplitude between 0.7 and 0.8. In case of the glycopolymer brushes, the samples were measured after purification with respecting solvents. The solution of diblock glycopolymers was spin

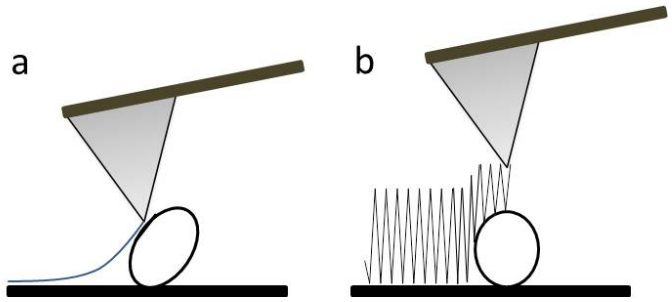

Figure 2.2: Comparison between the two AFM scanning types: (A) contact mode and (B) tapping mode (adapted from Ref. [100]).

coated onto a silicon wafer. In this case, the silicon wafer was pretreated by snow-jet as well as plasma of 0.2 mbar for 2 min.

Transmission Electron Microscopy (TEM)

Since the first TEM has been introduced by Knoll and Ruska in 1931[102], it has been used successfully in the atomic scale imaging of thin samples.[103] Traditionally, materials such as metals, alloys, ceramics, glasses, polymers, semiconductors, and composite mixtures of theses materials have been examined using TEM by material scientists. The ability of TEM to observe matter at dimensions of roughly 1 to 100 nm has been contributed to the development of nanoscale science.[104] A TEM can appear in several different forms such as high-resolution TEM, scanning TEM, and analytical electron microscopy. Here, the general concept of TEM will be introduced. In this work, TEM images were obtained using an Zeiss Libra^{TM} 120 Microscope (Oberkochen, Germany). The accelerating voltage of the electron beam was set at 120 kV. A drop of the sample was trickled on a carbon-coated copper grid. Then, the copper grid was air-dried under ambient conditions.

The imaging by TEM is achieved by an electron-optical system including an electron gun producing the electron beam and several magnetic lenses as shown in Figure 2.3. For the better understanding of the principles, TEM can be divided into three sections: the illumination system, the specimen stage, and the imaging system. The illumination system includes the electron gun and two or more condenser lenses that focus the electrons onto the specimen. The specimen stage holds the specimen in position and allows translation of the specimen for the detailed scan. The imaging system is composed with at least three lenses that together make a magnified image of the specimen.[105]

The electron gun produces an electron beam which can pass through the thin TEM specimen. The gun is formed from an electron source known as the cathode and an electron-accelerating chamber. A sufficiently good vacuum is necessary for the electron gun to prevent a high-voltage discharge and to avoid oxidation of the electron-emitting surface.

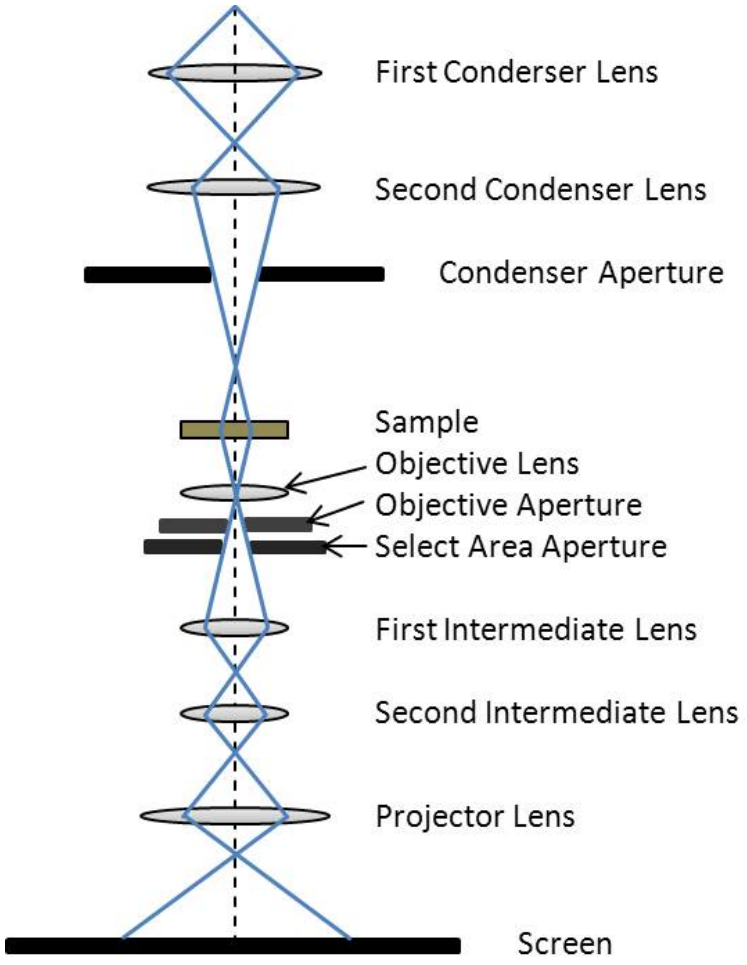

Figure 2.3: Schematic of the optical components in a basic TEM.

When electrons are emitted from the cathode, electrons are accelerated to an anode, a round metal plate containing a central hole. Most of the accelerated electrons are absorbed in the anode, while only 1% pass through the hole. Then, most of the electrons that pass through the specimen are focused on fluorescent screen by two or more condenser lenses. TEM specimens are circular with a diameter of 3 mm and made thin enough to allow electrons to be transmitted. The specimen stage holds the specimen as stationary as possible to minimize image drift. In addition, it is designed to allow the specimen to be inserted into the vacuum of the TEM column using an airlock. The resolution of the image is usually highly dependent on the first imaging lens, the objective. The objective lens must be cooled to get the high resolution image because of its high excitation current. In a modern TEM, the specimen is located close to the center of the objective lens. The pre-field of the objective is important to focus the incident illumination and the lens is called a condenser-objective. In the post-field of the objective, the first objective imaging lens with a small focal length is positioned to optimize the image resolution. The several lenses between the objective and the final (projector) lens are used mainly for the production of an electron diffraction pattern on the TEM viewing screen by changing the lens

excitation in big steps and for the change of the image magnification by changing the focal length in small steps. The projector lens produces an image or a diffraction pattern across the entire TEM screen. The resulting electron image is converted to a visible form by a phosphor screen.

Field Emission Scanning Electron Microscopy (FESEM)

Although Knoll presented a first "scanning microscope" in 1935, the first scanning electron microscopy (SEM) had some discriminations such as the low resolution limit by scanning a very small raster and the high magnification using demagnifying lenses. Then, the scanning microscopy was developed toward observing the surface of samples, while the resolution for thin specimens at TEM was very difficult to compete. SEM provides not only information on surface topography, but also crystalline structures, chemical composition and electrical behaviour of the top 1 μm or so of the specimen. A significant improvement in SEM instrumentation was succeeded by the development of field emission scanning electron microscope (FESEM). In the 1980s, the FESEM became commercially available. In the FESEM, a field emission gun is used for electron beam generation and provides an electron probe with a diameter of about 0.5 nm. FESEM allows the imaging of specimens with high resolution at low acceleration voltage, even below 1 kV. Recently, high-resolution FESEM was possible thanks to the improvements in electron optics and electron detectors and in specimen preparation. At an electron energy of 30 kV, these modern high-resolution FESEMs have a specified resolution power in the secondary electron mode in the range of 0.1-1 nm. Therefore, the high-resolution SEMs are able to cover six orders of magnitude for the surface characterization.[106, 105] In this work, FESEM imaging was performed with a FESEM HITACHI S-4800 instrument. The sample was fixed on a holder and then transferred to the high vacuum chamber.

2.2.2 Ellipsometry

Generally, non-contacting and non-invasive manner of the measurement is expected for ideal sensors. Spectroscopic ellipsometry is a powerful technique, because this method measures the sample in a non-destructive contactless manner. Hence the sample can be used for further studies. In addition, this instrument can precisely measure thickness and compositions of multilayer structures in situ and in real time.[107, 108] Although the principles of ellipsometry were established more than a century ago, the first ellipsometry was introduced 1988 by Drude.[109] The ellipsometry technique is an optical measurement technique and based on the measurement of polarization transformation. The transformation occurs when a beam of a polarized light is reflected obliquely from or transmitted

through a medium.[110, 111] The name 'ellipsometry' originated from the fact that the light often gets elliptically polarized after passing a polarizer.

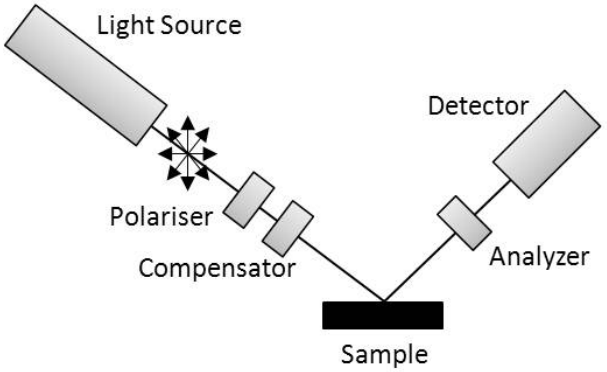

Figure 2.4: Schematic of the spectroscopic ellipsometer.

Figure 2.4 shows the schematic illustration of ellipsometer set-up. This instrument utilizes the so-called polarizer-modulator-sample-analyzer arrangement.[108, 112] The input rail is composed with a Xe arc lamp, polarizer and modulator. Light from an arc lamp passes through a monochromator and then through a polarizer. The polarizer changes the angle of incidence, until the reflected light from the sample is linearly polarized. The output rail (after the sample) contains the analyzer and photodetector. The analyser prism is adjusted to an angle, to extinguish the polarized light as detected by a photodetector. Ellipsometry measurements is typically expressed as two values (ψ, Δ). These values are related to the amplitude ratio and the phase difference between light waves known as p- and s-polarized light waves.[113]

$$\frac{R_p}{R_s} = tan\,\psi\, exp(i\Delta) \tag{2.1}$$

where R_p and R_s are the light components polarized parallel and normal to the plane of incidence. In spectroscopic ellipsometry, spectra are measured by changing the wavelength of light and the measurement is generally performed in the ultraviolet/visible region. In general, the polarization changes are so sensitive that the presence of a thin film or a layer of adsorbed molecules can be characterized. However, the surface roughness of samples should be rather small. If the value of surface roughness exceeds 30 % of a measurement wavelength, the ellipsometry measurement becomes difficult due to the increased errors. In addition, the measurement can be carried out just at oblique incidence. Therefore, an incidence angle is usually chosen to maximize the measurement sensitivity.[114]

In this work, ellipsometry measurement was performed with an OMT instruments using VisuEl software (version 3.4.1; Optische Messtechnik GmbH). This instrument was used at an angle of incidence of 70° and a spectral method in the wavelength range from 460 to

870 nm. The azimuthal angle (rotating angle around an optical axis; ϕ) was maintained at 15° to measure ultrathin layers. For these measurements at least 5 areas of the sample surface were used to determine the average thickness.

2.2.3 Contact Angle (CA) Measurement

The CA is a very common method to quantify the wettability of a surface and often used to measure the hydrophobicity of a flat surface. Young[115] has first recognized the relationship between surface tension and contact angle. When a liquid droplet is located on an ideally flat and homogeneous surface at the triple-point of the three-phase lines, an equilibrium contact angle θ is formed between the liquid and the solid surface. The Eq. (2.2) is known as Young's equation, where γ_{SV}, γ_{SL} and γ_{LV} refer to the interfacial surface tensions with S, L, and V as solid, liquid, and gas respectively as shown in Figure 2.5.

$$\cos\theta = \frac{\gamma_{SV} - \gamma_{SL}}{\gamma_{LV}} \tag{2.2}$$

The determination of the contact angle by adjusting the Young-Laplace equation and the analysis of drop shape considering physically correct deformation of the droplet under the influence of gravity can enhance the accuracy of contact angle value. This method can be applied only in the configuration used in a symmetrical cross section of droplet. The pressure difference across the curved interface (radii of curvature R_1 and R_2) describes the Young-Laplace equation. The index LV for liquid vapor at the surface tension will be omitted in the following, i.e. $\gamma_{LV} \rightarrow \gamma$:

$$\Delta p = \gamma \cdot (\frac{1}{R_1} + \frac{1}{R_2}). \tag{2.3}$$

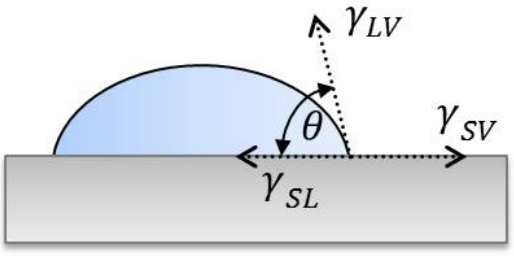

Figure 2.5: Schematic of the contact angle between a drop of water and solid surface.

A hydrophilic surface is arbitrarily defined as a surface with a contact angle of $< 90°$ between the surface and a drop of fluid resting on it, whereas a hydrophilic surface is

defined by CA > 90°.[116, 117, 118] Despite of wide acceptance of Young's Law, it has never been verified experimentally because of the difficult measurement of the surface tension of solids. Therefore, Youngs' Law has been modified in cases of various types of surfaces.[119, 120]

In practice, two types of CA values, static and dynamic CAs, are used. For the static CA measurements the interaction of the droplet with the substrate is dependent on recent history. Experimentally, static CAs are obtained by sessile drop measurements, where a drop is deposited on the surface and the CA values are measured by a goniometer. In case of the dynamic CAs, the droplet is in motion and the CA values are determined during the growth (advancing CA, θ_a) and shrinkage (receding CA, θ_r) of a water droplet. The difference between the maximum (θ_a) and the minimum (θ_r) CA values are defined as CA hysteresis ($\Delta\theta$). There are two major reasons for CA hysteresis: (i) surface roughness or (ii) surface and liquid inhomogeneities. As an example, a surface with CA higher than 150° is known as superhydrophobic and has very little CA hysteresis.[121, 122]

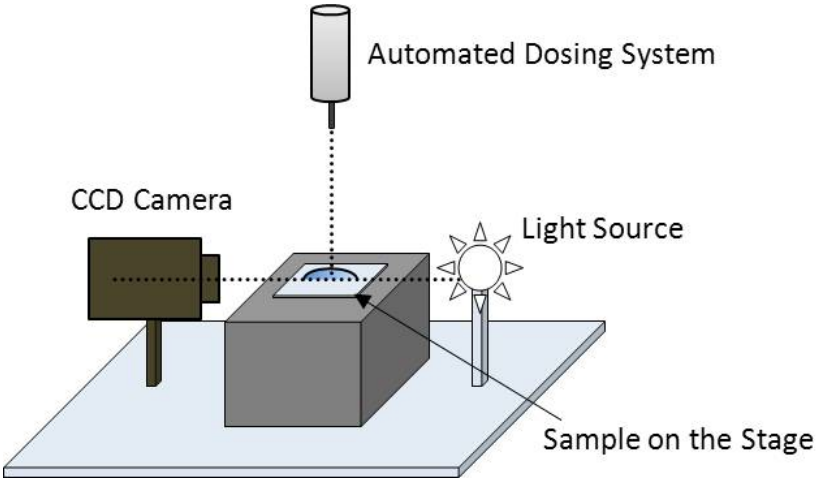

Figure 2.6: Experimental setup to measure the contact angle.

Herein we focused on the static CA and the measurements were performed in sessile drop configuration as shown in Figure 2.6. Milli-Q water was used as dispense medium on a DSA 100 tensiometer from KRÜSS. For the dosing system a blunt end cannula with a diameter 0.517 mm was used. The sample was put on a stage which could be moved in x-, y- and z-direction. A 1 µL water drop was generated by the dosing system and placed on the sample surface. Then, the CCD camera captured the profile of the backlit droplet and the image was anaylzed by "Drop Shape Analysis" software. The software identifies drop contour and baseline with the substrate. The area of the three-phase contact point was evaluated and fitted using Young-Laplace fits. The arithmetic mean and the standard deviation were calculated from each of at least 5 individual measurements at different points of a surface. All measurements were carried out at room temperature.

2.2.4 Enzyme-linked Lectin Assay (ELLA)

Lectins can be utilized for the glycoanalysis implemented in a number of different formats, for example microarray techniques.[123, 124, 125, 126, 127] An enzyme-linked lectin assay (ELLA) is the most simplistic format of lectin used for the glycoanalysis. This assay is performed on microtiter plate and based on the same principles in a manner analogous to the standard enzyme-linked immunosorbent assay (ELISA). ELLA has been developed to detect specific carbohydrate units on the cell surface. It allows the analysis of glycoproteins and lectin-carbohydrate interactions. The common procedure of ELLA begins with the immobilization of glycoconjugates on the ELISA plate, subsequent blocking of the plate surface, and then measuring with biotinylated lectins.[128] The critical step of this assay is the blocking of ELISA plate due to the lack of suitable blocking reagents for ELLA. That is why only small subsets of specific lectins have been investigated by the ELLA technique.[129, 130]

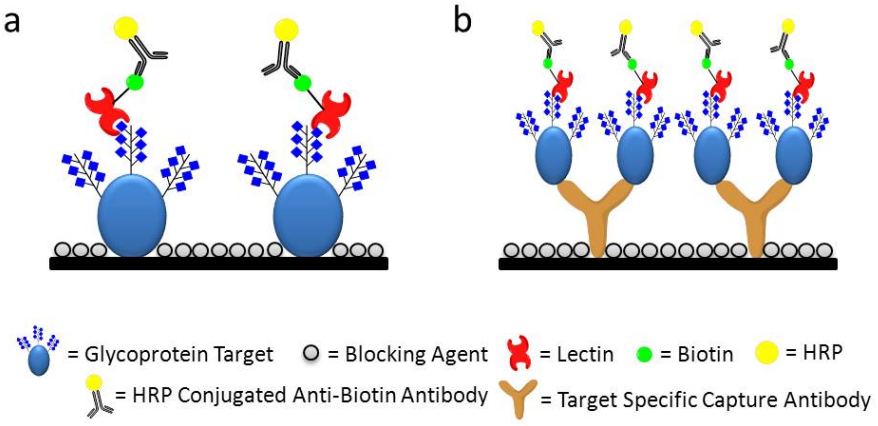

Figure 2.7: Schematic of the enzyme-linked lectin assays using horseradish peroxidase (HRP).

In Figure 2.7, the schematic of the ELLA method is illustrated. In case of Figure 2.7a, target glycoproteins are immobilized by nonspecific absorption on the surface of an ELISA plate. Subsequently, the plate surfaces are blocked with blocking agents and then the biotinylated lectins bind to the target glycoproteins. Bound lectins are detected by the binding with streptavidin or anti-biotin antibody. As an alternative, a specific antibody can be immobilized on the ELISA plate surfaces and then the surfaces are blocked (see Figure 2.7b). The target glycoproteins can bind specifically to the immobilized antibody. Further recognition steps are the same as in Figure 2.7a. This form of assay enables the selective capture of a target molecule from the sample mixture, but the glycans of the capture antibody have to be removed before the immobilization to prevent use as an assay component.[131, 132] In this work, fluorescent labelled lectins have been applied in combination with ELLA due to easy visualization and characterization.

2.2.5 Electrochemical Impedance Spectroscopy (EIS)

The concept of EIS has been introduced by Oliver Heaviside in 1872. This technique uses alternating current impedance measurements and these measurements are succeeded by a wide range of frequencies. EIS allows to prove the features of surface-modified electrodes. A small amplitude is applied to the electrochemical cell, and the current response is measured. The different regions of the material are characterized according to their relaxation times or time constants. EIS is usually easy to handle and able to apply to a wide range of materials. Therefore, EIS has become a major tool to investigate the characterization of electroceramics, the study of solar-cells, as well as the production of polymer coated microarry electrodes.[78, 133, 134] Recently, it has been applied even to generate novel sensor systems such as impedimetric immunosensors, DNA-sensors, and enzyme biosensors.[135, 136, 137, 79, 138]

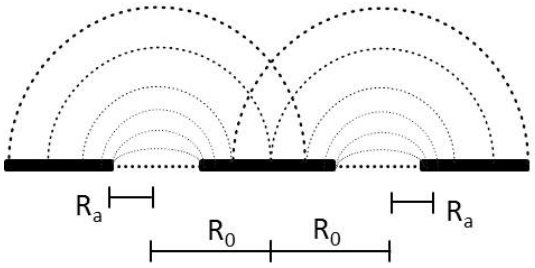

Figure 2.8: Schematic of the diffusion profiles of microarray electrodes.

Figure 2.8 shows the diffusion profiles of microarray electrodes. R_a is the radius of the microelectode and R_0 is the radius of the inactive area surrounding the microelectrode. The dashed line marks the diffusion layers. These diffusion layers are separated at short times or high frequencies, whereas they are overlapped at long time or low frequencies.

In this work, we introduced a new platform of multivalent glycopolymer brushes for lectin diagnostics using EIS technique. The used device is composed with three parts: microfluidic device, contact part and impedance analyzer. If lectins bind to the glycopolymer surface, the change of impedimetric signal was measured by the analyzer. Figure 2.9 illustrates the configuration of the impedimetric glyco-biosensor (IGB).

Deposition of the ATRP Initiators on EIS Chips

Gold interdigital electrodes (gap 10 µm, width 10 µm, length 3885 µm, count 100) on silicon wafer were used for all EIS experiments. One EIS chip contained six electrodes (see Figure 2.10) and 25 µm thick SU8 photoresistor was photolithographically structured between the electrodes and the silicon wafer. The SU8 layers were used later to build microfluidic channels. For the modification of the electrode surfaces, the EIS chips were

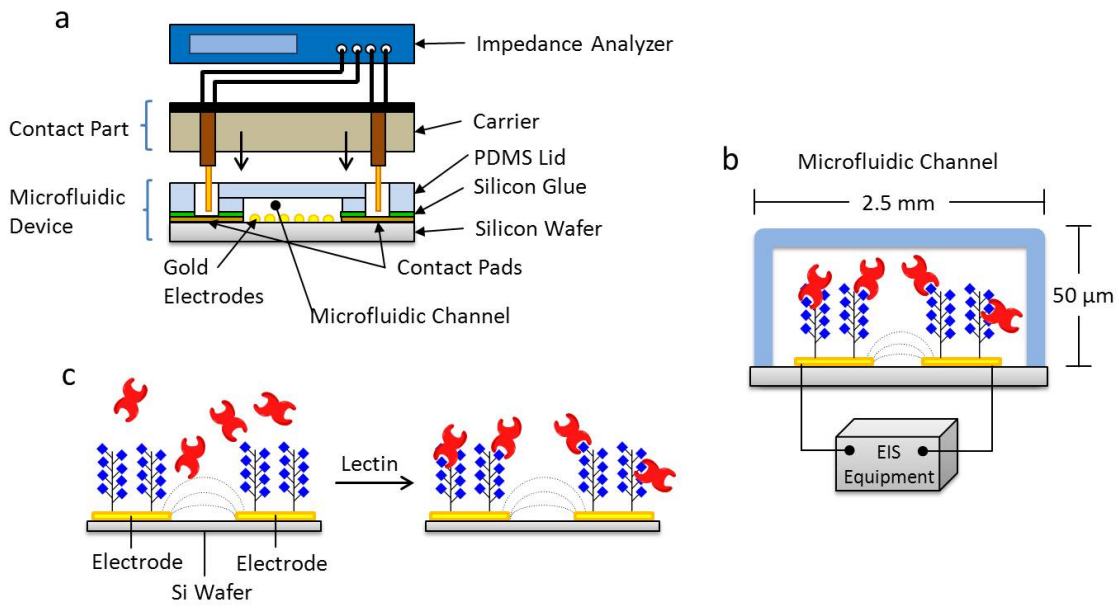

Figure 2.9: Schematics of glycochips for the lectin binding using on-chip electrochemical impedance spectroscopy (EIS). (a) The whole EIS measurement system containing the silica chip with the micropatterned electrodes. (b) Microfluidic channel including the sample and the interdigitated electrodes. (c) Concept of binding: multivalent presentation of glycan structures of glycopolymer brushes on gold electrodes and lectin binding. The dashed line represents the inner edge of the microfluidic chamber.

cleaned sequentially in aceton, 1-propanol, ethanol, and water. The surface was oxidized for 5 min in air plasma (0.2 mbar, 18 W, PDC-32 G, Harrick). Then, the self-assembled monolayers of ATRP initiators were prepared according to the literature from Hendrick and coworkers.[139] The freshly cleaned chips were immersed in 6.12 µL of a 2 mM solution of the ATRP initiator Bis[2-(2'-bromoisobutyryloxy)ehtyl]disulfide using ethanol as solvent at room temperature. After the reaction time, the chips were rinsed with ethanol and then dried with a stream of nitrogen.

Synthesis of Glycopolymer Brushes on EIS Chips by ATRP

The scheme of the initiator deposition on a silicon wafer and the subsequent polymerization is shown in Scheme 2.4. A representative procedure is the following: a initiator modified EIS chip was placed in a reaction flask under a stream of nitrogen. A 50 mL reaction flask was equipped with 2.10 g (6.30 mmol) GlcNAcEMA which was dissolved in 20 mL methanol/water = 1/1 (v/v). The solution was degassed through nitrogen bubbling for 20 min. Then, 49.90 mg (0.50 mmol) CuCl, 28.14 mg (0.13 mmol) $CuBr_2$ and 196.79 mg (1.26 mmol) bpy were added and stirred under a nitrogen stream until a homogeneous dark brown solution formed. The reactor was degassed through nitrogen bubbling for 20

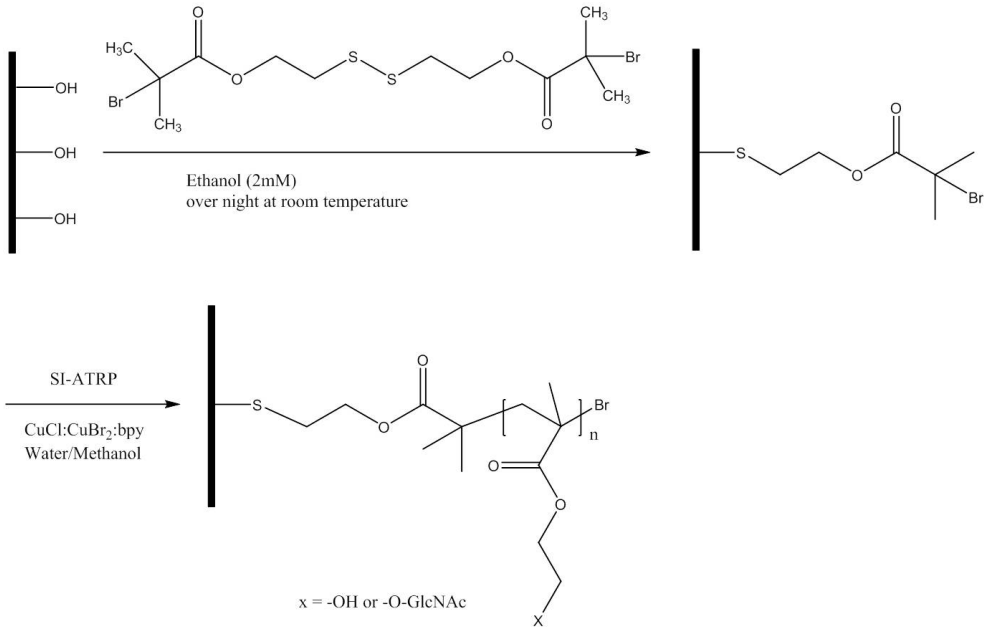

Scheme 2.4: Surface modification of gold-electrodes with glycopolymer brushes

min at room temperature and then transferred into the flask containing EIS chips. The polymerization proceeded at room temperature for a defined reaction time. Then, the chips were thoroughly rinsed with water, methanol and ethanol and dried in a nitrogen stream.

Impedance Measurements

To build the walls of a microfluidic channel of 2.5 mm width, a polydimethylsiloxane (PDMS) lid with inlet and outlet was bound to the SU8 photoresistor under the polymer grafted gold electrodes. Three electrode pairs were placed within one microfluidic channel (see Figure 2.10).

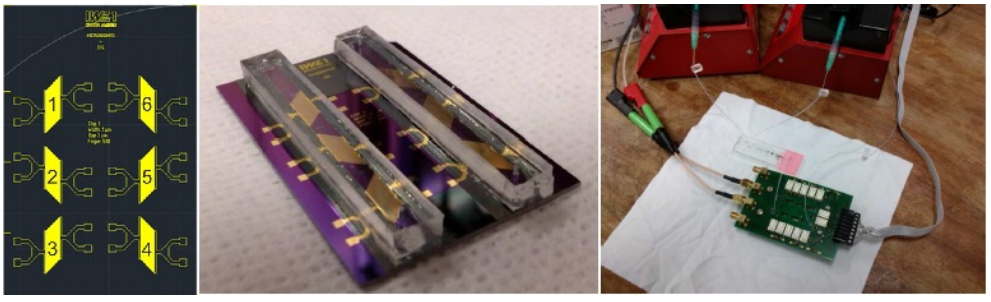

Figure 2.10: Schematic illustration and measurement setup for microfluidic IGB devices. Left: Illustration of a chip with six Au electrodes. Pictures of a EIS chip with PDMS lid and the used microfluidic device (Right).

Contact pads of the interdigital electrodes on the chip were applied to electrical contact

by the spring-loaded contacts which were soldered on a printed circuit board (PCB) with multiplexer unit and realized by relays circuit (OMRONG G&K-2P, OMRON Japan). The PCB was fixed in a polymethyl methacrylate carrier. Then, the contact part and the microfluidic device were clamped together for the good temporary contacts. Syringe pumps (LA-100, Landgraaf Laborsysteme HLL GmbH, Germany) and a PDMS based microfluidic distributor were utilized for the supplying of the liquid probes into the inlet of the microfluidic channel. The insertion of liquids were succeeded through flexible teflon tubes and microfluidic experiments were usually performed using a flow rate of 8.33 $\mu L \cdot min^{-1}$. Solartron 1260A impedance analyzer (Solartron Technologies GmbH & Co. KG) in combination with a front end EG&G potentiostat (EG&G, USA) was used for impedance measurements. To minimize the effect of cable impedances itself, the analyzer was connected to the PCB by four Bayonet Neill-Concelman (BNC) cables in a kelvin measurement mode. The data was read out to a PC by Z-Plot (Scribner Software) and further processed by in-house written Python control program for continuous signal monitoring. To select desired electrode pairs and to manage the syringe pumps, Labview Software NI-6021 USB card (National Instruments) and a simple current amplifying circuit were utilized. For the data analysis, spectra between 10 Hz and 200 kHz and signal amplitudes of 10 mV were evaluated. Prior to loading the lectin solution, the microfluidic channel was flushed with ethanol and PBS buffer solution. All electrochemical measurements of glycochips were performed in the Institute für Werkstoffe der Elektrotechnik at RWTH Aachen University.

Surface Plasmon Resonance

Surface plasmon resonance or SPR is well known and a popular sensing method for the observation of biochemical reactions. SPR has some advantages such as the high resolution and the detection efficiency of unlabelled analytes. SPR is a collective oscillation of conduction electrons taking place at the interface between a negative and positive permittivity media (metal-dielectric). In general (see Figure 2.11), excitation of surface plasmon is based on total internal reflection when an incident light strikes an electrically conducting gold layer at the interface. At a given angle, the excitation of surface plasmons results from a reduced intensity of the reflected light. A slight change at the interface, e.g. binding of molecules to surface-immobilized receptors, alters the refractive index (RI) of the medium near the surface layer of a sensor chip. In this way, precise measurements of thin film properties and molecular interactions can be measured in real-time.[140] Besides the aforementioned capability of real-time quantitative analysis and label-free detection, there are several advantages of using SPR technology. For example, SPR has a high sensitivity of up to 1 nM for a 20 kDa protein, automated performation possibility, thus increasing sample throughput. However, there are also several disadvantages of SPR such as hard discrimination between specific and non-specific interactions with the sensor surface,

thus needs of reference material or control samples. Furthermore, the detection sensitivity of low molecular weight compounds is low because it is based on mass sensitive technique.[141, 142] Therefore, new applications such as localized SPR have been demonstrated to diminish these drawbacks.[143, 144]

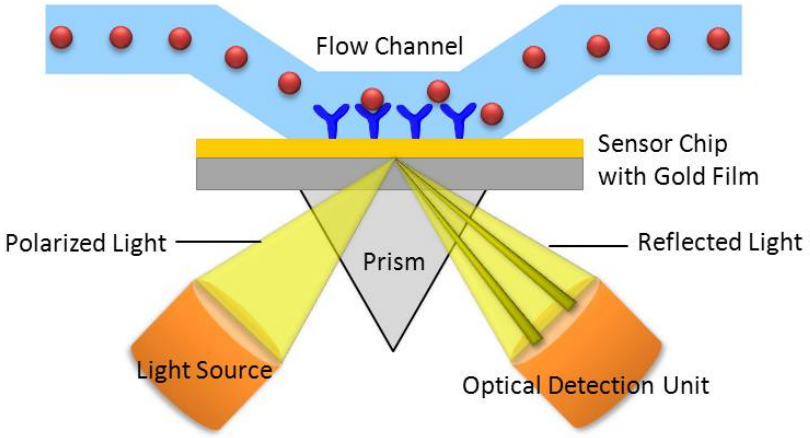

Figure 2.11: Typical setup for an SPR biosensor (adapted from [140]).

In this work, we manufactured an advanced plasmonic flow-through biosensor using glycopolymers. This novel glyco-biosensor is based on the sensor chip developed by Buchenauer et al.[145] A polycarbonate membrane was used and its surface modified with glycopolymer brushes.

Surface Acoustic Wave

In recent years, surface acoustic wave (SAW) began to receive more attention for microfluidic use. Although SAWs have been already introduced by Lord Ryleigh in 1884 [146], SAWs have been particularly developed recently. To date, these technologies have been often used for the biological/chemical sensing and in telecommunication industry for applications such as touch-sensitive screens. SAW is an acoustic wave propagating along the surface of an elastic material. In general, SAW devices use acoustic waves based on one or more interdigital transducers (IDTs) on the surface of a piezoelectric crystal to generate acoustic waves and to detect electrical signals, and vice versa. The use of 10-1.000 MHz acoustic waves enables fluid manipulations at microscale and beyond. Such high-frequency acoustics are strongly confined at the surface of the device in the acoustic wavelength scale regardless of the thickness of the complete substrate. Therefore, any change on the surface such as mass loading, viscosity and conductivity can be detected with a high sensitivity.[147, 148, 149] In this work, a novel microfluidic SAW chip was fabricated for the online monitoring of the ATRP process. This new platform is beneficial for the fundamental understanding as well as the up-scaling of the polymerization.

3 Glycopolymer PGlcNAcEMA Brushes on Silicon Surface

3.1 Introduction

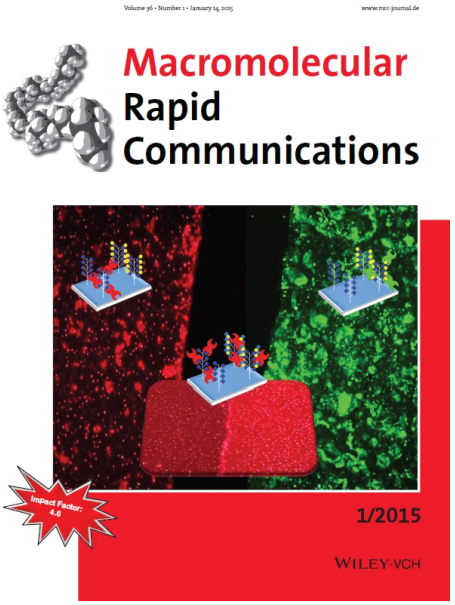

Carbohydrates on cell surfaces present important epitopes and play essential rolls in cell-cell and cell-matrix interaction, cancer invasion and metastasis as well as viral and bacterial cell infections. Therefore, the preparation of artificial surfaces which mimic external cell surfaces may provide an important route not only to understand carbohydrate-receptor interactions but also to develop biocompatible surfaces.[67] The characterization of such surfaces may contain a vast number of biological information because of the diversity of glycan structures with their complex stereo- and regiochemistry. In general, the effective *in vivo* control of events mediated by protein-carbohydrate binding requires significantly greater affinity.[7] However, the coiled form of the glycopolymeric chains in solution often results in a low protein recognition activity. Hence, growing glycopolymer brushes from surfaces represents an attractive alternative as the grafted glycopolymer chains adopt a stretched conformation to avoid overlap.[67, 150, 151] The fabrication of multivalent glycopolymer layers, in particular, will foster the understanding of carbohydrate-protein (lectin) interactions[21]. It is crucial for selective and specific biomedical applications of lectin interactions with their glycan ligands, including novel biofunctionalized biomaterials for tissue engineering, diagnostics, and therapy.[66, 152]

The amino sugar *N*-acetylglucosamine (GlcNAc) is found as a major component of microbial cell walls and extracellular matrix of animal cells. It is well known for its structural roles at the cell surface. Recent studies have also introduced new roles for GlcNAc in cell signaling.[153, 154] GlcNAc is an essential building block for *N*-acetyllactosamine (LacNAc) disaccharide which is a common structure of glycoproteins and -lipids on the

cell surface. The linear oligosaccharide of repeating LacNAc units, Poly-LacNAc, binds specifically with galectins which play a significant roll in cell adhesion, immune response, and tumor progression as well as metastasis.[95] For the better accurate application, we prepared a novel platform of variable multivalent GlcNAc containing glycopolymers and investigated direct modification of GlaNAc to oligosaccharides on the surface.

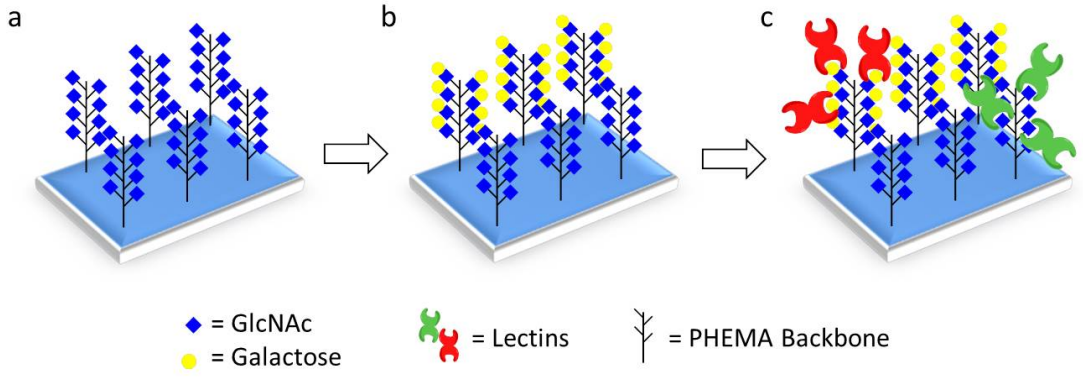

Figure 3.1: Schematic of the glycopolymer brushes on solid substrate. a) Glycopolymers with PHEMA backbone and pendant sugars are grown from a solid substrate. b) The GlcNAc monosaccharids are extended with galactose to LacNAc disaccharides. c) Lectins can bind specifically to the sugars of glycopolymers.

In this chapter, both the synthesis of a glycopolymer brushes and the modification of the sugar pendants of the glycopolymers are described. Surface characteristics of the grafted glyco-brushes are analyzed by using AFM, FESEM, CA and ellipsometry measurements. The biological activity of the grafted glycopolymers is investigated in detail. Figure 3.1 illustrates the schematic of the glycopolymer brushes on solid surface such as silicon substrate. Black tree-like backbones represent the PHEMA polymer chains, blue diamond shapes pendant GlcNAc monosaccharide, yellow circles galactose monosaccharide, and red and green X-shape figures two different lectins. It will be presented that the fabricated glycochips are highly specific and selective surfaces for lectin binding.

3.2 Results and Discussion

3.2.1 Fabrication of PGlcNAcEMA Glycopolymer Brushes

The sugar-based monomer 2-O-(N-acetyl-β-D-glucosamine)ethyl methacrylate (GlcNAcEMA **4**) was synthesized according to Scheme 2.1 in chapter 2.1.1. This unprotected monomer was employed for the polymerization from the surface of a silicon wafer by SI-ATRP. For the formation of densely packed monolayers of initiator on silicon wafers, the initiator was stirred in ethanol containing 8.4% (v/v) ammonia following a well-

established technique (Scheme 2.2).[155] The ATRP of the GlcNAcEMA **4** was carried out from the initiator-modified silicon surface at room temperature. The polymerizations were performed using CuCl/2,2' -bipyridine as the catalyst system in a methanol/water mixture.

Generally, in surface-initiated ATRP, the extremely low concentration of initiator grafted on the surface prevents the formation of a sufficient amount of the Cu^{II} complex to control the polymerization process.[156] To overcome this problem, it is necessary to add predetermined amounts of soluble free initiator or Cu^{II} complex into the reaction mixture at the beginning of the polymerization.[157, 158] In this work, the soluble free initiator, EBiB (1.7 mol % relative to monomer), and the Cu^{II} deactivator (24 mol % relative to Cu^{I}) were added at the beginning of the reaction. It is known that the amount of water in the solvent system plays an important role and polymerizations in less polar media show slower kinetics and longer propagation times.[159] Therefore, a 1/1 (v/v) water/methanol mixture was chosen as solvent system which yielded a good control over the polymerization of GlcNAcEMA 4 and 2-hydroxyethyl methacrylate.

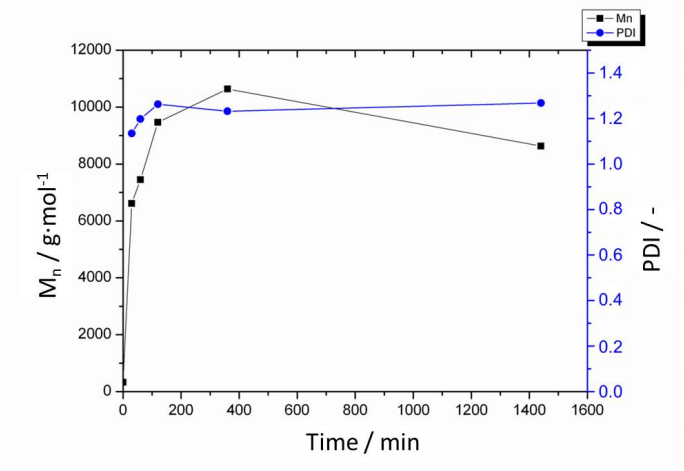

Figure 3.2: Dependence of molecular weight and polydispersity on polymerization time. ATRP of soluble free GlcNAcEMA **4** glycomonomer in 1/1 (v/v) water/methanol mixture. Polymerization condition: [m]/[CuCl]/[$CuBr_2$]/[bpy] = 50/4/1/10 mol, soluble free initiator: ethyl α-bromoisobutyrate was used.

The amounts of glycopolymers which can be cleaved from the surface were too small to analyze. Therefore, the molecular weights of the free polymer in solution have been used to estimate the length of the grafted polymer chains (Figure 3.2). During the polymerization, the mixtures were collected and purified as mentioned in chapter 2.1.3. The polydispersities of soluble polymers are below 1.3 for all polymerization times which implies a well-controlled polymerization reaction. However, a rapid termination reaction can be observed after one hour. This early termination might result from the disproportionation of the copper bromide.[67] The free glycopolymers were also analyzed by GPC. The refractive index responses for variable polymerization time are shown in Figure 3.3. The

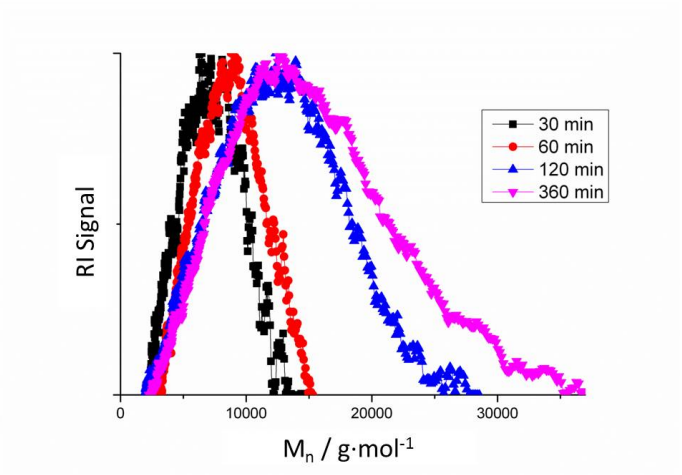

Figure 3.3: Refractive index responses for variable polymerization time for PGlcNAcEMA.

molecular weight of glycopolymers increased with the reaction time and the data corresponding to 360 min show a very broad distribution which is correlated with the highest polydispersity value.

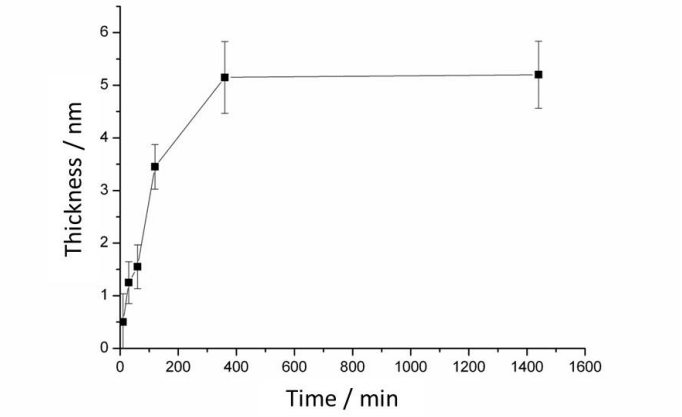

Figure 3.4: Evolution of the thickness of the PGlcNAcEMA **5** glycopolymer brush on a modifided silicon surface with polymerization time. Polymerization condition: [m]/[CuCl]/[$CuBr_2$]/[bpy] = 50/4/1/10, methanol/water = 1/1 (v/v). As soluble free initiator ethyl α-bromoisobutyrate was used. The thickness was determined using ellipsometry.

The polymer layer thickness on the silicon wafer is measured by ellipsometry. The value of an untreated silicon wafer is set as the basis for the further analysis. Figure 3.4 shows the increase of the PGlcNAcEMA **5** layer thickness as a function of polymerization time. The thickness increases linearly to 3.5 nm ± 0.4 nm during the first 2 h and then very slowly increases further up to 5.2 nm ± 0.6 nm after an extended reaction time of 24 h. The inhibition of the polymer growth with extending time can be explained with the termination events on the surface.

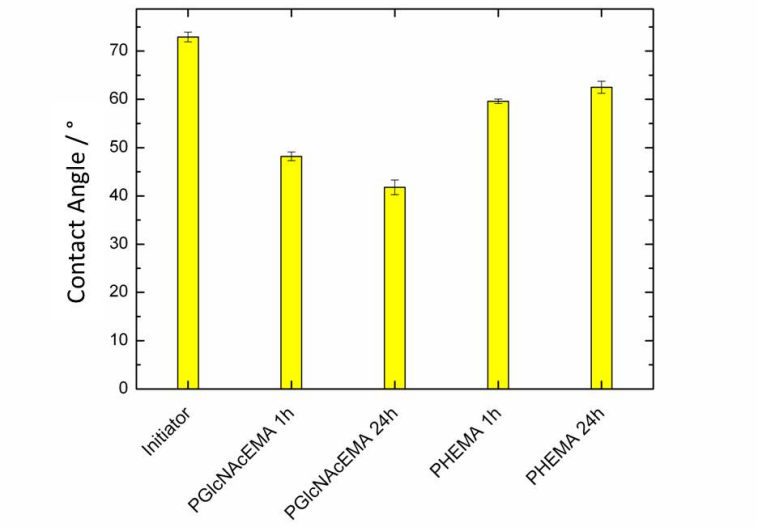

Figure 3.5: Results of the water contact angle measurements of initiator modified silicon wafer and PGlcNAcEMA **5** and PHEMA grafted wafers (after 1 h and 24 h reaction time).

After each step of the modification of the surface, the wafers were investigated by the water contact angle measurement. The initiator modified wafer showed value of 72.9° ± 1.0°. This highly hydrophobic surface shows after 24 h polymerization time less hydrophobic surfaces. The contact angle of PGlcNAcEMA and PHEMA grafted wafers was determined to be 41.8° ± 1.5° and 62.5° ± 1.3°, respectively (Figure 3.5). Due to the GlcNAc pendant groups, the surface of glycopolymer brushes is always more hydrophilic than the surface functionalized with pure PHEMA brushes.

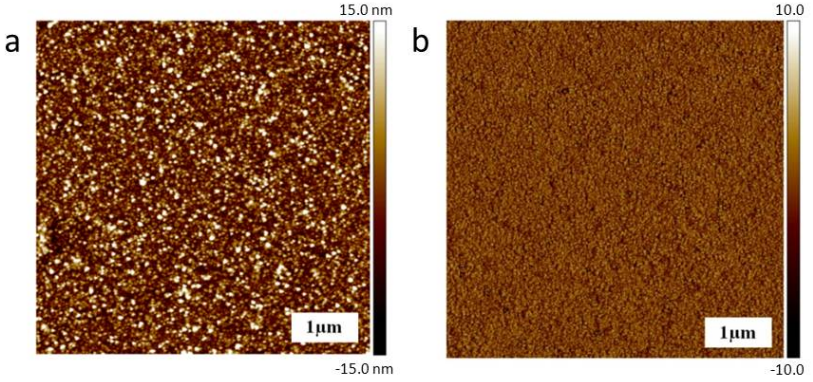

Figure 3.6: Tapping Mode AFM; (a) height and (b) phase image of PGlcNAcEMA **5** brushes prepared in methanol/water = 1/1 (v/v), 24 h polymerization time.

The polymeric surface was also characterized by Tapping Mode AFM. Figure 3.6a shows a typical AFM topography image of PGlcNAcEMA brushes. The glycopolymer brushes are homogeneous and completely cover the whole substrate surface. The phase image (Figure 3.6b) also illustrates a very uniform and completely covered silicon surface as the bare and hard silicon oxide should appear brighter compared to the softer polymer brush. The same

can be inferred from the field emission scanning electron microscopy images in Figure 3.7. With increasing time of polymerization much denser and packed polymer structures can be observed. Both AFM and FESEM data confirm a successful polymerization on the wafer.

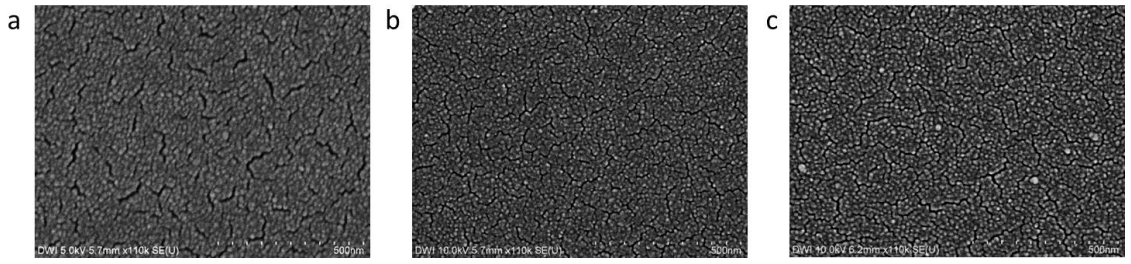

Figure 3.7: Micrographs of FESEM of PGlcNAcEMA brushes prepared in methanol/water = 1/1 (v/v) for (a) 10 min, (b) 2 h, and (c) 24 h polymerization time.

The protein recognition on PGlcNAcEMA glycopolymer brushes was investigated by binding of the two different lectins to the wafers.[160] They have different glycan binding specificities: for example, GlcNAc-specific lectin GS-II and LacNAc-specific lectin *erythrina cristagalli* (ECL). Fluorescence readout verified that GS-II lectin bound to GlcNAc-presenting brushes whereas only a very weak signal was detected on PHEMA shown as Figure 3.8.

3.2.2 Enzymatic Modification of PGlcNAcEMA Glycopolymer Brushes

To prepare a more complex multivalent platform based on surface grafted glycopolymer brushes, it was tried to establish whether PGlcNAcEMA is accessible on the surface for enzymatic galactosylation by β4GalT-1.[93] The reaction scheme is illustrated in Scheme 2.3. The resulting disaccharide (Galβ4GlcNAc, LacNAc, compound **5a** in Scheme 2.3) is an important starting-point for the more complicated synthesis of complex oligosaccharides.[96] Galβ1,4GlcNAc-motifs specific ECL was used to detect the galactose transter.[161] Figure 3.8 illustrates the fluorescence analysis of lectin binding to the surface of the glycopolymer brushes. Figure 3.8a shows that the binding of GS-II to the surface relies on specific recognition of GlcNAc. These binding events do not occur for PHEMA which does not possess carbohydrate pendants. In Figure 3.8b, a strong fluorescence signal of the *N*-acetyllactosamine (LacNAc) containing surfaces is visible, whereas only a weak signal appears fot the GlcNAc containing wafer. This strong increase in fluorescence signal indicates the enzymatic transfer of Gal and formation of LacNAc (Galβ4GlcNAc) on the glycopolymer brushes. This enzymatic modification of GlcNAc to LacNAc could also be proved by an oxidation method (Figure 3.8c). When the Gal transfer to GlcNAc is successfully performed, galactose of LacNAc can be specifically oxidized by galactose oxidase. Then, the subsequent reductive amination at its C6-position with a fluorescent dye can

give a signal on galactosylated brushes.[162] From the fact that the modified LacNAc wafer shows high fluorescent signal, it can be concluded that the enzymatic transfer of Gal and formation of LacNAc on the glycopolymer brushes have successfully taken place.

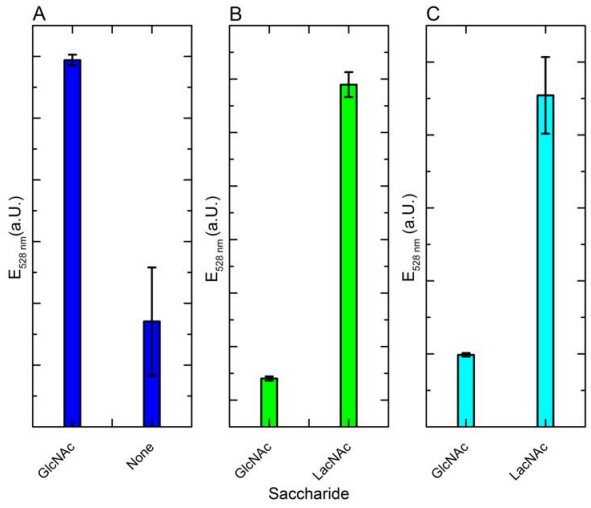

Figure 3.8: Fluorescence analysis of lectin binding to glycopolymer brushes. A: Binding of GlcNAc-specific GS-II to glycosylated (PGlcNAcEMA **5**) and non-glycosylated brushes (PHEMA). B: Binding of Gal-specific ECL to galactosylated (**5a**) and non-galactosylated (**5**) brushes. C: Fluorescent signaling of galactosylated (**5a**) and non-galactosylated (**5**) brushes (adopted from [163]).

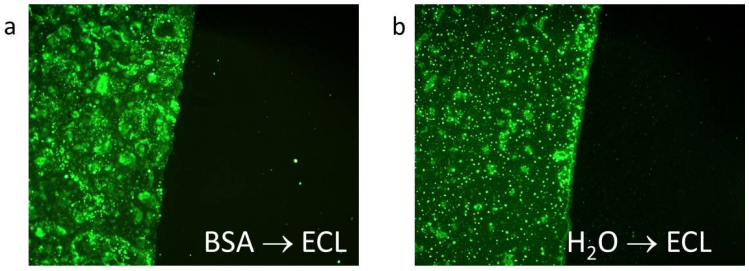

Figure 3.9: Investigation of the specific Lectin binding using BSA and FITC labelled ECL. One half of the PGlcNAcEMA brush was galactosylated and the binding of ECL to these surfaces was investigated. The figures present glycochips with and without BSA blocking.

For fluorescence microscopy measurements, we transferred galactose only onto one half of the PGlcNAcEMA brush-covered wafers, thereby creating an intrinsic negative control. Thus, only the half side of glycochips was enzymatically modified. We investigated the binding of ECL to these surfaces. Figure 3.9 present both glycochips with and without BSA blocking. Figure 3.9a represents the galactosylated side of glycochips and hence the glycopolymers contain LacNAc pendants. Figure 3.9b presents the PGlcNAcEMA brushes containing GlcNAc pendants. Interestingly, unspecific adhesion of the lectins was not detected. This indicates that blocking of the surfaces by inert proteins prior to lectin incubation seems to be eluded.

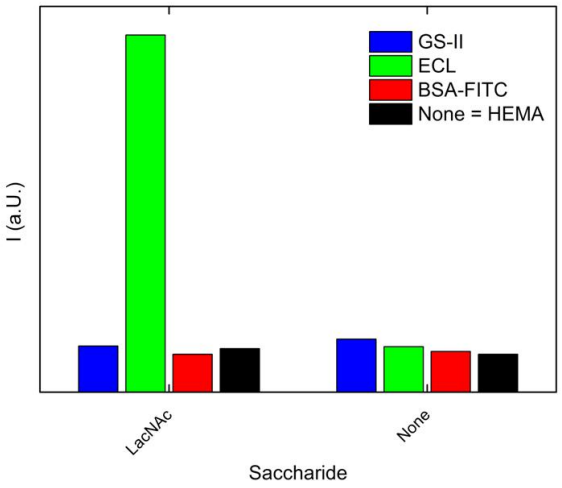

Figure 3.10: Binding of GS-II, ECL and BS-FITC to brushes consisting of PLacNAcEMA **5a** or PHEMA. Note, that there is almost no unspecific adhesion of the proteins to the polymer.

To prove that the unspecific adhesion of proteins to this material is minimal, the wafers were also incubated with FITC-BSA. After washing and drying of the wafers we measured the fluorescence signal but could not detect any difference in emission behavior. It proves conclusively that BSA does not bind to the wafers as shown in Figure 3.10. From these results, it is confirmed again that the glycopolymer brushes can capture the lectins very specifically even without using blocking agents. These findings facilitate the handling of the surfaces dramatically, because the simplified probing procedures can be further reduced using introduced glycochips.

Competition as well as displacement studies were performed with ECL on **5a**-presenting brushes with lactose as inhibitor and revealed an IC_{50} value of 0.3 mM.[163] In the literature, an IC_{50} value for lactose of 0.5 mM has been reported in case of using human serum α1-acid glycoprotein.[96] The similarity of these values shows that the glycopolymer surface can present almost the same surface as the human serum α1-acid glycoprotein. Therefore, it can be concluded that the prepared glycopolymer surface is able to bind strongly to lectins due to its multivalent presentation.

The specific binding of GS-II and ECL to half-galactosylated wafers is shown in Figure 3.11. The fluorescence images of lectin binding revealed a remarkable selectivity of both lectins to their specific sugar ligand on the wafer (Figure 3.11a and b). Consequently, GSII and ECL only bind respectively to the non-galactosylated half and galactosylated half of the wafers revealing absolute differentiation of the glycopolymers by the specificity of the lectins. Subsequent enzymatic transfer of GlcNAc onto **5a** on the galactosylated side of the wafer results in PGlcNAcLAcNAcEMA (compound **5b** in Scheme 2.3) which

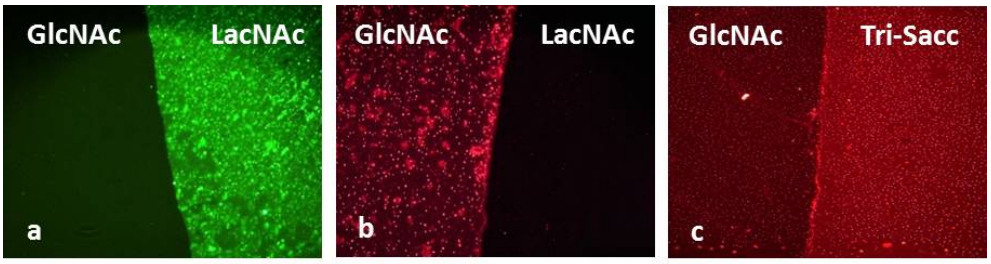

Figure 3.11: Binding of ECL (a, green) and GS-II (b, red) to brushes where the right wafer side is galactosylated. ECL binds only to the Gal presenting side (LacNAc) and GS-II binds only to the GlcNAc presenting side. The binding of GS-II to the whole wafer can be reconstituted by enzymatic transfer of GlcNAc forming a tri-saccharide on the right wafer side (c).

is then detected by GS-II (Figure 3.11c) because now terminal GlcNAc is exposed on the tri-saccharide. In agreement with our fluorescence spectroscopy analysis (see below) the fluorescence signal of GS-II was approximately double as high with **5b** compared to **5** indicating the preference for longer glycans by this lectin.

Oligo-LacNAc structures on PGlcNAcEMA brushes were also synthesized by an enzymatic cascade reaction (Scheme 2.3).[95] The alternating use of β4GalT-1 and β3GlcNAcT generates glycan oligomers up to a hexasaccharide presenting three LacNAc units. In this way glycan oligomers of variable length with GlcNAc or Gal at their non-reducing ends were ready for testing with lectins. The ongoing glycosylation processes were investigated with the lectins GS-II and ECL. Both lectins have shown a distinct different binding behavior on growing glycan chains (data shown in [163]). The fluorescence signals of the both lectins were measured on the wafers presenting different saccharides. GS-II has shown good binding to brushes presenting a terminal GlcNAc moiety indicated by stronger signals with the mono- (**5**), tri (**5b**)- and penta (**5d**)-saccharide compared to di (**5a**)-, tetra (**5c**)-, and hexa (**5e**)-saccharide presenting brushes. With the lectin GS-II, the multivalent presentation of GlcNAcβ1,3Gal-units on glycopolymer brushes have represented to a two-fold higher fluorescence intensity compared to internally presented GlcNAc moieties of LacNAc terminated brushes. ECL shows a clear preference for Gal-terminated glycopolymer brushes. PGlcNAcEMA brushes have shown almost no signal, whereas LacNAc carrying brushes (**5a**, **5c**, **5e**) presented a burst in signal intensity with each additional LacNAc unit. In contrast to GS-II, the fluorescence intensity rose with each LacNAc unit about 1.5 times. This could be explained by a higher amount of ECL proteins interacting with the growing glycan chain on the brushes. The same as GS-II, ECL could also recognize internal LacNAc units which might become better accessible due to the higher flexibility of the multivalent glycopolymer scaffolds on longer glycan chains. In conclusion, some detailed informations such as the kind of terminated saccharide, Gal or GlcNAc, and differences in the number of LacNAc units on multivalent glycopolymer brushes can be distinguished by both lectins. Thus, the enzymatic cascade reaction provided a unique platform for in-

vestigating the binding of lectins to a defined multivalent environment presenting complex glycan-oligomers.

3.3 Conclusion

We prepared multi-variant glycopolymer brushes containing LacNAc-oligomers on a silicon substrate by SI-ATRP, and enzymatic polymerization methods. The structural features of glycopolymers were studied by ellipsometry, atomic force microscopy and scanning electron microscopy. The presented platform is quite unique in terms of process stability and versatility. The well-controlled surface-initiated polymerization of the glycomonomers results in homogeneously covered surfaces with remarkable re-usability of the functionalized wafers. Most of the experiments were carried out on one set of wafers validating the reusability and robustness of the presented material. Additionally, our platform shows very good ligand accessibility for lectins and higher binding signals achieved with longer glycans. Enzymatic modifications of the sugar units are possible directly on the surface and enable building up linear oligo-LacNAc structures in a highly multivalent manner. The specific binding of lectins revealed the preference for longer glycan chains. Surfaces with multivalently presented glycan structures in a homogeneous layer of glycopolymer brushes proved to be suitable for highly selective and specific lectin capture and analysis. These developments of bioactive glycopolymers have a significant potential in a number of novel practical applications such as adhesive materials, cell culture materials, templates for bioanalysis, and tumor diagnosis.

4 Gradient Glycopolymer PGlcNAcEMA Brushes on Silicon Surfaces

4.1 Introduction

Surface gradients have recently become a hot issue, especially in material sciences and biophysical researches. A gradient means that chemical or physical properties of components attached on substrates themselves gradually vary along one or more given directions. Gradients play an important role *in vivo*, they drive a range of biological processes from matter transport across biological membranes to the motion of proteins. Engineering gradients on surfaces could thus provide not only in vivo models for better understanding of biological processes, but also tools to mimic the biological functions. Usually, the surface gradient of polymer brushes is divided into a physical and a chemical gradient. In most cases, the chemical gradient of polymer brushes concentrates on the gradual variations of grafting densities and/or molecular weights of polymer chains along one or more directions. They are generally prepared by employing various gradient fields on the initiator densities or polymerization processes for polymer brushes. Those gradient fields include a temperature gradient, a concentration gradient derived from the diffusion in gas or in solution, and a gradient of the exposure time under UV light, ozone, or monomer solution.[164] For instance, Genzer and co-workers have fabricated orthogonal polymer brush gradients with varied grafting densities and molecular weights in orthogonal directions.[165, 166] They have shown the tailored adhesion of cells on such gradient substrates. These gradients are sufficient for those applications which do not need a precise boundary of polymer brush gradients. However, new approaches such as various lithographical techniques may elaborate confined gradients or predefined complex gradients on the nanometer scale.

Generally, the "grafting from" strategy is used to prepare polymer brushes. For the fabrication of gradient polymer brushes, two strategies can be used to combine self-assembled monolayers (SAMs), surface-initiated polymerization (SIP), and lithographies: (i) performing SIP after the lithography process of SAMs and (ii) processing pre-prepared polymer brushes by lithographies. The lithographies based on electron beams, X-rays, lasers, and probes have been developed to design confined polymer brush gradients. Confined gradient polymer brushes may present a powerful platform to investigate adhesion, migra-

tion, culture, and differentiation of cells as well as the adsorption of proteins. Bhat and co-workers demonstrated that gradient polymer brushes are a useful tool for fundamental research into surface texture and nature on the control of protein adsorption and cell behavior (*i.e.*, adhesion and differentiation).[166] This can be useful for practical applications such as implantable materials and tissue engineering.[164]

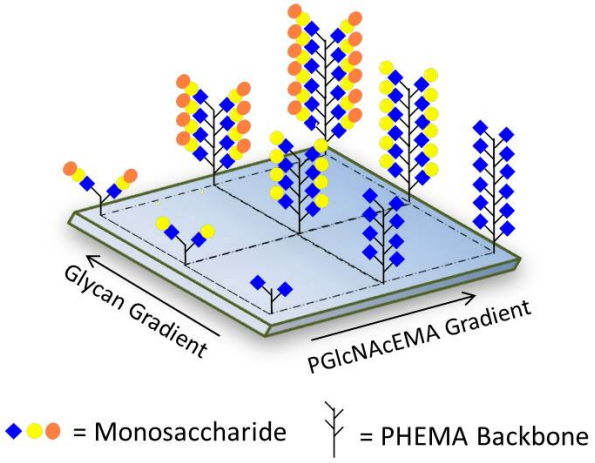

Figure 4.1: Schematic of the glycopolymer brushes on solid substrate with a molecular- and an orthogonal glycan-gradient.

In this chapter, the formation of a gradient of molecular weight of glycopolymer brushes and the modification of the sugar pendants of the glycopolymers are described. Surface characteristics of the grafted glyco-brushes were analyzed by AFM and ellipsometry measurements. The biological activity of the grafted glycopolymers were determined by FLLA. Figure 4.1 illustrates the schematic of the gradient of glycopolymer brushes on solid surfaces such as silicon substrates. As described in Chapter 3, Black tree-like backbones represent the PHEMA polymer chains, blue diamond shapes pendant GlcNAc monosaccharide, yellow circles galactose monosaccharide, and red and green X-shape figures two different lectins. As illustrated here, the fabricated glycochips form highly specific and selective surfaces for lectin binding. Figure 4.2 illustrates the scheme of the experimental steps proceeded in this work for the formation of gradients.

4.2 Results and Discussion

For the formation of glycopolymer molecular weight gradients, the SI-ATRP technique was chosen for the polymerization of glycomonomer GlcNAcEMA. Hereby, a dip-coating process was used to manufacture the molecular weight gradient of PGlcNAcEMA. To make surface gradients, two different approaches have been developed in this work: (1) glycopolymer gradient grafted from iniator monolayer or (2) glycopolymer polymerization from initiator gradient. The former approach was almost similar as the preparation of

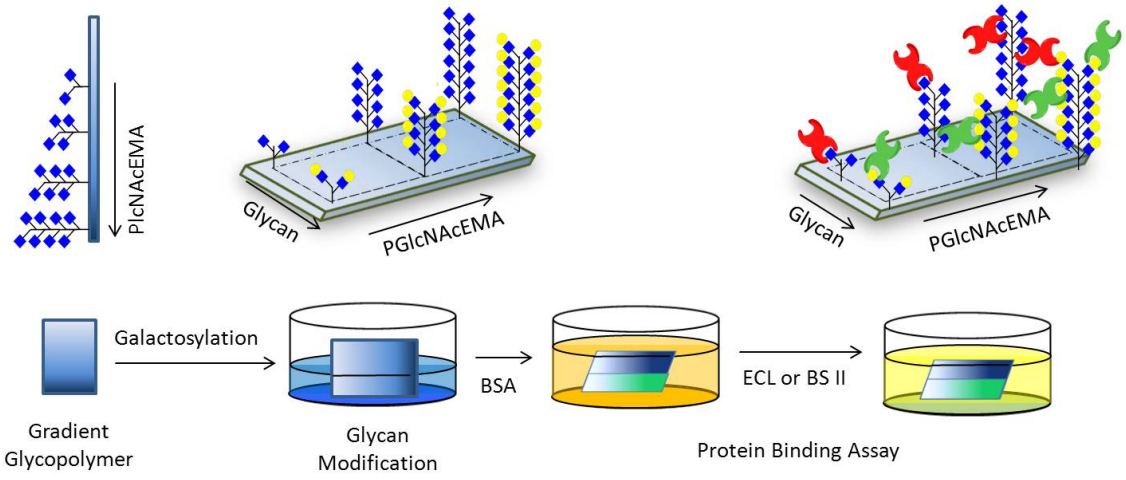

Figure 4.2: Schematic illustration of the experimental steps to the formation of gradients.

glycopolymer brushes in Chapter 3. However, the silicon wafer with initiator monolayer was dip-coated during the polymerization for the gradient formation. For the latter approach, gradients of polymerization initiator were prepared by combining with SI-ATRP. Both methods, well-defined gradient PGlcNAc surfaces were prepared to study about carbohydrate-lectin binding. In this work, a custom-made dip-coater has been used to manufacture gradients as shown in Figure 4.3.

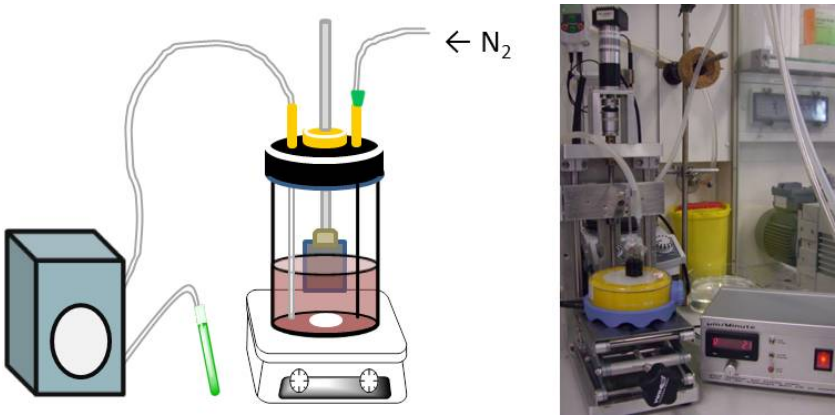

Figure 4.3: Experimental setup of dip-coater.

4.2.1 PGlcNAcEMA Glycopolymer Molecular Weight/Glycan Length Orthogonal Gradient

A silicon wafer was cut into 1 × 1 cm^2 rectangles and rinsed with toluene. Then, the wafer was cleaned in a stream of CO_2 crystals ("snow jet") and treated in plasma oven (0.2 mbar, 18W, PDC-32 G, Harrick) at 0.2 mbar for 2 min. The self-assembled initiator monolayers were prepared by stirring in ethanol as described in Chapter 2.1.2. The initiator modified substrate was hold on the dip-coater and the custom-designed polymerization reactor was

flushed with nitrogen. In a separate flask, the polymerization mixture was prepared as described in Chapter 2.1.3. After transfer of the solution into the reactor, the initiator covered substrate was completely lowered vertically into the reaction mixture and the ATRP of GlcNAcEMA proceeds at room temperature. The polymerization took place only on those parts of the substrate, which were in contact with the reaction mixture. Hence, the length of polymer chains at a given point on the substrate grew proportional to the contact time with the reaction mixture. The dip-coater withdrew gradually the wafer from the reaction vessel of the polymerization medium. Therefore, the area of the contact area with the polymerization medium was slowly decreased with increasing reaction time. As a result, a gradient in molecular weight of GlcNAcEMA was formed along the length of the substrate. The brush molecular weight gradient could be varied and tuned by adjusting the withdrawal speed and/or the ratio of reaction components. After polymerization, the substrate was thoroughly rinsed with water, methanol and dried in a nitrogen stream. The PGlcNAcEMA dry thickness was determined by an ellipsometry measurement. At the beginning of gradient formation, the brush thickness was near to zero which represents almost the same thickness of the initiator layer. With increasing contact time with polymerization medium, the polymer brush presents enlarged thickness (data not shown). In case of a gradient brush, the exact determination of thickness at a given point on the wafer was difficult because the evaluating area on the surface is not evenly formed. Therefore, the dry thickness of brushes were measured only for the control of the polymerization reaction. However, the general development of the thickness was proportional to the polymerization time.

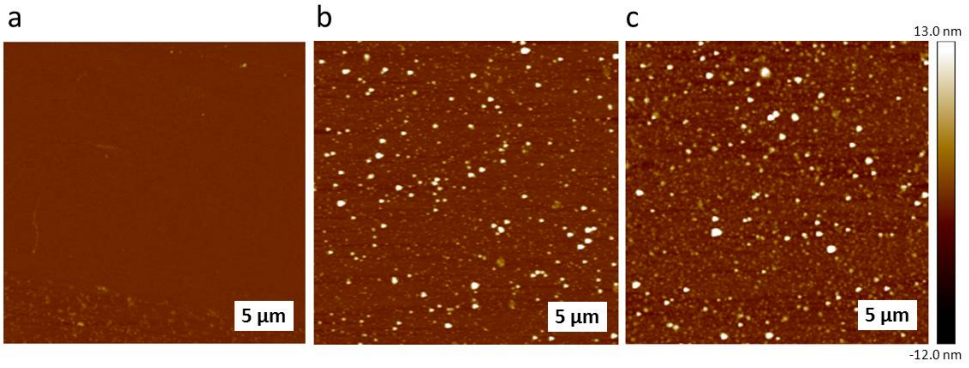

Figure 4.4: Height image of glycopolymer brush gradient using Tapping Mode AFM; (A) Top, (B) middle, and (C) bottom of the glycopolymer molecular gradient on the silicon substrate; PGlcNAcEMA prepared in methanol/water = 1/1 (v/v), 53 µm·min^{-1}.

The resulting grafted-from polymer gradients were studied by AFM. Figure 4.4 shows the height images at the three different positions on the PGlcNAcEMA wafer. The polymerization was performed while pulling out the substrate with a speed of 53 μm·min^{-1}. The top of the silicon wafer was incubated in the ATRP reaction mixture for a very short time, while the bottom of the wafer has contacted with reaction medium for a whole reaction

time. The top of the wafer (Figure 4.4A) shows almost no polymers, whereas the others (Figure 4.4B and C) present much more polymers. However, there are still differences between the middle and bottom of glycopolymer grafted wafers. In the bottom position of the glycochip, the polymer chains are distributed much denser than in the intermediate region. In addition, the size of dots became larger with increasing polymerization time. Thus, the surface tethered PGlcNAcEMA brushes show gradually grown brushes along the substrate.

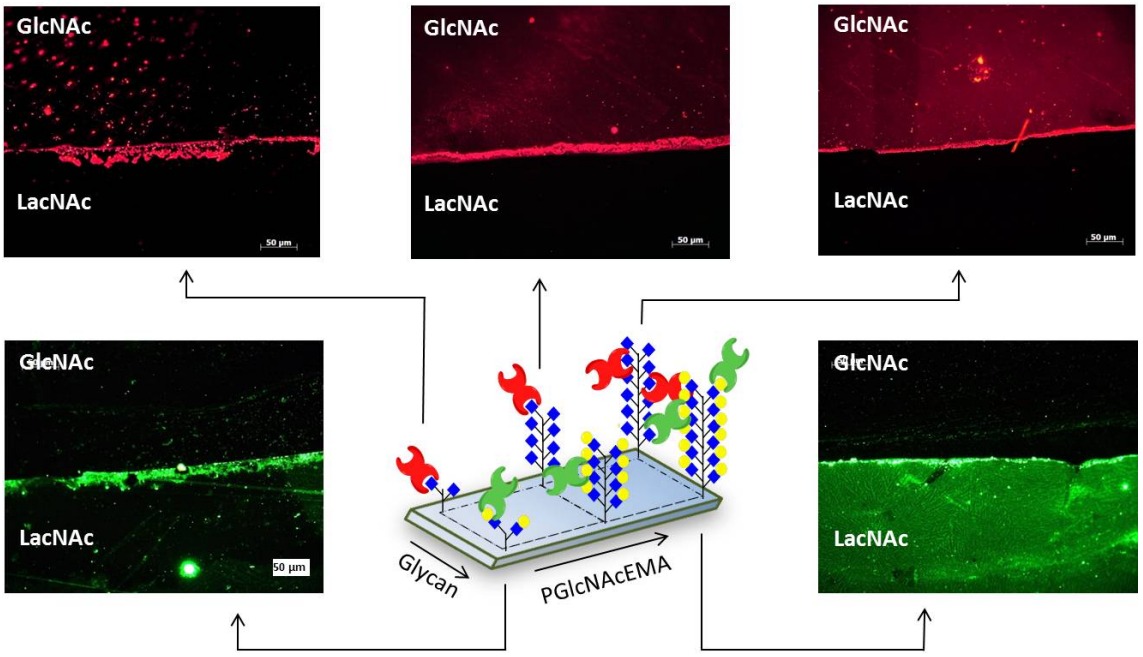

Figure 4.5: Fluorescence image of glycopolymer brush gradient using FITC labelled GS-II and ECL; (Top) specific GS II binding to the GlcNAcEMA molecular gradient. (Bottom) ECL binding to the LacNAcEMA molecular gradient. PGlcNAcEMA was prepared in methanol/water = 1/1 (v/v), 53 μm·min^{-1}. PLacNAcEMA was prepared by the enzymatic extension of the GlcNAc moieties on the half of the gradient wafer.

The enzymatic modification of GlcNAc monosaccharides to LacNAc disaccharides was carried out on the gradient PGlcNAcEMA brushes. For the generation of glycan length orthogonal gradients, only one half of the PGlcNAcEMA gradient wafer was placed horizontally in the reaction solution. The further experimental processes of the enzymatic synthesis were the same as described in Chapter 2.1.4 and Chapter 3.2.2. The glycan gradients gave a more complex multivalent platform based on surface grafted glycopolymer brushes. The resulting substrate included gradients in glycopolymer molecular weight, polymer chain composition and a combination of these gradients. As shown in the middle of Figure 4.5, one half of the PGlcNAcEMA gradient contained LacNAc glycans, while the other half exhibited GlcNAc glycans as pendant groups. Therefore, the region with GlcNAcs could be recognized by monosaccharides binding lectin such as GS-II and the region with LacNAc glycans by disaccharides binding lectin such as ECL. To determine

these properties of gradient wafers, we investigated the binding of GS II and ECL to these surfaces (see Figure 4.5). As expected, these fluorescence images revealed a remarkable selectivity of both lectins to their specific sugar ligand on the wafer. Upper three micrographs of Figure 4.5 present the GS II binding to the non-galactosylated half of the brush gradient. In addition, the binding intensity of GS II lectin on the surface is proportional to the length of the glycopolymer brushes. The lower two images illustrate the specific ECL binding the the galactosylated half of the brush gradient. The enhancement of the lectin binding intensity can be also observed with the increased polymer length. Currently, the oligo-LacNAc gradient along the PGlcNAcEMA gradient is prepared and the complex properties of will be reported later on for details.

4.2.2 PGlcNAcEMA Glycopolymer Grafting Density Gradient

Washburn and co-workers have reported a technique to prepare a polymerization initiator gradient, which was combined with SI-ATRP to produce a PHEMA gradient substrate.[167] They have observed different polymer chain structures at low and high grafting densities. The film thickness was measured across the gradient and the results showed smoothly varied values. Bhat et al. fabricated surface-grafted orthogonal gradient involving the formation of concentration gradients of initiator molecules and the growth of surface-tethered polymer chains with a molecular weight gradient in a direction perpendicular to that of the initiator concentration gradient.[168] They have demonstrated some application possibilities of orthogonal polymer brush gradients to understand the formation of polymer brush-nanoparticle composite assemblies, protein adsorption and cell adhesion, and chain conformations in anchored diblock copolymers exposed to selective solvents. Herein, we prepared a concentration gradient of the initiator to combine this with GlcNAcEMA polymerization on the solid substrate. Hence, a PGlcNacEMA surface with a gradient in grafting density was fabricated in a well-defined manner.

The concentration gradient of the polymerization initiator was formed on a solid substrate by dip-coating. A reaction mixture containing 200 µl 3-(trimethoxysilylpropyl)-2-bromo-2-methylpropionate, 2.1 ml ammonia (29 %) and 25 ml ethanol was preheated at 70 °C. A freshly cleaned silicon wafer placed on the sample holder of the dip-coating system was then vertically lowered into the reactor. The initiator modification proceed at 70 °C with a drawing speed of 350 μm·min^{-1}. After dip-coating, the wafer was removed from the solution, rinsed repeatedly with ethanol and dried in a nitrogen stream. The substrate is then placed into a polymerization reactor and GlcNAcEMA was grown from the initiator gradient as described in Chapter 2.1.3. Usually, we prepared the initiator monolayer at room temperature (See Chapter 2.1.2). However, an elevated temperature (70 °C) was employed for the generation of the initiator gradient. Otherwise, the overall duration of the initiator modification might be too long to be applied for the dip-coating method. As

a result, the generation of initiator gradient was proceeded at 70 °C to reduce the reaction time and to ensure the covalent binding on the surface.

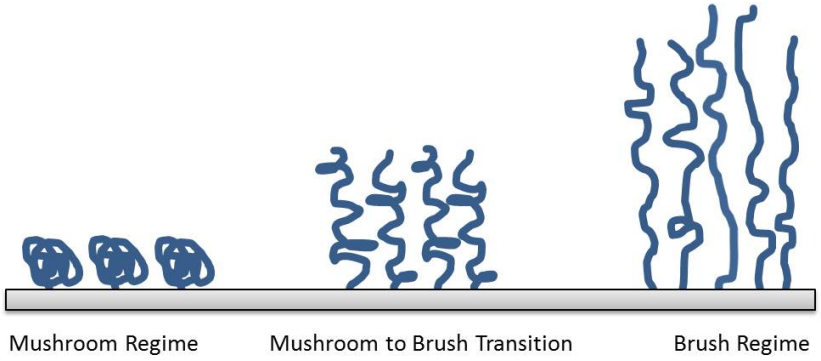

Scheme 4.1: Schematic illustration of polymer conformations in the mushroom and brush regimes and the mushroom-to-brush transition.

In Scheme 4.1, the schematic of polymer conformations, the so-called the mushroom-brush transition regime, is plotted. Polymer brushes consist of polymer chains that are anchored with one chain end to an interface. It is known that the conformation of those polymers can dramatically change with graft density. At low graft density, the polymer chains have enough space between each other to adopt various conformations, which are generally referred to as a mushroom. The mushroom conformation with the coil dimension is assumed similar to that of ungrafted free polymer chains. At high grafting densities, the polymer chains are packed tightly. Hence, steric repulsion between the neighboring chains leads to chain stretching and forms a brush structure.[169, 167]

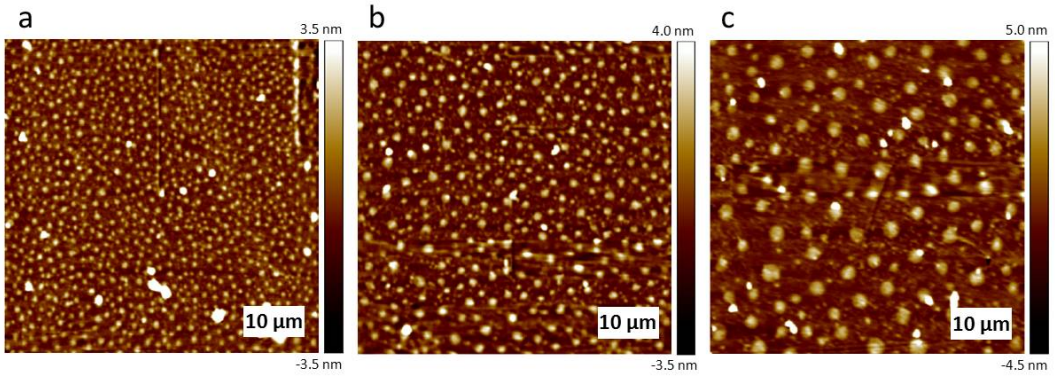

Figure 4.6: AFM height image of glycopolymer brushes polymerized along the initiator gradient; (a) Top, (b) middle, and (c) bottom of the PGlcNAcEMA grafted wafer. The initiator gradient was prepared at a dipping speed of 350 μm·min^{-1}. PGlcNAcEMA was prepared in methanol/water = 1/1 (v/v) for 2 h.

Figure 4.6 shows the representative AFM images of the PGlcNAEMA brushes grown along initiator gradient. The obtained 10 × 10 µm^2 height images show a difference in morphology along the initiator concentrations. Compared with the AFM image of

PGlcNAcEMA grown from initiator monolayer (Figure 3.6), it is obvious that the polymer chains are growing very far apart from each other. In addition, the spots of PGlcNAcEMA brushes grown along initiator gradient are quite big in comparison with those from initiator monolayer in spite of a acquired big area difference. This can be explained by the lower grafting density of the polymerization initiator after short modification time (maximal 25 min) of the silicon wafer. Hence, the polymers can form mushroom conformations. With increasing the grafting density, the polymer spots become larger and this can be estimated of the effect of mushroom-brush transition. At the low grafting density, the surface structure of the brushes show small and monodisperse spots (Figure 4.6a). At the middle of the gradient wafer (Figure 4.6b), the surfaces have larger polymer spots which look like to be coalesced into large grains. The highest initiator density of gradient results in monodisperse but much larger polymer structures (Figure 4.6c). Interestingly, the small spots in Figure 4.6a are shown still between the big spots. Hence, the coalescing of polymer chains can be a potential explanation of these observations.

The polymer brushes grown from initiator gradients have been also investigated using GlcNAc specific lectin GS-II. With increasing the initiator density on the surface, the fluorescence intensity is obviously enhanced. At the beginning of the polymerization, almost no binding of lectin on the surface can be observed (Figure 4.7a). Figure 4.7b illustrates the middle area of the gradient wafer and the GlcNAcEMA binding can be well observed. Figure 4.7c shows the highest binding intensity of GS-II on the surface. These measurements prove that the initiator concentration gradient is successfully generated and the grafted glycopolymers can be recognized specifically.

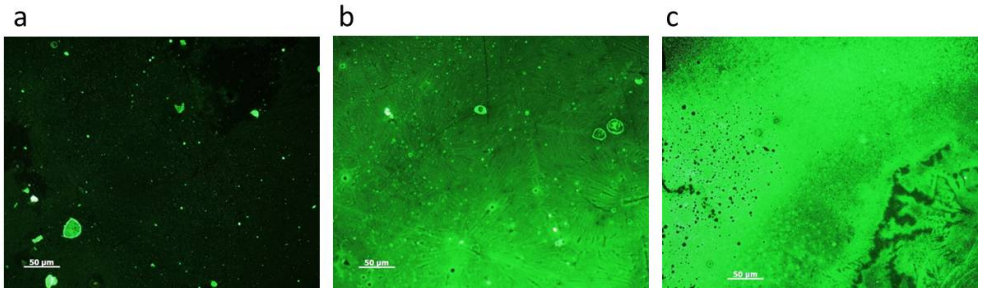

Figure 4.7: Fluorescence image of glycopolymer brushes polymerized along the initiator gradient (using FITC labelled GS-II); (a) Top, (b) middle, and (c) bottom of the PGlcNAcEMA grafted wafer. The initiator gradient was prepared at a speed of 350 μm·min^{-1}. PGlcNAcEMA was prepared in methanol/water = 1/1 (v/v) for 2 h.

In this case, the orthogonal gradient of glycans has not yet been fabricated. However, the initiator gradient brushes in the AFM images have shown different surface structures in comparison with the glycopolymer gradient brushes. The fluorescence microscopic micrographs have revealed again lectin specific binding surfaces. In result, the glycopolymer brushes along the initiator gradient have shown a quite large potential as a new multi-

functional glyco-surface.

4.2.3 Conclusion

In this chapter, we introduced a new method for the gradient glycopolymer synthesis. At first, a molecular weight gradient of glycopolymers was generated from initiator monolayers by using dip-coating method. The AFM images revealed well controlled gradient structures. Then, an orthogonal glycan gradient was synthesized in perpendicular with the molecular weight gradient. The investigation using FITC-labelled lectins showed very specific and selective lectin binding events on the surface. This proves that the expectation sketched as schematic illustration in Figure 4.1 was fulfilled well. The further modification of glycan for the gradient generation is on processing and the result will be reported later on. At second, an initiator concentration gradient was generated on a silicon wafer. The AFM images have showed a mushroom conformation of the brushes. Then, monosaccharide GlcNAc specific lectin was empolyed to investigate the biological activity of grafted polymers. The acquired images confirmed again that the gradient glycopolymer brushes possess a great potential as a new multivalent glycochip. In conclusion, the PGlcNAcEMA gradient on the silicon wafer was successfully performed. Detailed experiments will give much more information about the sugar-lectin binding events. This new platform combined with chemistry and biology can be widely used in the field of chemistry, biology, diagnostics, and biomedicine as a powerful synthetic material.

5 Impedimetric Glyco-Biosensor (IGB)

5.1 Introduction

The interest in grafted polymer chains on gold surfaces has been increasing in recent years.[139, 170] Synthesis of polymer layers using the "grafting from" approach actually leads to higher grafting densities because of easier diffusion of monomers than macromolecules. Hereby, stable attachment of initiators to the gold substrate is crucial. If the attachment is not strong enough to support the polymerization, the long polymer chains can be detached from the substrate. Organic thiols on Au are the most common system for anchoring reactive sites because they form well-defined self-assembled monolayers. However, Au-S bond is too weak to link the initiator layers to the surface. While the enthalpy of binding is in the range of 30-50 kcal·mol^{-1}[171], the free energy of binding is only 5 kcal·mol^{-1}.[172] The bound thioles can be thermally detached from the Au surfaces when the substrate comes into contact with hot organic solvents. Hawker and coworkers reported SI-ATRP of various vinyl monomers on Au substrates.[139] They modified the Au surface with the initiator at elevated temperature to prevent the thermal desorption of initiators during polymerization. Baker and coworkers reported free-radical polymerization of styrene initiated from azo-initiators attached to Au substrate.[170] They carried out a simple cross-linking procedure using mercaptopropyltrimethoxysilanes to overcome monolayer instability. The cross-linked poly(siloxane) primer layer stabilizes the initiator-containing surface to polymerization condition.

Glycopolymers on the Au surface have been also reported by many groups and typically explored to study the lectin interactions.[173, 174, 175] Gibson and coworker have introduced glycosylated gold nanoparticles that change their color due to lectin mediated aggregation. They used RAFT polymerization to generate gold nanoparticles coated with glycosylated polymers. They found that long glycopolymer chains hinder lectin binding and hence lead to a poor readout.[175] As mentioned in Chapter 1, carbohydrate-lectin interactions are implicated in numerous disease processes. Particularly, there is increased interest in real-time measurement of carbohydrate-lectin interactions. For example, Ramström and coworkers have introduced a method for quantitation of these interactions using the quartz crystal microbalance (QCM) technique.[176] Yeast mannan was immobilized on polystyrene-coated quartz crystals, and its interaction with concanavalin A was tested. Pei

and coworkers have developed a lectin-based suspension-cell biosensor for determination of protein-carbohydrate interactions on cancer cell surfaces using QCM.[177] This system evaluated glycosylation in real time on suspension cancer cell surfaces.

Recently, immunosensors using electrochemical impedance spectroscopy (EIS) have been reported by several groups.[135, 136, 138] Biosensors based on the impedimetric detection of biological binding events have been published in numerous articles.[178, 179, 180] The impedimetric detection method measures impedance changes produced by the binding events of target molecules to receptors. Receptors, for example antibodies or enzymes, are usually immobilized on the surface of microelectrodes. The preparation of the receptor immobilized electrodes is a complex and sometimes non-reproducible procedure. These electrodes are usually very sensitive to noise produced by the non-specific binding events of background contaminants. In addition, they are prone to drift. Although this method has some disadvantages, it is still a promising detection method due to its high sensitive and effective properties. If the drawbacks of the impedimetic detection method could be overcome, it might be a powerful sensing technique to investigate the biological interactions. However, there is still no literature describing real-time monitoring of sugar-glycan interactions. To enhance the detection possibility, glycopolymers can be used instead of a single glycan. In this work, we introduce a novel impedimetric glyco-biosensor (IGB) for the real-time measurement of the lectin-glycopolymer brushe interaction.

5.2 Results and Discussion

This work describes a new platform for the impedance spectroscopy of biological species. The fabrication of the IGB was succeeded by the chemical modification and the following electrochemical measurement using biological binding systems. Until now, there have been several reports about the modification of the Au surface. However, the detailed modification conditions have not been investigated yet. Before the fabrication of a IGB, it was necessary to find out important factors which may influence the chip production. The determination of critical parameters helps saving time, cost and materials. In this chapter, we will introduce how the optimal conditions for the IGB production were identified and how the characteristics of the fabricated IGB were measured. Then, we will present the results from the electrochemical measurements of EIS.

5.2.1 Optimization of IGB Production

The stripes of Au electrodes on a chip were so narrow (approx. 10 μm) that the characterization of each stripe was difficult. Therefore, the optimal conditions for the IGB

production were sought through the examinations of various parameters using flat Au wafers. We considered several parameters such as thickness and modification of Au electrodes, the way of production of Au electrodes, rinsing and storing in different solvents and so on. For the optimization of the attachment of polymer chains, we investigated flat Au surfaces, initiator modified Au surfaces, and polymer coated Au surfaces using CA measurement (see Chapter 2.2.3) and FLLA (see Chapter 2.1.5).

Characterization of the Au layers

First of all, we examined the effect of storing the substrates in air on the hydrophobicity with elapsed time. A 300 nm thick Au surface produced by vacuum deposition was used. As table 5.1 shows, the water contact angle (CA) of the Au surfaces increases with ongoing time. Thus, the pure Au surface becomes hydrophobic in air with time duration. Therefore, the Au surface was always prepared just before its application.

Table 5.1: Contact angle values of Au surface kept in normal air.

CA / °	fresh	1 day	7 days
L	37.2	45.2	65.9
R	38.2	45.0	66.0

Characterization of the initiator modified Au layers

There are some ATRP initiators which can be grafted on the Au surface. To determine the influence of initiators on protein binding, we used two different initiators for three different reaction times. The bromine containing ATRP initiators, bis[2-(2'-bromoisobutyryloxy)ethyl]disulfide (BisBIBED) and bis[2-(2'-bromoisobutyryloxy)undecyl]disulfide (BisBIBUD) were utilized. They are distinguished just by the length of the alkane chains between the disulfide and bromine group. As shown in Figure 5.1, both initiators show almost the same binding activity for three different modification times. Therefore, the short ATRP initiator BisBIBED was chosen due to its low cost and employed for the whole reactions.

The initiator modified Au surface (vacuum-deposited, d = 300 nm) was tested by FLLA using BSA-FITC. Initiator solution was prepared as described in Chapter 2.2.5. As shown in Figure 5.2, a longer incubation time led to a better protein binding. The fluorescence values do not stand represent absolute values, but fluctuate. For this reason, the graph contains relatively high error bars. The initiator modification on the Au surface would work better when it processes over 18 h rather than below 2 h. Therefore, the surface

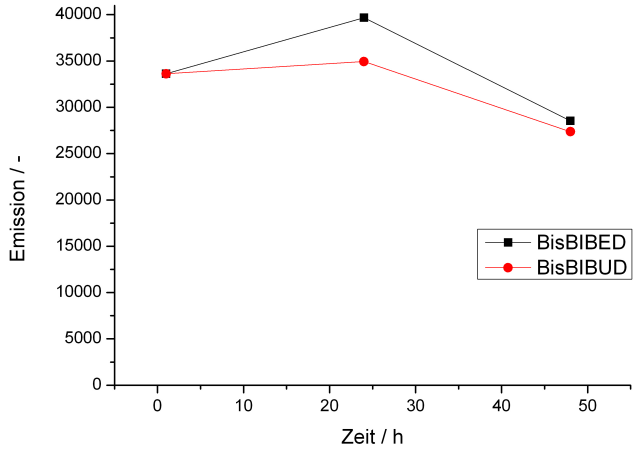

Figure 5.1: Influence of different ATRP initiators on the lectin binding (used FITC labelled *Ricinus communis*).

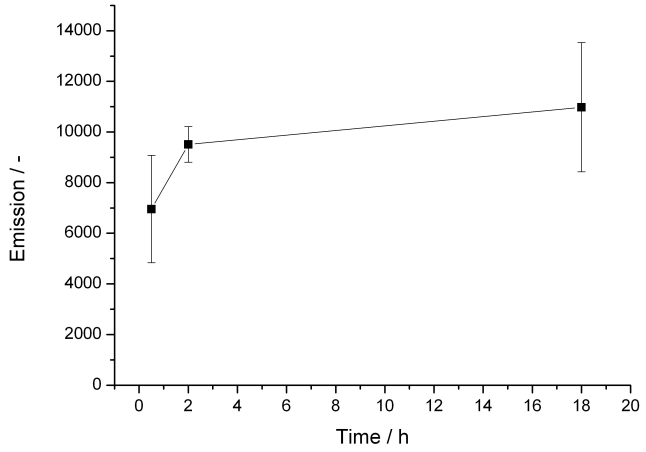

Figure 5.2: Dependence of BSA-FITC binding on the duration of Au substrates incubation in initator solution.

modification of Au was hereby always performed over night.

For the study about the relationship of Au thickness with protein binding, two different thicknesses of Au substrates (produced by vacuum-deposition) were used for FLLA with increasing incubation time in initiator solution. A freshly prepared Au wafer was used for the measurement as a reference. The fluorescence values fluctuated quite strongly, but the main tendency can be observed. The 100 nm Au substrate shows no appreciable changes in initiator solution during 18 h incubation time, whereas the 300 nm Au substrate exhibits very high protein binding on its surface on average. In addition, the 300 nm Au substrate displays enhanced fluorescence values with increasing incubation time. It confirms again

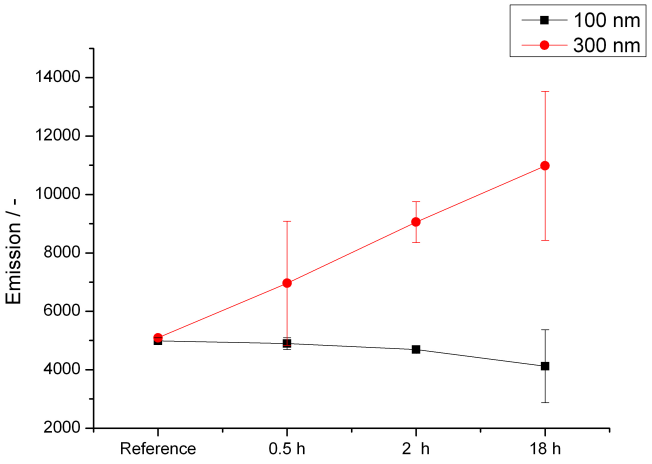

Figure 5.3: Dependence of BSA-FITC binding on the thickness of the Au substrate and the incubation time in the initiator solution.

the result of the former experiment (see Figure 5.2). For this reason, we choose the 300 nm Au wafer and 18 h of incubation time for the further experiments.

To find the best rinsing solvent and storing method, the initiator modified Au surface was stirred in various solvents and then investigated by FLLA using BSA-FITC. The wafers were measured twice; directly after initiator modification and after 24 h incubation in solvent. Water, methanol, ethanol, and PBS buffer solution were used as solvents. The freshly prepared wafers with initiator show relatively high emission values, while after 24 h incubation under stirring they reveal quite low emission values. Particularly, in air stored wafers exhibit the lowest fluorescence value. In case of methanol incubated wafers, the protein binding properties are just slightly reduced. Consequently, we avoided to store the initiator modified wafers in air and applied them immediately for the further modification. Lastly, the Au layers produced by vacuum deposition have been compared with the Au substrate deposited by sputtering on SiO_2. The sputtered Au layers showed a little better protein binding after initiator modification (data not shown). Hence, we used the Au layers deposited by sputtering on SiO_2 for the further experiments.

The influence of initiator treatment on protein binding was observed so far by choosing several parameters. Based on the results, we determined the optimal conditions for the initiator handling. The applicable parameters for the initiator modification and long time storing of initiator modified substrates may be summarized as follows. The thicker Au surface, the shorter ATRP initiators, and the longer treatment of initiators (at least over night) allow the better protein binding. In addition, to prevent altering of Au wafers, they should be modified freshly with ATRP initiators before further functionalization.

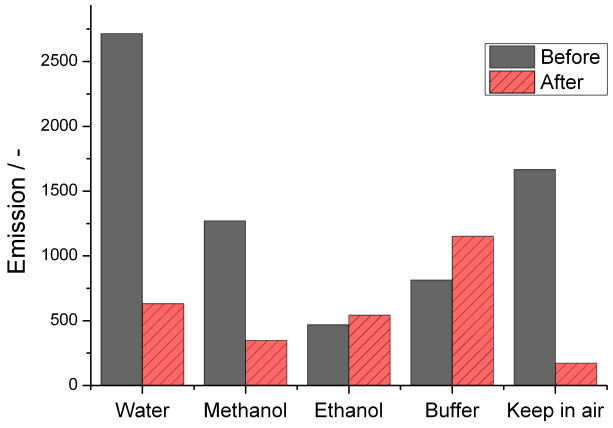

Figure 5.4: BSA-FITC binding properties of the initiator modified Au substrates before and after stirring in various solvents for 24 h. An initiator modified wafer was kept in air for 24 h and the binding intensity was measured.

Characterization of the PHEMA grafted Au layers

The PHEMA brushes on the gold coated chips were observed by AFM and FESEM to evaluate whether the polymerization was successfully made (Figure 5.5). The AFM acquired image reveals the PHEMA polymer spots distributed almost monodispersely. The FESEM image illustrates nearly the same structure as shown in Figure 3.7). These results convince the successful polymerization of HEMA on gold substrates.

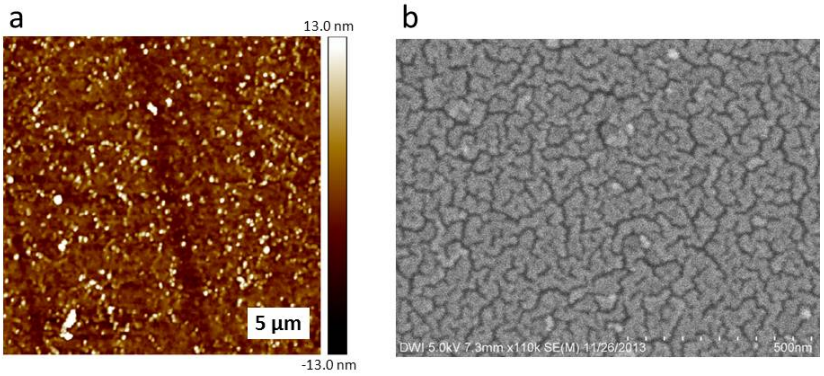

Figure 5.5: AFM height image (Left) and FESEM micrograph (Right) of PHEMA brushes on the Au coated wafer.

The BisBIBED modified Au surface was employed for the polymerization of HEMA to compare the surface characteristics before and after polymerization. Au coated wafers were examined with three different film thicknesses (100 nm, 150 nm, 200 nm). Here, the Au layers have been produced by sputtering on SiO_2. The polymerization was performed in

three Erlenmeyer flasks containing an initiator modified Au substrate, respectively. The flasks were degassed by purging with nitrogen. The monomer, catalysator, and ligand mixture was prepared separately in a 25 mL peer shaped flask for each reaction. A representative example for the preparation of polymerization mixture is the following: 0.38 mL (3.15 mmol) HEMA was added in 10 mL methanol/water = 1/1(v/v) and stirred under nitrogen at room temperature for 10 min. Then, 98.36 mg (0.63 mmol) bpy, 24.95 mg (0.25 mmol) CuCl, and 14.07 mg (0.06 mmol) $CuBr_2$ were added into the HEMA mixture and stirred under nitrogen further 10 min. The resulting dark brown mixture was transferred into the degassed Erlenmeyer flask and the HEMA monomer was polymerized from the Au surface for 2 h.

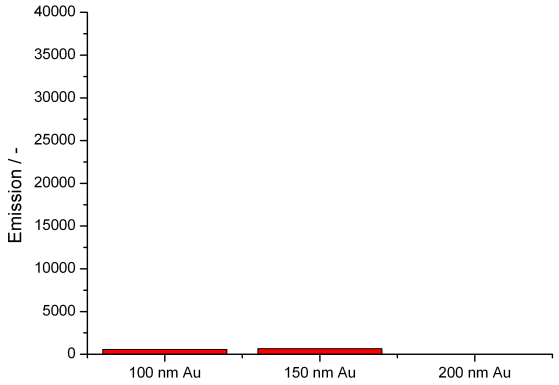

Figure 5.6: Protein binding properties of the PHEMA grafted Au substrates (used FITC labelled *Ricinus communis*).

Figure 5.6 shows the protein binding activity of the PHEMA brushes. All three Au surfaces exhibit very low adsorption of FITC labelled *Ricinus communis*. Nevertheless, the fluorescence of the Au substrate with 200 nm layer thickness shows much lower than that of 100 nm or 150 nm. These results indicate an extremely reduced protein binding property of the surface in comparison with the initiator modified substrate shown in Figure 5.1. Actually, PHEMA brushes on silicon wafers are known as anti-fouling substrates due to their inhibition properties of protein binding on the surface.[181, 182] Therefore, it is confirmed that the PHEMA brushes on the Au substrates are also coated well to repel the protein binding. For further experiments, the Au substrate with 200 nm film thickness has been used.

To exclude non-specific bindings of PHEMA on the Au substrate, three different experiments were performed in parallel. At first, Au surfaces were pretreated using plasma (0.2 mbar, 5 min, 18W, PDC-32 G, Harrick) and then immediately modified with the ATRP initiator for the fabrication under the optimal conditions (see page 55 and 57). After that, three different batchs were prepared: a typical ATRP reaction from the initiator

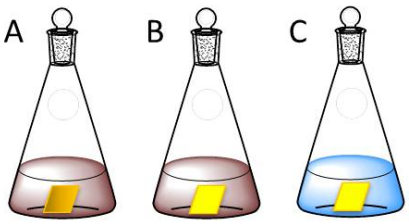

Figure 5.7: Experimental setup for the study of the non-specific bindings of PHEMA on the Au substrate. A: initiator modified Au substrate in the polymerization mixture, B: Plain Au substrate in the polymerization mixture, C: Plain Au substrate in PEHMA solution.

modified Au wafer (Figure 5.7A), a ATRP reaction from the Au wafer (Figure 5.7B), and an emulsion reaction of Au wafer in the PHEMA solution (Figure 5.7C). For reactions A and B, the reaction mixtures were prepared as described on page 59. For reaction C, a presynthesized white powder of PHEMA (Mn = 7359.1 g/mol, PDI = 1.13) was dissolved in ethanol (1 mg mL^{-1}). The ATRP of HEMA was performed in the reaction flasks (A and B) for 2 h. The incubation of the Au substrate in the PHEMA solution in the flask C was also performed for 2 h. After the reaction time, the substrates were rinsed with methanol, water or ethanol and dried in a nitrogen stream.

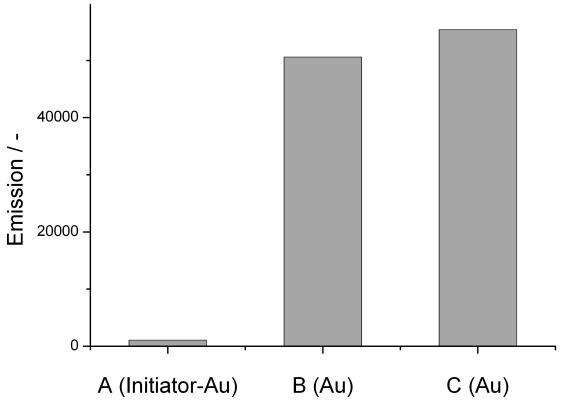

Figure 5.8: Protein binding properties of the substrates which were prepared as described in Figure 5.7 (used FITC labelled *Ricinus communis*). A: initiator modified Au substrate in the polymerization mixture, B: Plain Au substrate in the polymerization mixture, C: Plain Au substrate in PEHMA solution.

The wafers (Figure 5.7**A-C**) were incubated in the FITC labelled *Ricinus communis* lectin solution. Figure 5.8 shows the FLLA results of the substrates after the reactions. Through the typical polymerization reaction, the PHEMA brushes were grown from the initiator modified Au layers. The resulting brushes (**A**) show extremely low lectin adsorption. As expected, the polymerization from the Au surface without initiator layers (**B**) seems not working. The wafer shows very high non-specific lectin adsorption on the surface. This

represents that there are no PHEMA brushes on the Au layers and hence lectins bind non-specifically on Au. In case of the in PHEMA incubated Wafer, the adsorption value is similar high. This result denotes that the PHEMA cannot bind non-specifically on the Au layer. When PHEMA was grafted on the surface, the protein binding value should be reduced as shown in Figure 5.6. Therefore, we can conclude that the ATRP can just work from the initiator modified Au surface and almost no adsorption of PHEMA can take place on the plain Au layer.

To investigate whether PHEMA coated surfaces are resistant in the diverse solvents, the PHEMA grafted Au wafers were stirred in water, methanol, ethanol, and PBS buffer solution for 24 h. Then, the wafers were dried in a nitrogen stream and employed for the protein assay. In comparison with the initiator modified wafers in Figure 5.4, the entire results in Figure 5.9 show radically reduced values. This may result from the PHEMA coating on the Au surface which not only prevents the protein adsorption but also reduces the surface corrosion. Moreover, the values before and after the stirring in solution are almost unchanged in this case. Thus, the PHEMA grafted Au surfaces are much more stable than the pure or initiator modified Au surfaces.

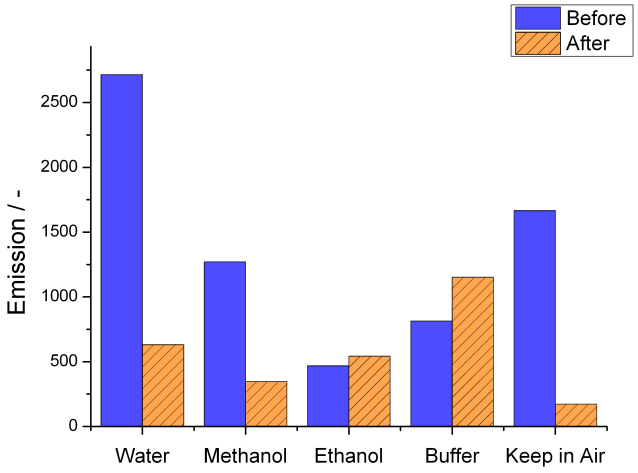

Figure 5.9: FITC labelled *Ricinus communis* binding properties of the initiator modified Au substrates before and after stirring in various solvents for 24 h. A PHEMA grafted wafer was kept in air for 24 h.

The PHEMA coated surface was also examined by the water contact angle (CA) measurement (Table 5.2). The CA values of PHEMA brushes were measured three times: immediately, 3 days, and 7 days after the synthesis. As shown in Table 5.2 the overall values within seven days did not fluctuate extremely. Instead, the CA values were almost stable within a week. This result confirms again that the PHEMA coating makes the Au surface very stable even against air in contrast to the result from pure Au surface (see page 55).

Table 5.2: Contact angle values of the PHEMA brushes kept in air.

CA / °	fresh	3 days	7 days
L	58.7	58.1	61.1
R	59.2	60.4	60.4

In summary, the pure Au surface, the initiator modified, and the PHEMA grafted Au substrates were investigated by using FLLA and CA measurements. The surface properties were characterized by testing optimal conditions to produce a stable surface against stress conditions such as exposure to air or solvents. As a result, the Au and the initiator functionalized substrate should be applied as soon as possible to the next modification. After PHEMA coating, the Au substrate shows to be a very resistant surface against the stressed conditions. Therefore, we adapted these results to produce the glycochips with the impedimetric detection property.

5.2.2 Fabrication of IGB

This chapter describes the fabrication and characterization of a microelectronic device prepared by the combination of chemical modification with impedance spectroscopy of the synthesized biochips. For the fabrication of IGB, a chip containing six Au electrodes was cleaned by diverse solvents and plasma treatment (Figure 2.10). The protective polymer coating on the electrodes has been removed by the rinsing with acetone, isopropanol, ethanol, and water. The electrical circuit was controlled to control the complete removal of coating and prevent using the chip with a short circuit. To reduce non-specific side reactions, the electrodes have been cleaned by plasma treatment at 0.2 mbar for 5 min. After that, the surface was modified with a thiol containing ATRP initiator, BisBIBED. The polymerization of GlcNAcEMA was performed under the same conditions like as the synthesis of PHEMA. The detailed experimental conditions are described in Chapter 2.2.5.

At first, we prepared an impedimetric glycochip containing three different surface structures. The surface of the electrodes was modified with different materials such as PHEMA, initiator, and PGlcNAcEMA. Here, the electrode 1 and 6 were coated with PHEMA, the electrode 2 and 5 with BisBIBED, and the electrode 3 and 4 with PGlcNAcEMA using the same ATRP method. After synthesis of polymers on the electrodes, the chip was covered with two PDMS channels to measure the changed impedance by a microfluidic system (see Figure 2.10). Finally, one chip has three different surface structures and two different fluidic measurement channels (1-3 and 4-6). The surface structure of the functionalized Au electrodes was investigated by AFM. The topographic images of these different surfaces are shown in Figure 5.10. The top and bottom images ensured that the polymerization

was successfully performed. The white dots in the images represent the grown polymers, whereas the dark brown background illustrates the initiator modified Au substrate. The PHEMA grafted electrode displays the most diverse colors which represent the most polymer growth from the substrate. In comparison with PHEMA, the PGlcNAcEMA surface shows relatively less white and smaller dots. However, the homogeneous distribution of dots can also be observed.

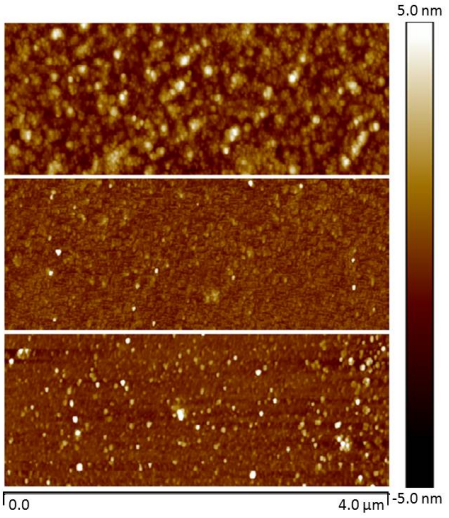

Figure 5.10: AFM micrographs of the modified Au electrodes. Top: PHEMA, Middle: initiator, Bottom: PGlcNAcEMA.

Then, an impedimetric glycochip containing a polymer gradient was prepared. A gradient of PGlcNAcEMA molecular weight was constructed using varying polymerization time. All of the six electrodes were coated with PGlcNAcEMA and the polymerization time was varied. The electrodes 1 and 6 were reacted for 10 min, the electrodes 2 and 5 for 30 min, and the electrodes 3 and 4 for 2 h respectively. This one chip also has three different surface structures and two different fluidic measurement channels (1-3 and 4-6) as shown before. The AFM height images are shown in Figure 5.11. The grown polymer chains are shown as the white dots here. All of theses Au electrodes have a homogeneous distribution of PGlcNAcEMA. While the surface after 10 min polymerization displays few and smaller polymers, after 2 h polymerization much more and larger polymers are visible. The progress of the polymerization with increasing time is clearly observable. In addition, the thickness of glycopolymers can be estimated from the result in Figure 3.4. The surface with short polymers after 10 min polymerization has around 0.5 nm thick, after 30 min 1.25 nm, and the long polymers after 2 h polymerization are 3.45 nm in thickness. The surface roughness of the respective surfaces are calculated using AFM analysis. The value changes from 0.243 nm $\pm$ 0.018 nm for the shortest PGlcNAcEMA and 0.387 nm $\pm$ 0.016 nm for the longest PGlcNAcEMA. These values are significantly low in comparison with a plain Au surface with 1.672 nm $\pm$ 0.231 nm in roughness. These observations can be explained as follows: the rough plain Au surfaces are flatted by the modified initiator and

then the surface roughness is increased again with increasing polymerization time.

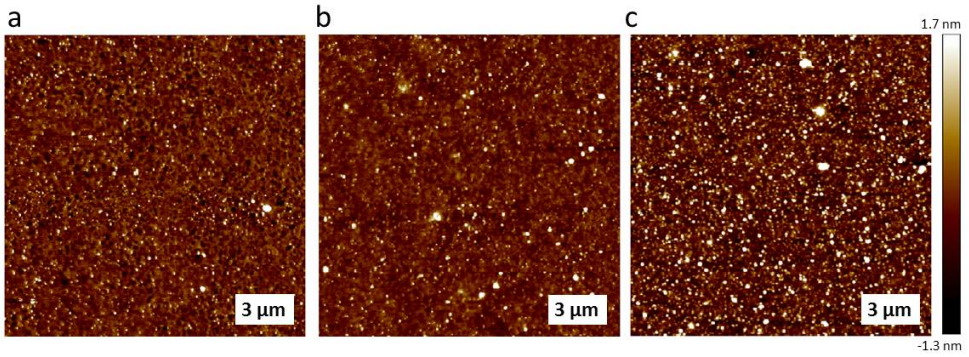

Figure 5.11: AFM micrographs of the PGlcNAcEMA grafted Au electrodes. a: after 10 min polymerization, b: after 30 min, c: after 2 h.

In order to determine the binding properties, the PGlcNAcEMA brushes on the Au electrodes were investigated using FITC labelled GS-II lectin. At first, the chip with gradients show protein binding on the whole surface which might be explained with high non-specific protein binding. However, the gradient of fluorescence intensity can be lightly observed. Then, we used several wash steps with PBS buffer solution. As the result, the chip shows very specific protein binding as shown in Figure 5.12.Almost no fluorescence can be observed for the spaces between the electrodes, whereas the Au electrodes show a bright green color. This represents that the sugar specific GS-II lectins bind just to the glycopolymer brushes on the Au electrodes. In addition, the for 10 min polymerized surface shows relatively weak fluorescence in contrast to the surface after 2 h polymerization. Therefore, the on the Au electrode polymerized GlcNAcEMA can be recognized by GlcNAc specific lectin GS-II and bound very specifically.

The pendant sugars of PGlcNAcEMA were enzymatically elongated as described in chapter 2.1.4. As illustrated in Figure 5.13, the GlcNAc pendant was extended with galactose and the glycopolymers with LacNAc disaccharide pendants were produced. Figure 5.13a shows no binding of the galactose specific ECL on the PGlcNAcEMA brushes. In contrast to PGlcNAcEMA, the PLacNAcEMA brushes (Figure 5.13b) show the ECL binding on the electrodes clearly. These observation confirms that the enzymatic modification of PGlcNAcEMA surface to galactose containing PLacNAcEMA was successfully done. In addition, both GS-II and ECL lectins can distinguish the surfaces and bind specifically to the corresponding sugars.

As shown here, both the PHEMA and PGlcNAcEMA brushes were successfully synthesized from the initiator modified Au electrodes by SI-ATRP technique. An EIS chip was processed to have three different surface characteristics in one direction and two microfluidic channels in the other direction. The specific functionality of glycopolymer brush surfaces shows the selective lectin binding ability. Herein, the electochemical properties

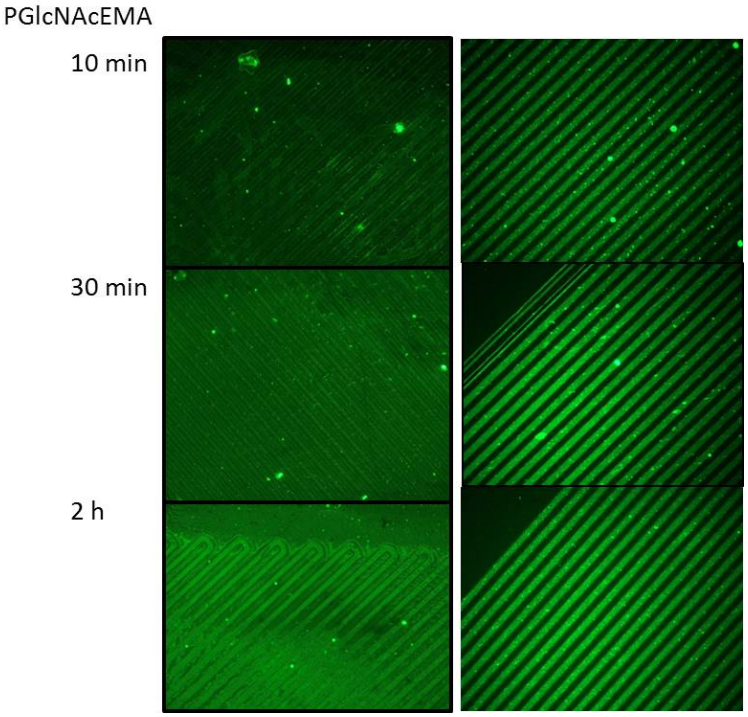

Figure 5.12: FITC labelled GS-II lectin binding on the PGlcNAcEMA grafted Au substrates before (Left) and after several wash steps (Right).

of glycochips was studied by the impedance spectroscopic measurement. To prove the reproducibility of the glycochip fabrication, all six electrodes of one chip processed under the same conditions and several chips were employed to measure. Two variant types of PGlcNAcEMA glycochips were prepared: 10 min and 2 h polymerized chips. Frequently, BSA is used as a blocking agent to prevent non-specific binding of proteins on the surface. For the IS measurement, the glycochips have not been blocked with BSA and they have been acclimated to PBS buffer solution for 20 min. After that, the corresponding protein was injected to the glycopolymer brushes using the microfluidic system for about 1 h. Then, the electrodes were washed again with buffer solution.

The shift in EIS value is recorded as function of time in the sensorgram. In Figure 5.14, the progress curve for 10 min polymerized PGlcNAcEMA is plotted. For a short period after the start of the GS-II injection, GS-II binds approximately linear to the surface. In this case, the initial rate period is estimated about 20 min. As the reaction proceeds and the protein is consumed, the binding increases steadily. Yet, the substrate did not reach a saturating level. After 70 min GS-II injection, the glycohip was washed by streaming the buffer solution. For 30 min washing time, the binding signal is not reduced to the initial value of the buffer solution. This could be due to GS-II lectins binding specifically and strongly to the surface.

In comparison with 10 min polymerization, the 2 h polymerized glycopolymers show rel-

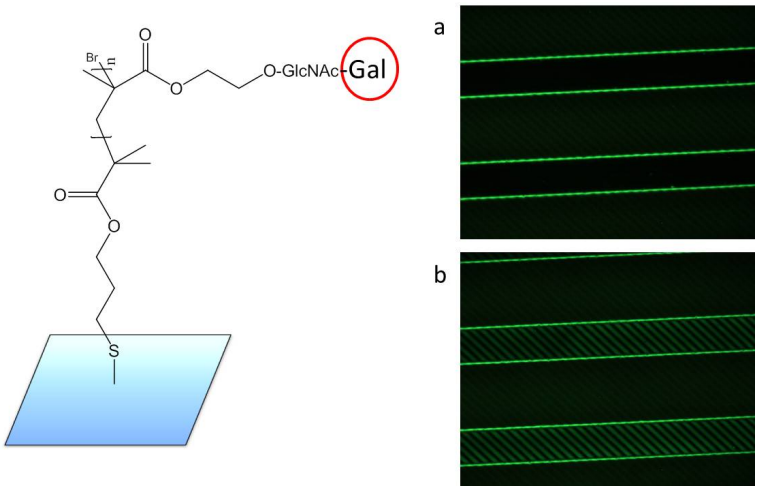

Figure 5.13: FITC labelled GS-II lectin binding on the different glycopolymer brushes. Left: Illustration of enzymatic elongation of galactose from the surface grafted PGlcNAcEMA. Right: a) No ECL binding on PGlcNAcEMA brushes, b) ECL binding on PLacNAcEMA brushes on the Au electrodes.

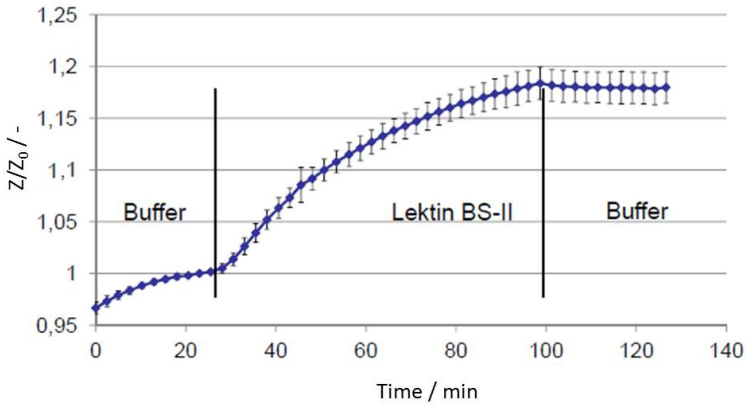

Figure 5.14: Sensorgram of GS-II binding on the 10 min polymerized PGlcNAcEMA chips.

atively fast protein binding and early saturation. To evaluate detailed binding characterization, the electrical signals were plotted at the various frequencies. The results revealed that electrical areas placing much far from the surface could be measured at elevating frequencies. This means that the parts of glycopolymer brushes which are close to the Au electrode would be measured better at a low frequency. In contrast, the top of glycopolymers which come in best contact with proteins could have the best signal at a high frequency (data not shown in this thesis). The detailed results and discussions about the impedimetric measurements are submitted for publication in Macromolecular Rapid Communications.

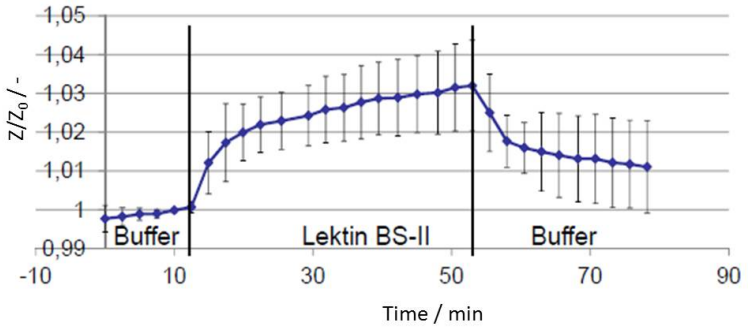

Figure 5.15: Sensorgram of GS-II binding on the 2 h polymerized PGlcNAcEMA chips.

5.3 Conclusion

Here, we described the fabrication processes of microfluidic glycochips for impedance spectroscopy measurement. One of the most interesting point of the introduced IGB was the combination of several techniques such as glycomonomer polymerization from the Au electrodes using ATRP, the enzymatic elongation of sugar pendants of glycopolymers, the measurement of biological interactions between the grafted glycopolymers and sugars, and the real-time monitoring of the recognition and specific binding process. Particularly, IGB has shown the opportunity for the detection of small quantities of lectins (approximately 20 $\mu g \cdot ml^{-1}$). The surface structure of the fabricated glycochips was characterized by AFM and the biological activity was analyzed by impedance spectroscopy as well as FLLA. The resulted glycopolymer brushes have shown a homogeneous surface structure and selective lectin binding properties. In addition, the glycochips introduced in chapter 4 showed that the use of labelled lectins is essential. Although the IGBs have used unlabelled lectins, the lectin binding to glycopolymers could be successfully proven by electrochemical measurements. Furthermore, the intrinsic insufficiency of the electrochemical measurement was overcome by the combination with chemical modifications. Thanks to the use of intact proteins, the screening of lectins from food products or bodily fluids is a potential applications. For the realization of these further applications, the more detailed investigation of IGBs is necessary as a next step. Studies about the dependence on different polymer length, various lectin concentrations, and diverse electrical frequencies for the EIS measurement are already on processing. Researches of IGB as an alternative to commonly used SPR biosensor systems are submitted for publication.

6 Generation of New Sensors Using Microfluidics

Microfluidics is the science and technology of systems that process or manipulate small (10^{-9} to 10^{-18} liters) amounts of fluids. It deals with channels geometrically constructed to a small scale of tens to hundreds of micrometers. Typically it is used in the development of medical diagnostics and bio-sensing. Many practical applications and integration of complex functions on chips have been reported since the last decades. The main advantages of microfluidic technologies are devoted to the copabilities of handling small sample sizes and saving reagents. It results in the enhanced efficiency of the assays and the reduction of cross-contamination. These advantages could potentially lower the total cost of the assays.[183, 184] Microfluidic biosensors have been usually involved in manipulations of small fluidic volumes and following optical detection. However, in Chapter 5 we introduced the electrochemical characterization of biological binding to the surface grafted glycopolymers using a microfluidic system. Herein, we want to present microfluidic sensors including integrated systems such as optical detection, chemical synthesis, or electrical measurements. At first, a plasmonic flow-through glyco-biosensor will be described as a new SPR-based platform. Then, a new polymerization monitoring system based on surface acoustic wave (SAW) technique will be presented.

6.1 Plasmonic Flow-Through Glyco-Biosensor (PFGB)

6.1.1 Introduction

SPR is well known and a popular sensing method for the observation of biochemical reactions. Figure 6.1 is a schematic diagram of the typical binding cycle observed by SPR measurement. A molecule is immobilized to the sensor surface as a receptor and an analyte flows over the sensor surface. The binding affinities and kinetics of the interaction with analytes are determined. At the beginning, buffer solution flows through a microfluidic flow cell. As the analyte binds to the surface, the refractive index of the medium near the surface increases. With increasing interaction of receptor and analyte, an increasing resonance signal is detected [displayed in response units (RU)]. The association rate k_a

can be determined by analysis of this part of the binding curve. At equilibrium, the amount of analyte that is associating and dissociating, is equal and the maximal binding is specified as R_{max}. The injection of the analyte is stopped by replacing the system back to buffer and the receptor-analyte complex starts to dissociate. Then, the dissociation rate constant k_d can be calculated by analysis of this curve. In many cases, the analyte is not dissociated completely after a reasonably long time. Therefore, an injection of an appropriate regeneration solution is necessary to disrupt binding and regenerate the free receptor. After this regeneration time, the resonance signal should be reached to the baseline response level. The affinity of the interaction can be determined from the ratio of the rate constants ($K_D = 1/K_A = k_d/k_a$).

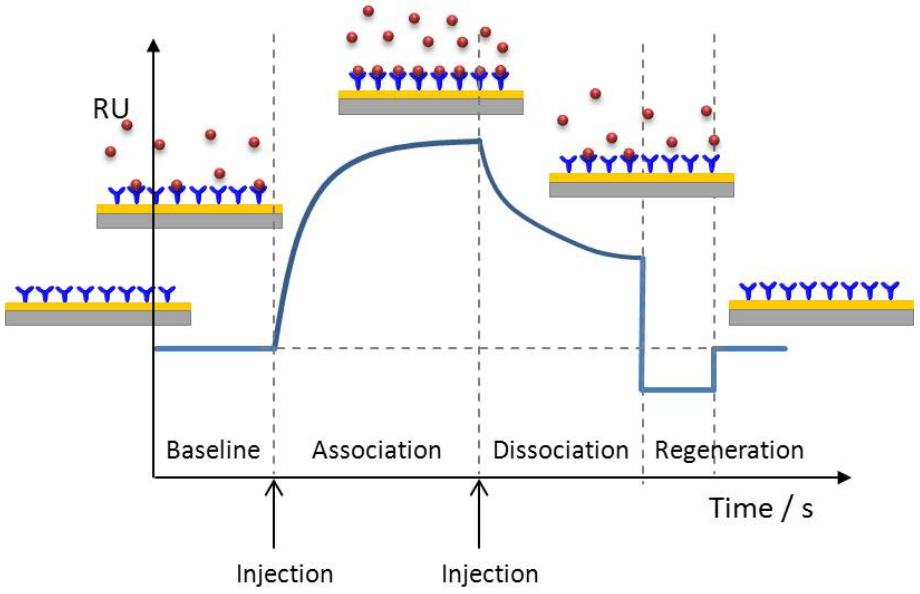

Figure 6.1: Typical sensorgram obtained by SPR measurement (adapted from [140]).

Commercial plasmonic materials like BIAcore® allow to monitor the thermodynamics and kinetics of biological binding processes by using SPR spectroscopy. They are based on thin (˜50 nm) metal films as the sensing platform. The BIAcore chips are especially more expensive than other affinity-based chips because they contain gold.[185] Buchenauer and coworkers have published a more rational and cost-effective strategy for the biosensors. They have manufactured a biosensor using a perforated polycarbonate membrane with an Au layer on one side.[145] They used the commercially available polycarbonate filter membrane as a substrate for plasmonic flow-through biosensing. The membrane has been modified by gold sputtering on its surface. Then, its sensitivity to changes of bulk refractive index has been evaluated by transmission measurements. The maximum sensitivity reached 117 nm·RIU^{-1} (refractive index units) and the average standard deviation was measured at 0.005 nm and the resolution was $4.1 \cdot 10^{-5}$ RIU. This substrate was explored using BSA and a simplified immunoassay using protein A, an IgG antibody and its corresponding antigen.

In this work, we manufactured an advanced plasmonic flow-through glyco-biosensor (PFGB). PFGB is based on the sensor chip developed by Buchenauer et al.[145] A polycarbonate membrane was used and its surface modified with glycopolymer brushes. This PFGB can not only offer an inexpensive substrate for SPR measurements, but also allows monitoring of selective and specific sugar-lectin interactions. Herein, the potential of PFGB as a diagnostic tool will also be proven using multiple modifications of gold surfaces and diverse lectin assays.

6.1.2 Results and Discussion

For the PFGB production, we used the polycarbonate filter membrane ISOPORE HTTP01300 (Millipore) with pore diameters of 400 nm. Both sides of the polycarbonate membrane were coated with an Au layer of 114 nm thickness (Figure 6.2). The gold coated polycarbonate membranes were provided by the Institute für Werkstoffe der Elektrotechnik at RWTH Aachen University and the plasmonic flow-through measurements were also performed at the same institute. The gold layers were prepared by a sputtering process. After sputtering, the membranes were stored under nitrogen atmosphere. For the fabrication of PFGB chips, the membranes were cut into the size of 1×1 cm^2. These substrates were cleaned with a solution of ammonium hydroxide (2.8-30%, Sigma-Aldrich), hydrogen peroxide (30 wt. % in H_2O, Sigma-Aldrich), and Milli-Q water; 1:1:8 (v/v), respectively. After 10 min, the membranes were immersed over night in a 2 mM solution of the ATRP initiator BisBIBED. Then, they were rinsed thoroughly with ethanol and dried by flowing a stream of nitrogen. The polymerization from the initiator modified polycarbonate membrane was performed almost in the same way as described in Chapter 2.2.5. Whereas the glycochips in Chapter 3 have been manufactured on a silicon surface, the PGlcNAcEMA were prepared from the Au coated surface as same as the IGB chips in Chapter 5. However, the total volume of the reaction mixture could be reduced to the volume of 2 ml due to the downsized PFGB chips.

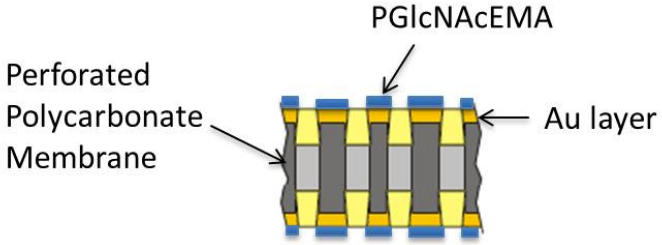

Figure 6.2: Schematic illustration (side view) of the perforated polycarbonate membrane. Both sides of the perforated polycarbonate membrane are covered with gold.

A representative polymerization process is the following: a initiator modified membrane was placed in a reaction flask under a stream of nitrogen. Into a 5 mL reaction flask, 0.24

g (0.72 mmol) GlcNAcEMA was added and dissolved in 2 ml methanol/water = 3/1 (v/v). The solution was degassed with nitrogen for 20 min. Then, 5.74 mg (0.06 mmol) CuCl, 3.24 mg (0.01 mmol) $CuBr_2$ and 22.63 mg (0.14 mmol) bpy were added and stirred under a nitrogen stream until a homogeneous dark brown solution was formed. The reactor was degassed with nitrogen further 20 min at room temperature and then transferred into the flask containing PFGB chips. The polymerization was proceeded at room temperature for a defined reaction time. Then, the chips were thoroughly rinsed with water, methanol and ethanol, and dried in a nitrogen stream. After polymerization, the grown glycopolymer brushes on the gold surface were observed by AFM. Figure 6.3 present the surface structure of the perforated membrane after PGlcNAcEMA grafting. The pores of the PFGB chip are shown as dark black dots distributed irregularly. The polymer growth can be observed using a high magnification. We can observe the glycopolymer structures in Figure 6.3c, although the structure cannot be observed clearly in comparison with the Figure 3.6. However, the grain-like gold structures are still shown in the background.

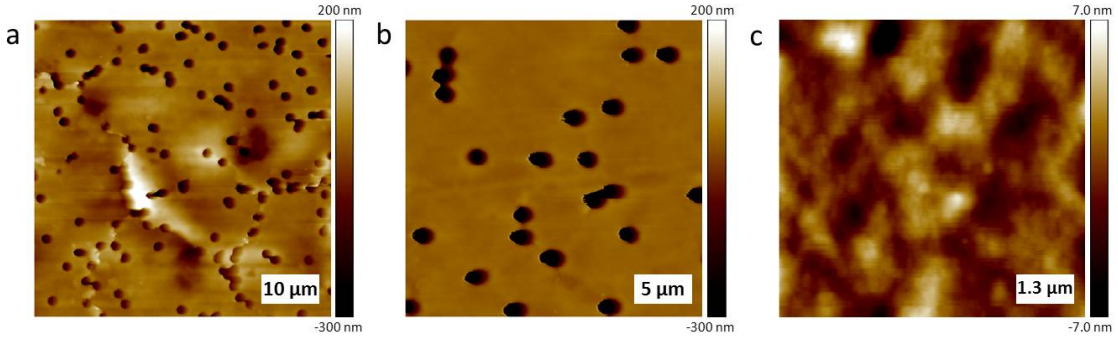

Figure 6.3: AFM height and phase images of PGlcNAcEMA grafted PFGB chips.

For the determination of the specific lectin binding to the PFGB chips, the glycans on the chip surface were enzymatically extended. The monomeric sugar pendant GlcNAcs were elongated to disaccharide LacNAc pendants. The experimental procedures were the same as described in Chapter 2.1.4. The lectin binding principle on the chip is exactly the same as shown in Figure 3.1. The lectin activities of the PGlcNAcEMA surface were also investigated by FLLA. The used FITC labelled GS-II, ECL, and His_6-SNAP-YFP-Gal-3 lectins were provided by the Lehr- Forschungsgebiet Biomaterialen (Institut für Biotechnologie und Helmholz-Institut für Biomedizinische Technik) at RWTH Aachen University. The whole measurement was done at the same institute. The detailed experimental procedures are shown in Chapter 2.1.5. Figure 6.4a shows the fluorescence and light micrographs of GS-II binding to the PGlcNAcEMA and PLacNAcEMA. The light micrographs (bottom) present no obvious difference, whereas the fluorescence images (top) are significantly different. The green fluorescence is clearly detected on the PGlcNAcEMA side, while no fluorescence was observed on the glycopolymer brushes with LacNAc pendants. The specific FITC-labelled GS-II lectin binding occurs just on the glycopolymers with GlcNAc pendants. Figure 6.4b shows the schematic illustration of the enzymatic galactosylation

on the surface. Thus, the modification of glycomonomer to glycodimer was successfully performed as the glyco brushes on silicon wafer in Chapter 3 and the impedimetric glyco brush sensor on Au substrate in Chapter 5.

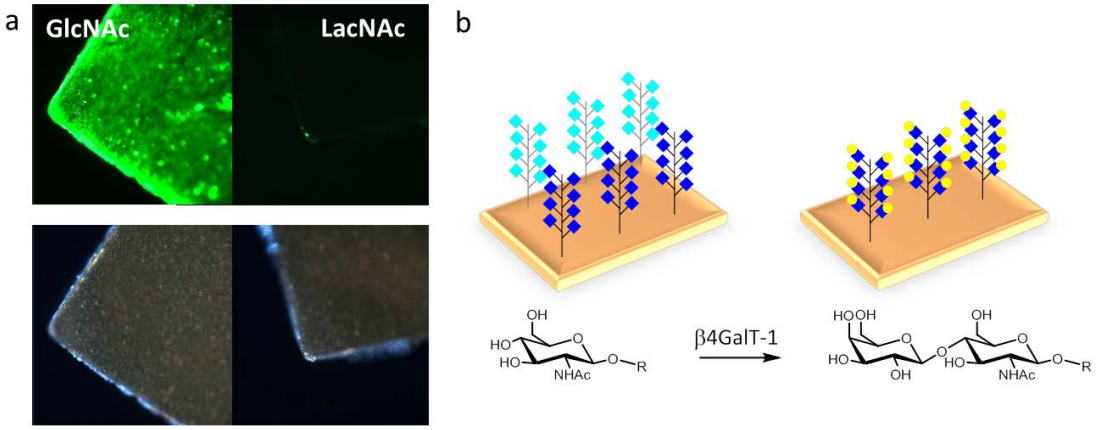

Figure 6.4: Binding of GS-II on PGlcNAcEMA and PLacNAcEMA grafted PFGB chips. a: Fluorescence (top) and light (bottom) micrographs after GS-II binding assay. b: Schematic illustration of the enzymatic modification of PGlcNAcEMA brushes to PLacNAcEMA brushes.

As next, two different lectins such as ECL and His_6-SNAP-YFP-Gal-3 were used for the binding assay. Figure 6.5a illustrates the ECL binding results. Whereas the light microscopic images present almost the same surface structure, the fluorescence micrographs show obviously difference. The galactose speceific lectin ECL binds only to the PLacNAcEMA brushes. This describes that ECL may also bind selectively to the glycopolymer brushes. As shown here, there is almost no unspecific binding on the PGlcNAcEMA grafted surface. In case of His_6-SNAP-YFP-Gal-3 lectin, the clear positive results are obtained as shown in Figure 6.5b. This Gal-3 lectin was produced by M.Sc. Sophia Böcker from Lehr- Forschungsgebiet Biomaterialien (Institut für Biotechnologie und Helmholz-Institut für Biomedizinische Technik) at RWTH Aachen University. Contrary to GS-II and ECL, this Gal-3 lectin stems from human body and plays an important role in numerous biological processes particularly in cancer. As expected, His_6-SNAP-YFP-Gal-3 shows the fluorescent marker only on the PLacNAcEMA surface containing galactose units. The light micrographs also reveal no difference between two chips. Therefore, it may be deduced that the modification of the gold coated membrane was successfully carried out and the grafted polymers were recognized by the diverse lectins very specifically.

The SPR availability of glycopolymer grafted surface was then investigated by a custom-made microfluidic equipment. Figure 6.6 shows the schematic illustration of the plasmonic flow-through measurement setup and a picture of the dissembled flow chamber on the optical microscope. The glycopolymer grafted membrane was placed in a flow chamber for

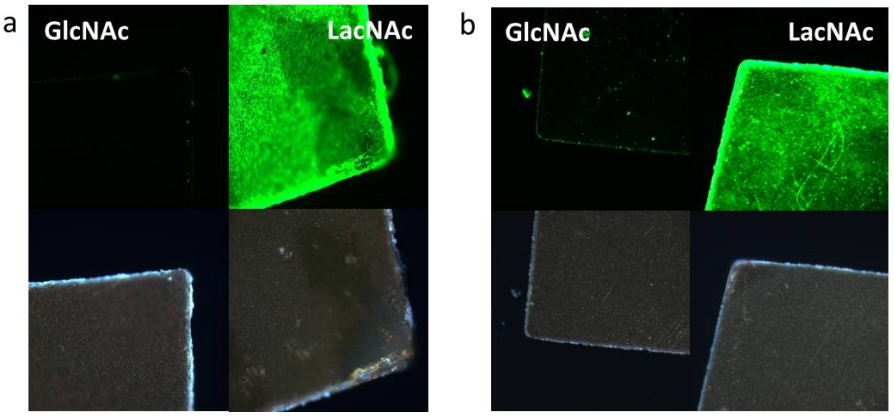

Figure 6.5: Binding of ECL on PGlcNAcEMA and PLacNAcEMA grafted PFGB chips. a: Fluorescence (top) and light (bottom) micrographs after ECL binding assay. b: Fluorescence (top) and light (bottom) micrographs after His_6-SNAP-YFP-Gal-3 binding assay.

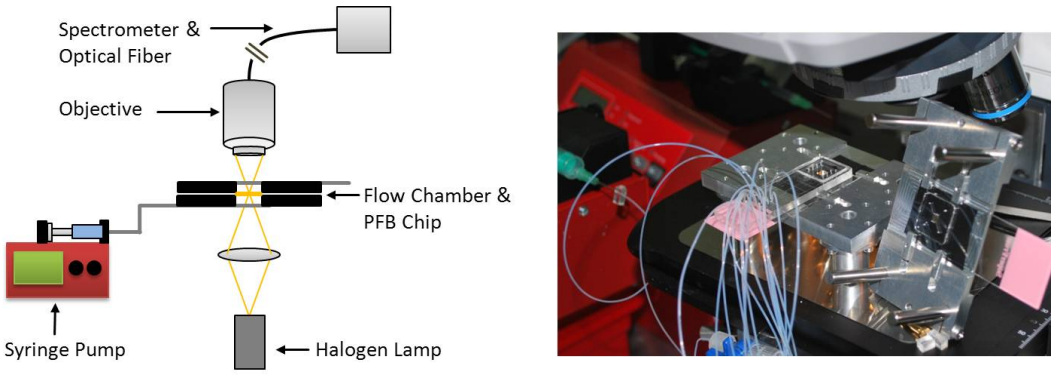

Figure 6.6: Plasmonic flow-through measurement setup. Left: Scheme of the transmission measurements carried out on an optical microscope with an attached spectrometer.[145] Right: The dissembled flow chamber with upper carrier.

the transmission measurements. A 1 mL syringe and a syringe pump (World Precsion Instrument) are used for the injection and the streaming of the fluid. During the measurement, the flow rate through the membrane is set to 0.5 $mL \cdot h^{-1}$. The transmission is measured with an optical microscope (Axioscope, Zeiss) and a spectrometer (HR2000+, Ocean Optics). The halogen lamp of the microscope was used as light source. Figure 6.7 shows a representative sensorgram of the SPR signal obtained by a plasmonic flow through measurement. At the beginning, PGlcNAcEMA immobilized PFB chips are equilibrated with HEPES buffer solution. After injection of GS-II in the microfluidic flow cell, the plasmonic signal increases. This increased signal represents the GS-II binding to the glycopolymer brushes on the Au coated membrane and hence the increase of the refractive index near the surface. An increased resonance signal is detected during the GS-II flow in the device. The signal progress is almost the same as the typical sensorgram obtained by SPR measurement (see Figure 6.1). After 1 h flow, the resonance signal reaches an equilibrium and the signal intensity is enlarged about 3 % in comparison with the initial

intensity. This signal difference is quite large to be detected, although a low concentration of protein (20 $\mu g \cdot mL^{-1}$) was used for the measurement. The injection of GS-II is stopped by replacing the system back to the buffer solution. The SPR signal then starts to decrease. This implies that the glycopolymer and the GS-II complex begin to dissociate. After 30 min, the GS-II lectin is injected a second time. The second binding plot shows almost the same progress as the first one. In this case, the equilibrium state can be more clearly observed after 30 min.

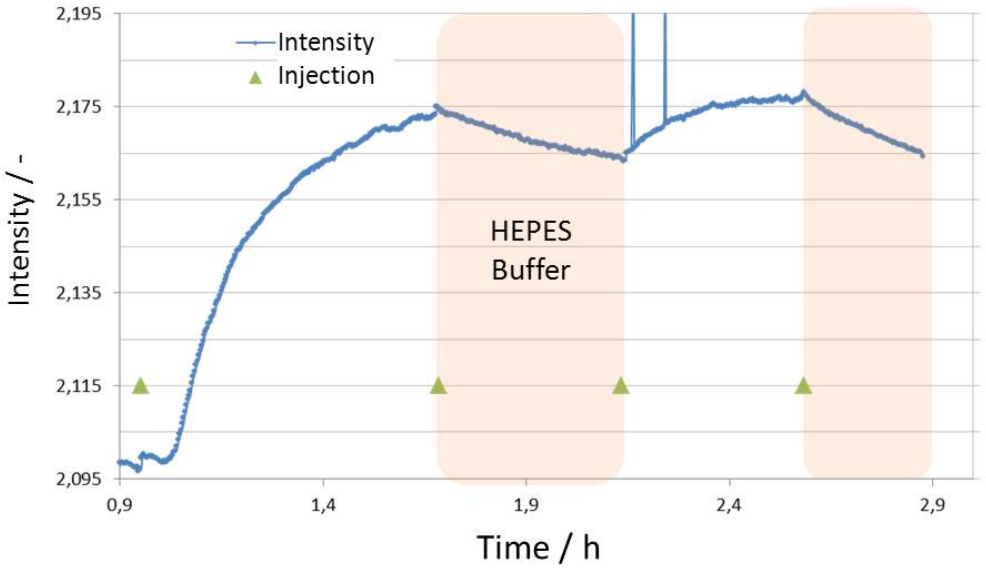

Figure 6.7: SPR sensorgram obtained by a plasmonic flow through measurement with increasing time. After GS-II saturation, HEPES buffer solution is injected and then the lectin binding test is repeated again.

Thus, the glycopolymer grafted PFGB chip has shown its applicability for the plasmonic transmission measurement. The binding events of lectin to the glycopolymer brushes could be observed very well. In addition, the measurement could be performed successively on each other. More detailed analyses were performed to ensure whether these chips can be used for diagnostic purposes. For example, the modified PLacNAcEMA brushes were employed to the SPR measurement using ECL or His_6-SNAP-YFP-Gal-3 lectin. The detailed results will be published as a journal paper soon.

6.1.3 Conclusion

Herein a commercially available perforated polycarbonate membrane was applied for the fabrication of a plasmonic flow through glycopolymer biosensor. The manufacturing of a new PFGB chip was performed by "grafting from" technique. The immobilized PGlc NAcEMA enabled a further modification of monosaccharides to disaccharides. The

different glycan pendants of the glycopolymers revealed a selective lectin binding characteristics on the chips. Furthermore, the synthesized PFGB chips have shown to be very stable and reproducible resonance signals which related with lectin binding could be obtained. In comparison with other SPR chips, these chips are very cost effective by using an inexpensive polymer membrane and multiply measurable as shown in SPR measurement. In addition, they have shown a very selective surface by direct glycan modification on the surface and could be recognized by recombinant lectin, namely His_6-SNAP-YFP-Gal-3 lectin. These results give a great potential of the PFGB chips as future diagnostic tools.

6.2 Surface Acoustic Wave Sensor for the On-line Monitoring of Polymerization

6.2.1 Introduction

As mentioned before, microfluidics has become more interest because of its combination ability with wide fields such as chemistry, biology and medicine. Microfluidics has been researched intensively to generate small-sized analytical devices so-called "lab-on-a-chip" devices. They have several advantages such as system miniaturization, automation, reduced amount of reagents, low cost, and precise microenvironment control. To improve their functionality, versatility and performance, many new microfluidic platforms have been introduced, for example, by the integration of new physical techniques.

Many polymerization technologies have been employed to control composition, thickness, topography, wetting, and viscoelastic properties of polymer brushes. However, there are very few reports to tackle actual brush growth on the surface.[186, 187, 188] Therefore, combining the SAW microfluidic technology with the ATRP polymerization technique will extend the respective system to create a versatile monitoring device. This new platform is beneficial for the fundamental understanding as well as the up-scaling of the polymerization. Herein, we describe real-time monitoring of PHEMA brush growth from the SAW chip surface and the potential applications of this technique will be discussed later.

6.2.2 Results and Discussion

In case of IGB and PFGB, the purification of the respective chips and modification with ATRP initiators were accomplished in different reaction flasks. The initiator modified chips were polymerized before they were assembled into the microfluidic chamber. The polymer coated chips could be then covered with polymer lid if necessary and placed in the corresponding devices. When the whole device was set up, the measurement could

be carried out. However, the SAW based microfluidic system was fully automated from purification to polymerization. This means the SAW chips were mounted at first on the equipment and then the solution of ammonium hydroxide/hydrogen peroxide/Milli-Q water = 1:1:8 (v/v) was flown through the PTFE microfluidic channel to clean the surface of chips. As next, the ATRP initiator was injected to the channel and let react over night. Because the ATRP system is very sensitive to oxygen, a special polymerization chamber was developed in-house to maintain the deoxygenated condition as shown in Figure 6.8b. Thanks to this reaction chamber, the polymerization of HEMA was performed after flushing ethanol in the channel. Therefore, only one reaction chip was necessary for the whole procedure. This is a great advantage of the SAW chips described here.

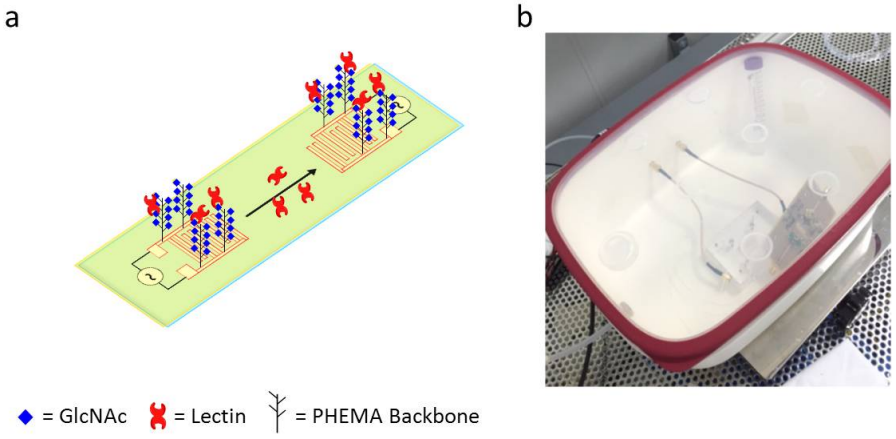

Figure 6.8: SAW measurement setup. a) Schematic illustration of SAW device. b) The polymerization reaction chamber containing SAW device.

Figure 6.8a illustrates the schematic construction of a SAW chip which was developed by the Institute für Werkstoffe der Elektrotechnik at RWTH Aachen University. The SAW chips were manufactured on the silicon wafer and the electrodes were made by gold sputtering. The Au electrodes were covered with a silicon lid and hence a microchannel was produced. 1 mL syringe and a syringe pump (World Precision Instrument) are used for the injection and the streaming of the fluid. During the measurement, the flow rate through the membrane is set to between 0.5 $mL{\cdot}h^{-1}$ and 1 $mL{\cdot}h^{-1}$. The piranha solution was flown through the PTFE tube in the microchannel. After purification, a 2 mM solution of the ATRP initiator BisBIBED was prepared and injected in the microfluidic channel. The modification of the Au coated SAW chip was processed overnight. Then, ethanol was used for the rinsing to remove the remaining initiator. Before the polymerization, the chip was accommodated with a mixture containing catalyst and ligand. This mixture was prepared using the same amounts of catalyst and ligand which were used for the polymerization of HEMA, without HEMA monomer in this mixture. The mixture was also degassed for 20 min and then injected to the microchannel. The only difference between this mixture and the polymerization solution was the monomer HEMA. Therefore, the measured signal might result from the growth of HEMA from the surface of the SAW chip. In addition, the

lectin binding properties may be investigated on the PHEMA coated SAW chip. However, we will focus on the monitoring of HEMA polymerization in this work.

The polymerization solution was prepared as described in Chapter 5.2.1. 0.38 mL (3.15 mmol) HEMA was added in 10 mL methanol/water = 3/1(v/v) and stirred under nitrogen at room temperature for 10 min. Then, 98.36 mg (0.63 mmol) bpy, 24.95 mg (0.25 mmol) CuCl, and 14.07 mg (0.06 mmol) $CuBr_2$ were added into the HEMA mixture and stirred under nitrogen further 20 min. The produced dark brown mixture was transferred into the degassed SAW chamber. The change of the frequencies due to the growth of polymer on the surface was monitored during the polymerization. A high frequency around 129 MHz ± 1 MHz was set for the SAW measurement. The frequency signal was passed into the electronic counter and the variation of the resonance frequency was monitored continuously with a time resolution of 10 s. To study the effect of HEMA on polymerization, the same mixture which did not contain the monomer HEMA was flushed in the microfluidic chamber. Any change of signal might be caused only from the conversion of HEMA. As the mass increases on the surface, it decreases the frequency in the oscillator circuit. Consequently, an increased resonance frequency could be observed during the polymerization.

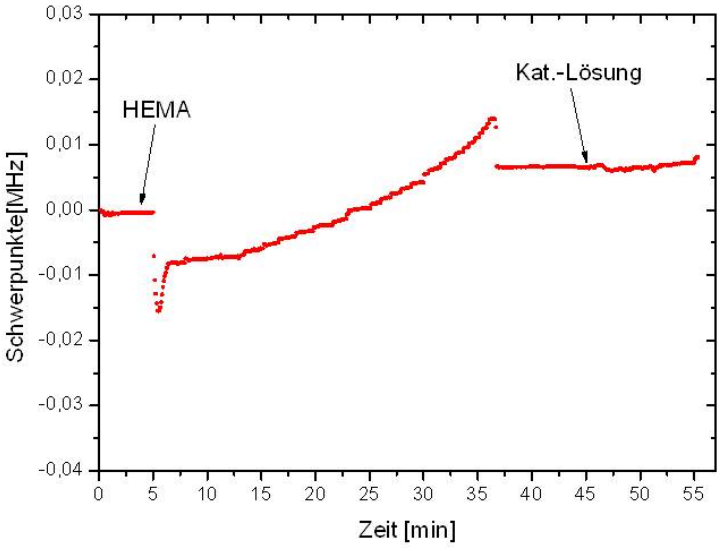

Figure 6.9: SAW sensorgram illustrating SAW signal against time. The solution containing HEMA was injected at 5 min and the polymerization of HEMA was observed for 30 minutes.

Figure 6.9 shows the SAW sensorgram during the HEMA polymerization. After HEMA injection, the resonance frequency increased until the injection of the catalyst and ligand mixture. Because HEMA is the only difference between the rinsing solutions, the increased resonance frequency may result exclusively from the adsorption of HEMA monomer on the

surface. As shown here, the growth of HEMA indicates nearly a linear behaviour. After washing with catalyst/ligand solution, no growth was observed. The linear growth of HEMA on the surface could be clearly observed by the linear error adjustment (data not shown). However, the growth of polymer chains is quite slow in comparison with Figure 3.2 in Chapter 3. The detailed analyses of e.g. the thickness of the grown polymer and the relationship between the concentration and the polymer growth are necessary to clearly understand the polymerization process. The detailed experiment will be reported later on.

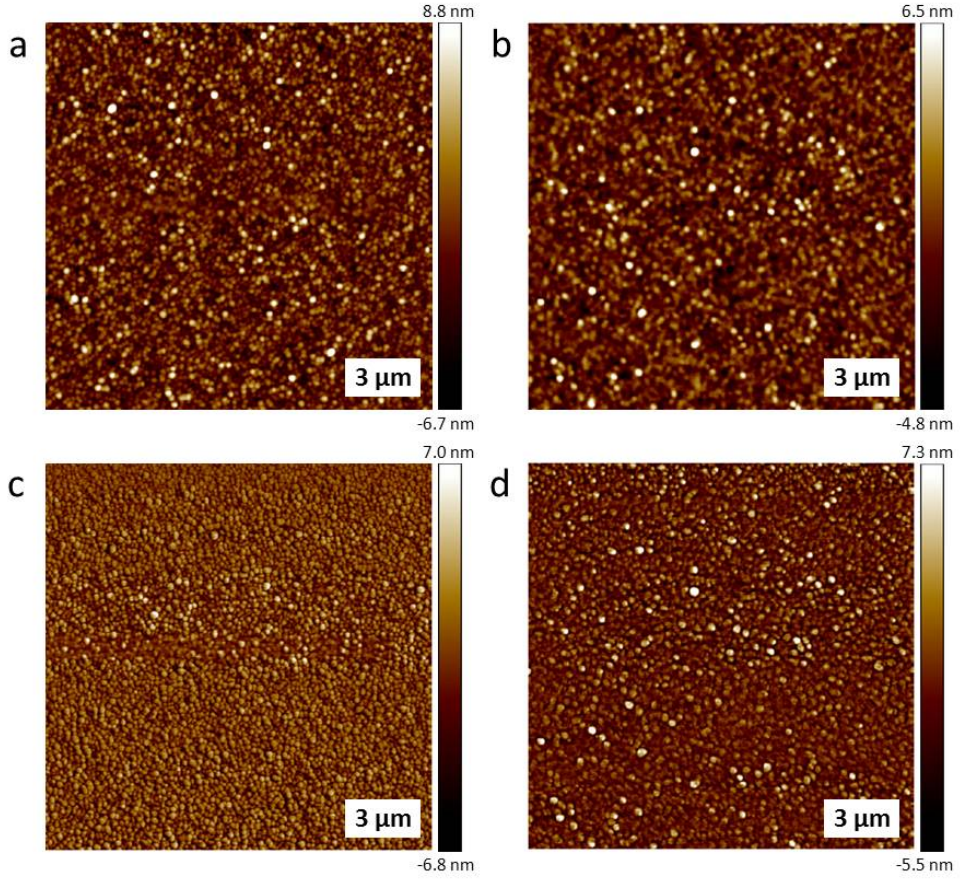

Figure 6.10: AFM micrographs of pure Au surfaces (a, c) and PHEMA grafted Au surfaces (b, d). top) Height images and bottom) phase images.

It is difficult to measure convincing AFM images of the Au electrodes of SAW chip because of their narrow bands. Therefore, pure Au surfaces were undergone by Au sputtering on glass and the HEMA polymerization was performed the same as for the SAW chip. After the polymerization of HEMA on Au, it was rinsed by methanol/water followed by pure water using the microfluidic system. Then, the PHEMA coated surface was compared with a pure Au surface to determine the actual PHEMA formation. Figure 6.10b and 6.10d present AFM micrographs of PHEMA grafted Au surfaces and 6.10a and 6.10c the pure Au surface. In the first view, it seems that there are no differences between pure and PHEMA coated surfaces. However, the small spots of Au elements shown on the pure Au

surface (6.10a and 6.10c) are not observed from the PHEMA surface (6.10b and 6.10d). Instead, little larger points of PHEMA are visible here. The relatively rough Au surface seems to be filled with PHEMA brushes and hence the polymer coated surface seems to be a much more even surface. This estimation was proven by the calculation of surface roughness using AFM analysis. The value is 1.623 nm ± 0.052 nm for the pure Au surface and 1.128 nm ± 0.032 nm for the PHEMA brushes. This result not only confirms the statement about the filling of the rough surface with polymer but also agrees well with the result from Chapter 5.2.2. However, the thickness of PHEMA brushes measured by AFM is significantly reduced in comparison with that of Figure 5.5. This result might refer to the slow growth of PHEMA chains observed from the SAW measurement (Figure 6.9). Such a polymerization using a microfluidic device may decelerate the polymer chain growth significantly to downsize the length of polymer chains.

6.2.3 Conclusion

In this chapter, a novel microfluidic SAW chip was fabricated for the online monitoring of the ATRP process. The measured frequency signals showed a linear progress. There are still ambiguities concerning the polymerization kinetics and the thickness of the polymer coated chip. However, the feasibility of a SAW chip as a potential "lab-on-a-chip" could be clearly noticed. Therefore, this novel platform might enable the deeper understanding of polymerization processes and pursue for extended applications such as SAW biosensors.

7 Silica-Polymer Core-Shell Microspheres via ATRP

7.1 Introduction

Silica-polymer hybrids are the most commonly used materials among the numerous organic-inorganic hybrid materials. Silica nanoparticles (NPs) have a broad application range such as filters, rubber products, and plastic binders. The surface modified silica particles are used for versatile applications including chromatography stationary phases and heterogeneous supported catalysts. Silica particles have several known advantages such as easy synthesis, precisely controllable size and distribution.[189] A simple generation process of monodisperse silica particles was discovered by Stöber et al. in 1968.[190] The Stöber method is a one-pot synthesis which is carried out under alkaline conditions in ethanol. The size-controlled Stöber silica particles are prepared by a sol-gel methodology in which the hydrolysis and condensation of tetraethyl orthosilicate (TEOS) are performed. The hydrolysis reaction is initiated by hydroxyl anions on TEOS molecules. The chemical reaction can be represented using a chemical equation as follows:

$$\mathrm{Si(OC_2H_5)_4 + 4\ H_2O \rightarrow Si(OH)_4 + 4\ C_2H_5OH} \tag{7.1}$$

$$\mathrm{Si(OH)_4 \rightarrow Si(O)_2 \downarrow + 2\ H_2O} \tag{7.2}$$

After the hydrolysis reaction (Eq. 7.1), the condensation reaction (Eq. 7.2) follows immediately.[191] The overall reaction is expressed as follows:

$$\mathrm{Si(OC_2H_5)_4 + 2\ H_2O \rightarrow Si(O)_2 \downarrow + 4\ C_2H_5OH} \tag{7.3}$$

The hydroxy groups on the surface of silica particles can be easily modified with polymers.[192, 193, 194] In general, the main challenge in preparing silica particles is known as the controlled particle dispersing. The grafting polymer chains around the silica particles can control the particle aggregation by steric repulsions and improve the mechanical properties of the composite. There are potential uses of the polymer grafted silica particles

especially in material science as novel separation materials. Hollow polymeric nanocapsules using silica NPs may have another potential application such as encapsulation of drugs and dyes. Thus, silica particles have not only a large surface area, well-defined pore size and shape, but also specific binding sites for suitably substituted polymers. Matyjaszewski et al. have reported a simple and general procedure for preparing thermally stable Au-NPs via a one-pot SI-ATRP.[195] A thin cross-linked polymer shell was formed around the surface of each Au-NP before the polymerization of linear polymer brushes. The SI-ATRP was performed using a monomer/cross-linker pair with unequal reactivities such as *n*-butyl acrylate and ethylene glycol dimethacrylate. In addition, inter-particle coupling reactions were prevented by keeping concentrations (1.7 - 7.2 mg·mL^{-1}) of the nanoparticles low.

The multivalent presentation of glycopolymers could be realized by several methods including the surface immobilization of glycopolymers.[29] Usually, the surface grafting of glycopolymers on silica particles is done via thiol functional groups. Guo et al. have reported lactose-containing polymers synthesized via the RAFT technique.[196] The glycopolymers with dithioester residues were grafted onto the γ-methacrlyoxypropyltrimethoxy modified silica gel particles. Müller and co-worker have addressed about the synthesis of galactose-displaying core-shell nanospheres exhibiting both fluorescent and magnetic properties.[197] These nanoparticles were prepared by grafting a glycopolymer consisting of 6-O-methacryloylgalactopyranose and 4-(pyrenyl)butyl methacrylate onto magnetic silica particles. The grafting was succeeded by thiol-ene chemistry.

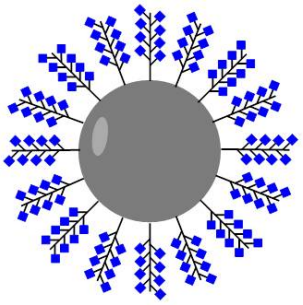

Figure 7.1: Schematic illustration of the cross-section view of a silica-glycopolymer core-shell particles. Silica particles act as the core and PGlcNAcEMA as the shell of the particles.

Herein, we describe a novel synthesis of silica-glycopolmyer core-shell particles by SI-ATRP from intiator grafted silica NP. Figure 7.1 presents the cross-section view of a silica-glycopolymer core-shell particle illustrating the multivalent presentation of glycopolymers. The silica NPs are prepared by the well-known Stöber method. The polymerization is performed from the initiator coated surface. The size of the synthesied core-shell particles was characterized by DLS and their structures observed by AFM, TEM and FESEM.

7.2 Results and Discussion

The silica microspheres surrounding glycopolymers were fabricated by the SI-ATRP technique. Figure 7.2 illustrates the reaction scheme for the synthesis of covalently attached PGlcNAcEMA on silica using the alkyl halide initiator EBiB.

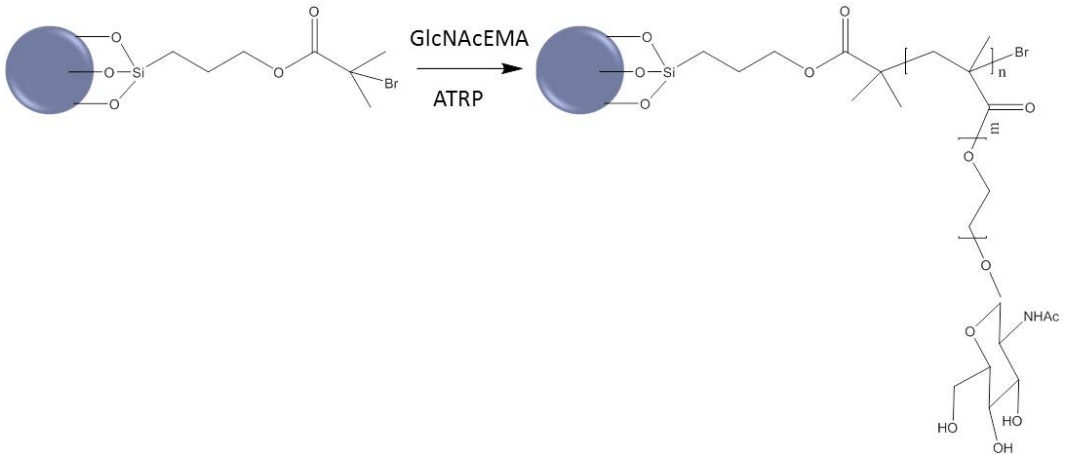

Figure 7.2: Synthesis of silica-glycopolymer core-shell particles.

The SiO_2 cores have been synthesized by the Stöber method. To get silica NPs, a mixture of 25 mL pure ethanol and 2.1 mL of ammonia were heated to 60 °C in a two-neck round flask equipped with a reflux condenser. After 30 min equilibrium time, 1.5 mL of TEOS (Sigma-Aldrich) were added to the solution under stirring at 100 rpm. The solution was stirred further for 18 h at 60 °C. The colloidal solution was then cooled down to room temperature and stored in a refrigerator (T ≈ 4 °C). The colloidal dispersion was purified by centrifugation at 8500 rpm for 30 min and redispersed in pure ethanol. For the functionalization of silica with the ATRP initiator, 20 μL of 3-(trimethoxysilylpropyl)-2-bromo-2-methylpropionate was added to 5 mL of the SiO_2 dispersion. The mixture was stirred at room temperature overnight, followed by heating to 70 °C for 1 h to ensure covalent bonding. The colloidal solution was cooled down to room temperature and centrifuged at 8500 rpm for 1 h. The functionalized silica was redispersed in 15 mL solvent and centrifuged. This procedure was repeated two times in ethanol and two times in water. Then, the particle size of 143 nm ± 6.5 nm in diameter was determined by DLS and the particle structure was observed by TEM (Figure 7.3) and FESEM (Figure 7.4). For the microscopic measurements the silica solution was diluted with water and spin-coated on the plasma treated silicon wafer. TEM as well as FESEM micrographs present the spherical silica particles. The particles are proven to be very homogeneously in size distribution and the measured size corresponds well to the DLS measurement.

The HEMA and GlcNAcEMA monomer were polymerized from the initiator layer by SI-ATRP. The feasibility of the polymerization from the silica particles was investigated and

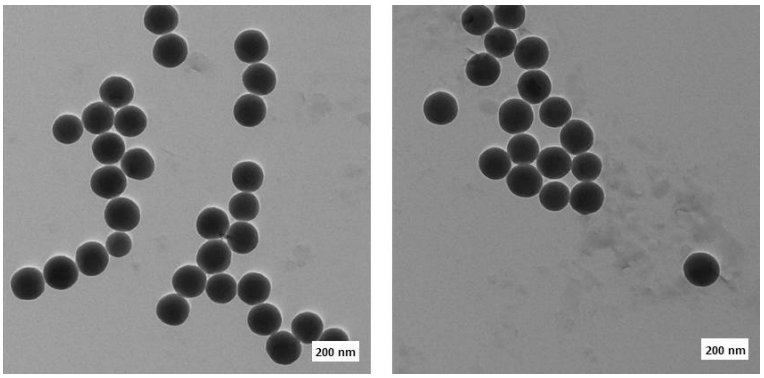

Figure 7.3: TEM micrographs of initiator modified silica NPs.

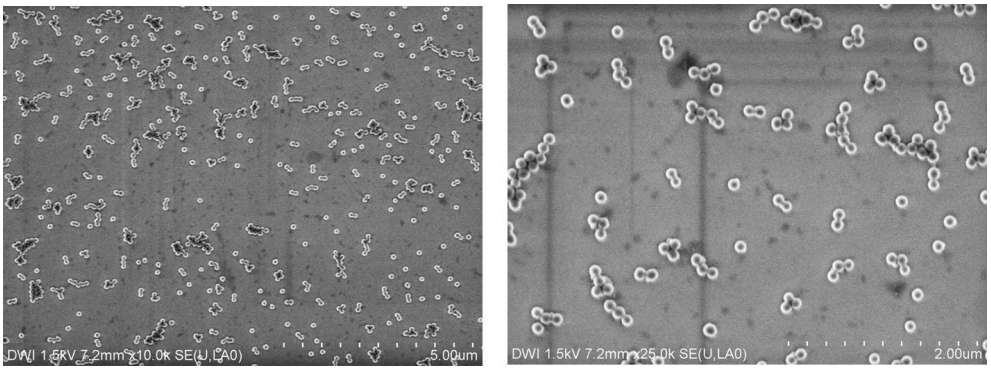

Figure 7.4: FESEM micrographs of initiator modified silica NPs.

the difference between these two polymers was observed by microscopic measurements. We started with HEMA to polymerize in order to find the optimal conditions of the polymerization, because HEMA is a commercially available monomer. The polymerization process of GlcNAcEMA was adapted to almost in the same conditions as that of HEMA, because the GlcNAcEMA is distinguished mainly in the monomeric sugar unit. In a typical HEMA polymerization, 170 µL (1.40 mmol) HEMA and 100 µL silica dispersion were mixed with 12 mL of methanol/water = 1/1 (v/v). The mixture was stirred under nitrogen for 20 min. After that, 21.87 mg (0.14 mmol) bpy and 10.04 mg (0.07 mmol) CuBr were added into the solution and degassed with nitrogen for further 20 min. The tube was sealed and stirred at room temperature for 24 h. The solution was purified by centrifugation (8500 rpm, 1 h) and then redispersed in water. This step was repeated three times. The TEM micrograph presents the core-shell particles very well as shown in Figure 7.5a. The thickness of the polymer is estimated to 8.9 nm ± 1.1 nm from the TEM images. The silica NP with PHEMA coating have a size of ± 7.6 nm in diameter. However, the particle size determined by DLS records 572.4 nm ± 95.04 nm in diameter. This large difference of the measured size between DLS and TEM might result from the agglomerates of PHEMA coated silica particles. In particular, Figure 7.5b and Figure 7.6 show the agglomeration of PHEMA grafted silica particles obviously. Although the SI-ATRP was performed successfully from the silica NPs, the controlled particle dispersing

is still left as a challenge to overcome. The polymer coated silica particles reveal the tendency to build inter-particle aggregation.

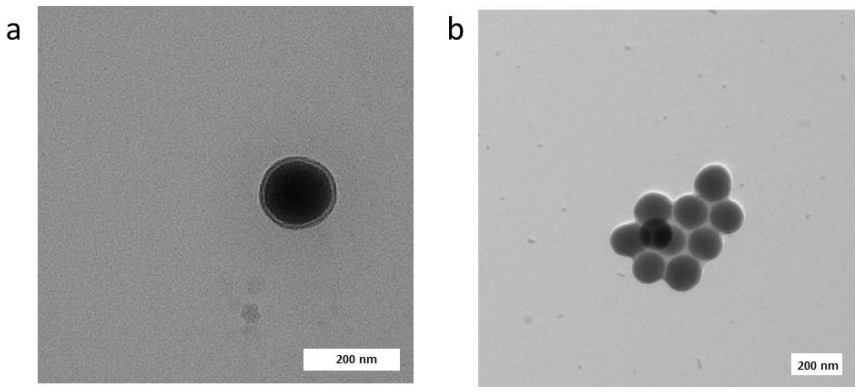

Figure 7.5: TEM micrographs of PHEMA coated silica NPs.

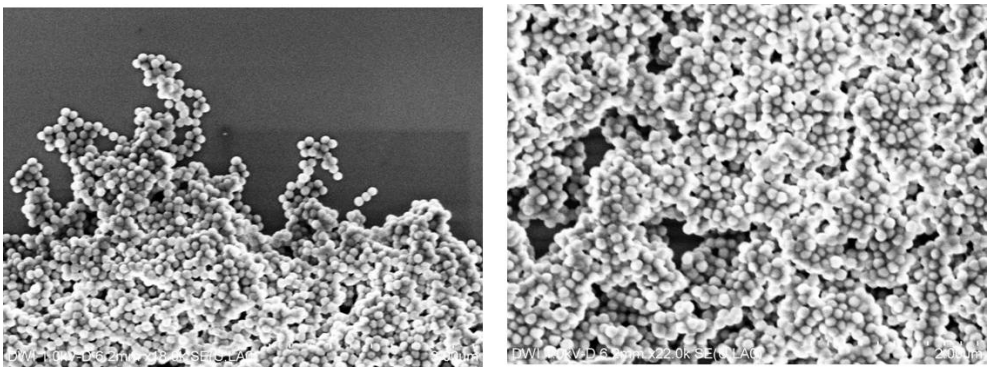

Figure 7.6: FESEM micrographs of PHEMA coated silica NPs.

As next, we prepared PGlcNAcEMA grafted silica particles using the same procedures as for PHEMA-silica particles. Typically in the polymerization process, 624.16 mg (1.87 mmol) GlcNAcEMA glycomonomer and 12.48 μL of the initiator functionalized silica solution were mixed with 3.1 mL of methanol/water = 1/1 (v/v). The mixture was stirred under nitrogen streaming for 20 min. Then, 58.49 mg (0.37 mmol) bpy, 14.83 mg (0.15 mmol) CuCl and 8.36 mg (0.014 mmol) $CuBr_2$ were added into the solution. The mixture was degassed with nitrogen for further 20 min. The reaction tube was sealed and stirred at room temperature for 24 h. The solution was purified by centrifugation in the same way for the HEMA polymerization. The DLS measurement determines an average particle size of 557.0 nm ± 11.31 nm. The TEM (Figure 7.7) and FESEM (7.8) images show the successful polymerization of GlcNAcEMA on silica particles. In particular Figure 7.7 presents clearly the formation of core-shell structure. In TEM micrographs, the silica particles are shown as dark circles and the PGlcNAcEMA as light gray layers surrounding the particles. Composing with the thickness of polymer layers estimated around 10 nm, we could characterize the size of particles to be around 153.5 nm. These PGlcNAcEMA grafted silica particles also reveal the agglomerated structures. The FESEM images present large agglomerations of particles. In spite of the huge size of agglomerates, the glycopolymer

layers surrounding silica particles can be also obviously observed.

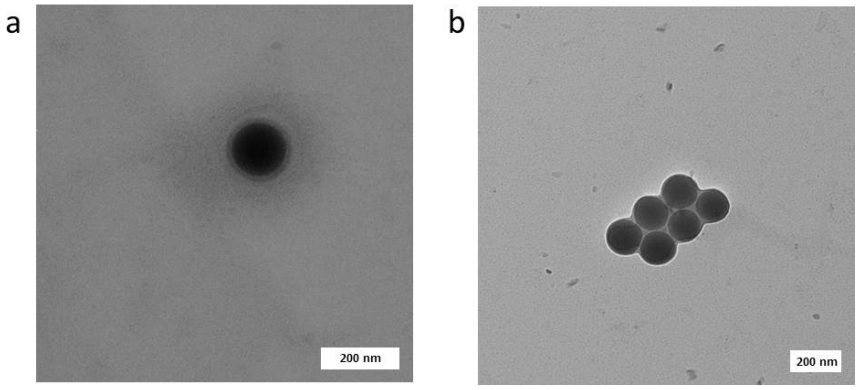

Figure 7.7: TEM micrographs of PGlcNAcEMA coated silica NPs.

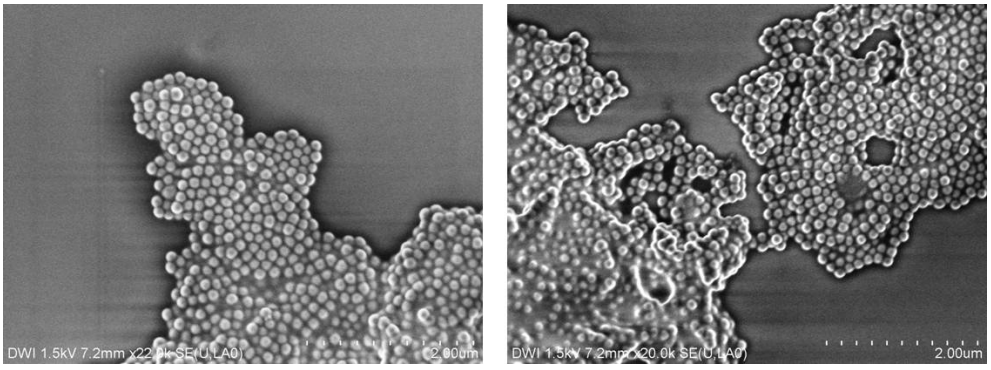

Figure 7.8: FESEM micrographs of PGlcNAcEMA coated silica NPs.

As shown before, the main problem in the preparation of the core-shell particles using the ATRP method was the tendency of particle agglomeration. This seems to be caused by inter-particle coupling reactions. Figure 7.9 presents the photographs of the silica particle solution. As shown here, the sample solution precipitated for 10 min represents that the silica paricles are not water-soluble any more after polymerization. In case of PHEMA grafted particles, this phenomenon may be caused by its water-insoluble polymer shells. For silica paricles with PGlcNAcEMA shells, the inter-particle coupling may result in the agglomerated glycopolymer particles. Hence, the large agglomerates might change the formation of hydrophilic sugar pendants. For better understanding of these results, more detailed analysis is required. To compare the particle size and structure, the differently coated silica particles are utilized for the AFM measurement. Figure 7.10 shows the AFM height images. The spheric silica particles are observed in Figure 7.10a and after initiator modification of silica NPs in labelled (b). No big changes in the silica particles were found especially in their structure. The polymerization of HEMA and GlcNAcEMA results in obviously changes of the particle shape. Figure 7.10c and d reveal polymer clouds surrounding the particles.

Although the polymerisation of HEMA and GlcNAcEMA was carried out successfully on

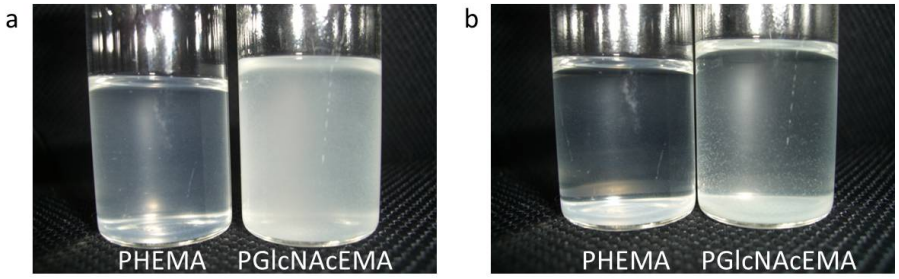

Figure 7.9: Precipitation of PHEMA and PGlcNAcEMA coated silica particles in water. a) Direct before the sample preparation. b) 10 min later after sample preparation.

the silica NPs, there are still some problems such as the agglomeration and precipitation of particles. To solve this problem, new experiments were performed using filtration and ultra-sonification. However, the solutions still contain agglomerated particles from this approach. As shown by TEM images before, the inter-particle interaction may be reduced by using a highly diluted silica NP dispersion for the polymerization.

7.3 Conclusion

In this chapter we described the feasibility of HEMA as well as GlcNAcEMA polymerization from the silica surface. The TEM micrographs of the silica particles revealed clear core-shell structures after polymerization of both monomers. The cloud-like shell structures of particles have shown to be beyond 10 nm thickness in water. The main problem of the synthesis was the particle agglomeration. Whether this phenomenon took place during or after the polymerization remains still an open question. However, some images of TEM have shown quite good single particle structures. Therefore, the problem may be solved by using highly diluted particle solutions. The detailed analysis of polymer grafted silica particles may also help to solve this issue. In addition, it is expected that the synthesized glycopolymer coated silica particles may present biological activity such as specific lectin binding and hence stimulate an application as screening materials of diverse lectins.

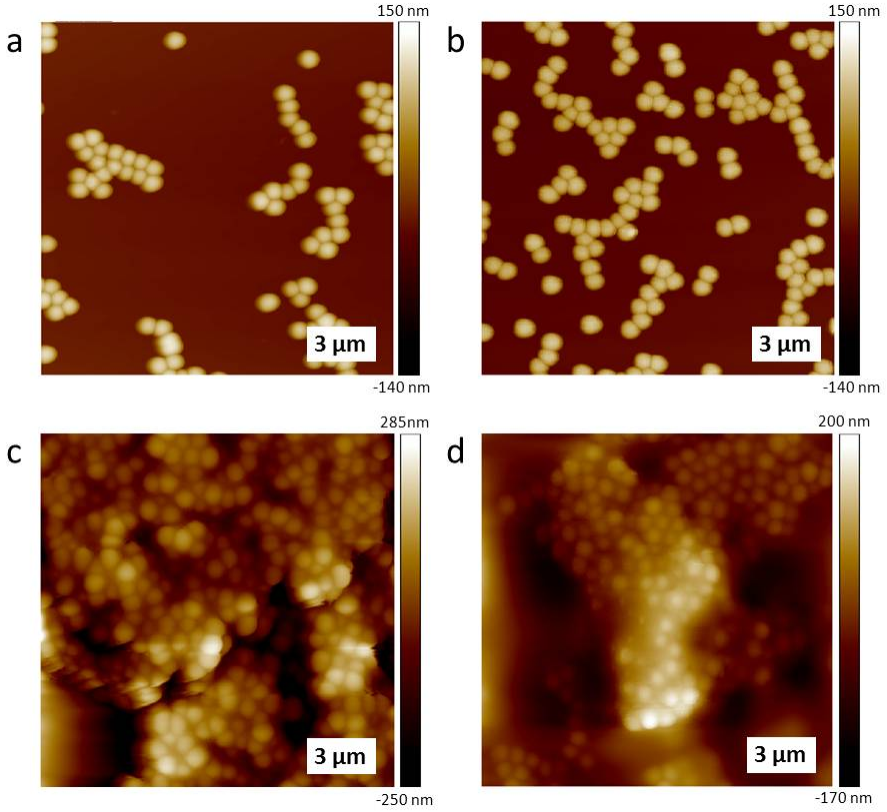

Figure 7.10: AFM micrographs of a) silica NPs, b) initiator modified silica NPs, c) PHEMA grafted and d) PGlcNAc grafted silica NPs.

8 Glycomicelles in Water

8.1 Introduction

In recent years, there has been an increasing attention in the use of the synthesis of polymerizable vinyl sugars. According to recent reports, it would be advantageous to synthesize polymerizable vinyl sugars thanks to their controlled polymerization property.[198, 41, 9, 24] Unlike polysaccharides, such polymers have an all-carbon backbone and pendant saccharide units. They are hydrophilic due to their large number of hydroxy groups and hence can be applied as water-soluble non-ionic polymers. These hydrophilic glycopolymers have been used to synthesize amphiphilic diblock glycopolymers by the construction with a hydrophobic glycopolymer block. These amphiphilic diblock copolymers can self-assemble into various architectures such as micelles or vesicle/liposomes. Their spherical and three dimensioned structures may display much higher affinity towards binding lectins due to their larger surface area as illustrated in Figure 8.1. However, the interaction between sugars and lectins needs to be carefully analyzed because glycopolymers are presented not in their linear configuration but in the form of aggregated structures.[10, 3]

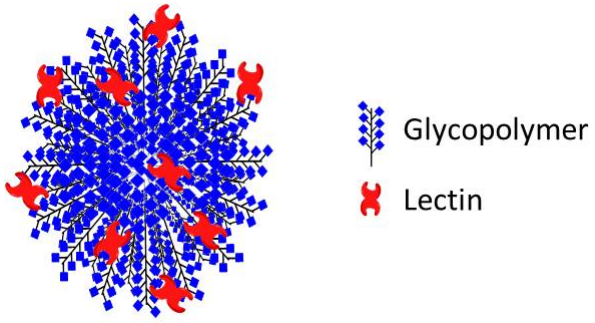

Figure 8.1: Schematic illustration of letin binding to a diblock glyco-copolymer micelle.

Ironically, not all the synthetic glycopolymers have a strong binding ability towards lectins in spite of their multivalent carbohydrate presentation. For example, León and coworkers have synthesized poly(butyl acrylate)-b-poly(2-[(D-glucosamin-2-*N*-yl)carbonyl]oxyethyl methacrylate) (PBA-b-PHEMAGI) diblock glycopolymer and PHEMAGI-b-PBA-b-PHEMAGI triblock glycopolymer.[3] These glycopolymers were self-

assembled in aqueous solution as spherical micelles with the coexistence of polymeric vesicles. In addition, the binding ability with the lectin Concanavalin A was influenced by the copolymer composition such as increasing the length of the hydrophilic glycopolymer segment in the block copolymer. However, the architecture of the block glycopolymers, di- or triblock copolymer, did not seem to have an influence on the lectin binding process. In contrast to this, Minoda and coworkers have shown a much increased recognition ability of amphiphilic glycopolymers toward lectin wheat germ agglutinin compared to monovalent GlcNAc itself and its oligomers. For the measurement, they used synthetic amphiphilic block copolymers of vinyl ethers having pendant GlcNAc residues synthesized by living cationic polymerization of isobutyl vinyl ether and GlcNAc carrying vinyl ether.[199] Thus, modified carbohydrate-based conjugates have been investigated not only for the study of carbohydrate-lectin interaction, but also for the application of therapeutic purposes recently.[200, 152]

Despite the advantages of synthetic amphiphilic glycopolymers, by far less research has been directed to their synthesis owing to the synthetic difficulty. In this work, ATRP was applied to the synthesis of a well-defined diblock glycopolymer being composed of a PHEMA and a PGlcNAcEMA block. First, the synthesized diblock glycopolymer was characterized by NMR spectroscopy, GPC and several microscopic measurements such as TEM, in situ TEM, AFM and FESEM. Then, dynamic light scattering (DLS) and fluorescence correlation spectroscopy (FCS) were used to investigate the lectin binding properties in detail.

8.2 Results and Discussion

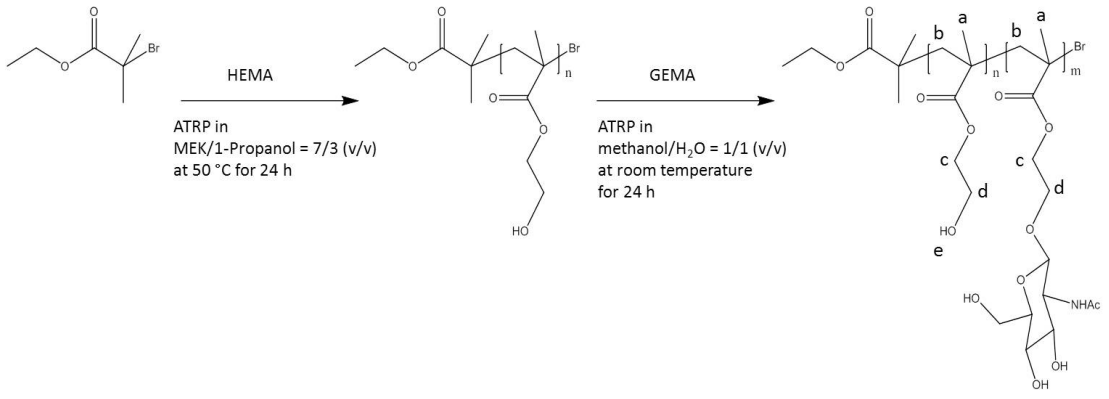

Figure 8.2: Synthesis of the diblock glyco-copolymer PHEMA-b-PGlcNAcEMA.

Figure 8.2 shows the schematic illustration of the diblock glyco-coplymer PHEMA-b-GlcNAcEMA synthesis. The polymerization of HEMA was performed in a 50 mL round bottom flask. 15.0 mL (123.50 mmol) HEMA was placed into the reaction flask and stirred

in 15.0 mL of methyl ethyl ketone (MEK)/ 1-propanol = 7/3 (v/v). The reaction mixture was degassed with nitrogen and preheated to 50 °C for 20 min. Then, 354.32 mg (2.47 mmol) CuBr, 0.77 g (4.94 mmol) bpy and 362.5 µL (2.47 mmol) EBiB were added and stirred under a nitrogen stream until a homogeneous dark brown solution was formed. The reactor was degassed with nitrogen for further 20 min. The polymerization was proceeded at 50°C for 24 h. The synthesized polymer was collected by passing through a column packed with silica to remove the catalyst. The polymer was precipitated from cold diethyl ether several times to withdraw traces of residual monomer and initiator. After filtration, the purified white polymers were dried in vacuum oven and analyzed by NMR spectroscopy and GPC. On top of the Figure 8.3, the ^{1}H NMR spactrum of PHEMA is displayed. The peaks around 1 ppm is attributed to methyl protons of HEMA segments and at 3.6 and 3.8 ppm are ascribed to methylene protons. The peak at 4.8 ppm is assigned to the hydroxyl group of PHEMA in the precursor polymer. The molecular weight of PHEMA amounts to $3{,}9{\cdot}10^3$ g·mol^{-1} with a low polydispersity of 1.14. These results demonstrate the polymerization process in a quite controlled manner.

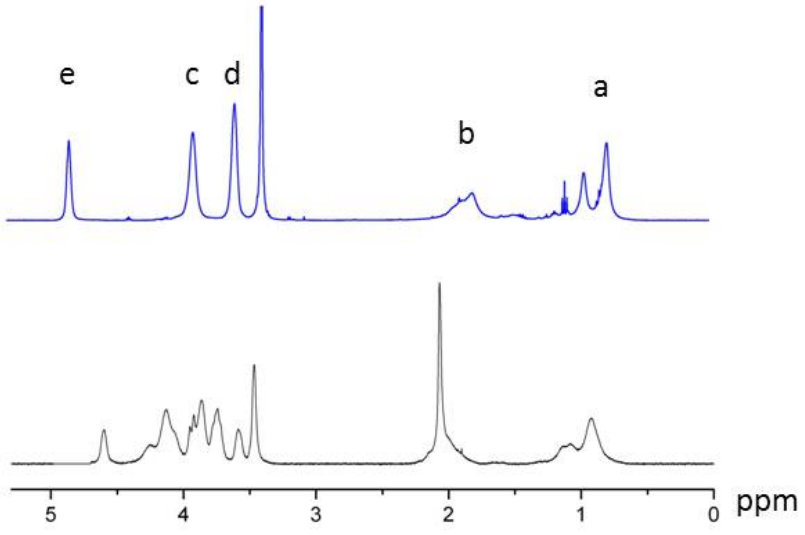

Figure 8.3: ^{1}H NMR spectrum of PHEMA and PHEMA-b-PGlcNAcEMA. (Top): ^{1}H NMR spectra of PHEMA. Polymerization condition: [m]/[EBiB]/[CuBr]/[bpy] = 50/1/1/2 mol in 7/3 (v/v) MEK/1-propanol mixture, at 50 °C for 24 h. (Bottom): ^{1}H NMR spectrum of PHEMA-b-PGlcNAcEMA. Polymerization condition: [m]/[PHEMA]/[CuBr]/[$CuBr_2$]/[bpy] = 50/1/0.8/0.2/2 mol in 1/1 (v/v) methanol/water mixture, at room temperature for 24 h.

As next, PHEMA was used as a macromolecular initiator for the diblock glycopolymer synthesis. The ATRP of GlcNAcEMA was performed in a 25 mL reaction flask. For the polymerization, 1.08 g (3.25 mmol) of the glycomonomer was stirred in 10 mL methanol/water = 1/1 (v/v) until complete dissolution. The solution was deoxygenated by nitrogen purg-

ing. 5.15 mg (0.052 mmol) CuBr, 2.90 mg (0.013 mmol) $CuBr_2$, 20.30 mg (0.13 mg) bpy and 291.64 mg (0.065 mmol) macroinitiator were added and stirred under a nitrogen stream for 20 min until a dark brown solution was formed. The reaction was performed at room temperature for 15 h. To remove the catalyst, the polymer was passed through silica gel. After removal of methanol im vacuum, the viscous polymer was dissolved in water. Then, the polymer was dialyzed against water to get rid of the residual monomer and initiator. The purified polymer was freeze-dried and a white polymer was obtained. The bottom of Figure 8.3 presents the ^{1}H NMR spectrum of the synthesized diblock glycopolymer PHEMA-b-PGlcNAcEMA. Comparing with the ^{1}H NMR spectrum of the parent polymer PHEMA, a new signal appeared between at 3.0 and 4.5 ppm which could be attributed to the GlcNAc protons. The molecular weight of diblock glycopolymer was determined by GPC and amounted to $5.5{\cdot}10^3$ g·mol^{-1} with a low polydispersity of 1.11. DMF was used as solvent (flow rate 1.0 mL·min^{-1}). MZ-SD-plus gel columns and a Jasco 2075 detector were used for the measurement. For calibration, poly(methyl methacrylate) standards were used. The molecular weight of PHEMA-b-PGlcNAcEMA was 6230.0 g·mol^{-1}, measured by MALDI-TOF mass spectrometry. The measurement was performed on a Bruker ultrafleXtreme equipped with a 337 nm smartbeam laser in the reflective mode.

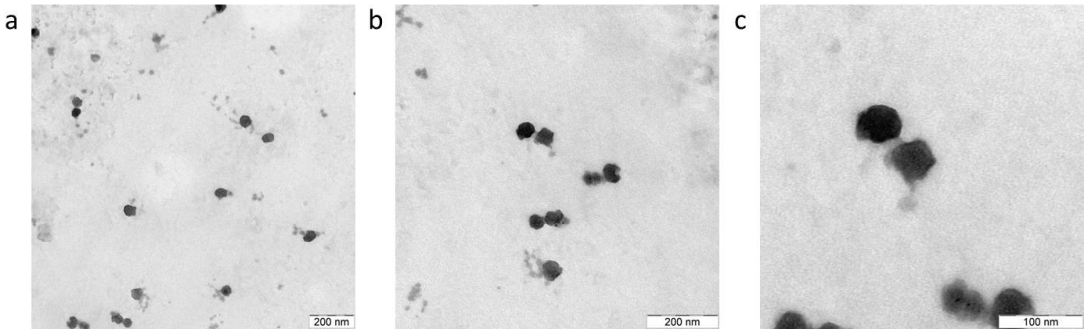

Figure 8.4: TEM micrographs of PHEMA-b-PGlcNAcEMA in different magnification.

For the microscopic measurement, the diblock glycopolymer was dissolved in water and a molar concentration of $3.2{\cdot}10^{-4}$ mol·L^{-1} (2.0 mg·mL^{-1}) was applied. The solution was vortexed for a few minutes to generate monodisperse polymer particles. Actually, these block copolymers are composed of two hydrophilic blocks: the water soluble glycopolymer with very hydrophilic sugar pendants and the water swellable PHEMA block. In spite of two hydrophilic blocks, the synthesized diblock glycopolymers self-assemble to a spherical shape in water. Figure 8.4 presents the TEM images of PHEMA-b-PGlcNAcEMA. Dark spherical structures are obtained at different magnifications. These spherical particles are distributed uniformly and their sizes are around 32 nm in diameter. Interestingly, the particles present uniform light gray spots on the particle surfaces. These spots indicate probably the hydrophilic block with sugar pendants presented on the surface. To clarify this assumption, the polymer solution was also investigated using in situ TEM. This microscopic technique was employed because of its high resolution and quantitative observation

of deformation behavior in thin films as well as nanostructured materials. Figure 8.5 shows the in situ TEM images of PHEMA-b-PGlcNAcEMA at the same concentration. The particles appear with little small sizes around 28 nm in diameter. In the Figure 8.5b, large aggregates of these particles can be observed. However, the large aggregates in the Figure 8.5c resembles as flower-like structures, and d and e are obtained at elapsed time within few minutes. As indicated with red circle, we observe that some aggregates are moving during measurement. This reveals a real time observation by situ TEM measurement. As shown here, the block copolymer containing PHEMA and relative hydrophilic glycopolymer may form spherical micelles in water. We supposed that the PHEMA blocks would form the core of the particles because of their relative hydrophobicity and the PGlcNAcEMA blocks would build the hydrophilic shell.

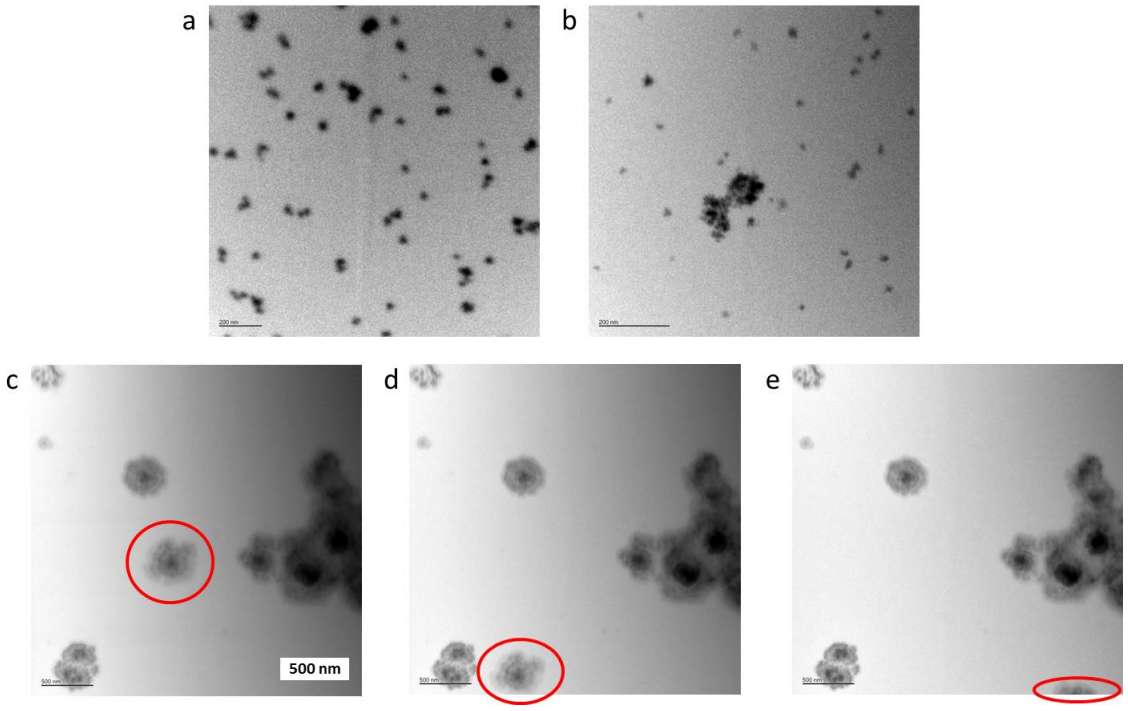

Figure 8.5: In situ TEM micrographs of PHEMA-b-PGlcNAcEMA.

As next, the diblock glycopolymer solution was examined to exclude a possible assumption such as the micellization resulted from residual catalysts. For the measurement, 10 µL of 10 mg·mL^{-1} $CuBr_2$ solution were added into the 100 µL polymer solution with a molar concentration of 2.4·$^{-4}$ mol·L^{-1} (1.5 mg·mL^{-1}). Changes of micelle structures were observed by TEM. Figure 8.6 shows three images which were taken with few minutes interval. We can observe the movement of micelle structures, because of the still wet sample solution on the TEM grid. The resulting structures present micelles with dark cores and gray shells. They are around 23 nm in diameter and almost monodispers in size. From the image of Figure 8.6a to 8.6c, the movement of micelles can be observed. They build large aggregates after a few minutes. This appearance gives significantly different structures in comparison with that shown in Figure 8.4. This implies that the possibly remaining

catalysts after the ATRP reaction has no influence on the micell formation. Otherwise, the micelles should have almost the same structure before the $CuBr_2$ addition.

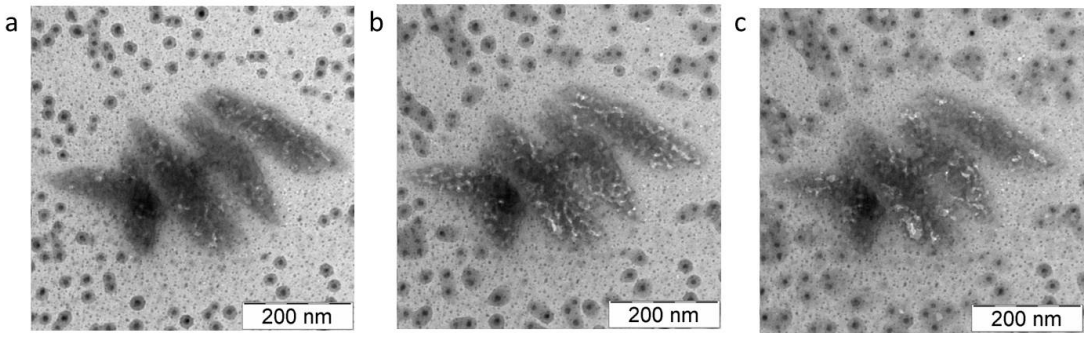

Figure 8.6: TEM micrographs of the $2.4{\cdot}10^{-4}$ mol·L^{-1} (1.5 mg·mL^{-1}) PHEMA-b-PGlcNAcEMA solution after addition of 10 µL of 10 mg·mL^{-1} $CuBr_2$ solution.

The lectin binding activity of these micelles was also investigated using 100 µL of $3.2{\cdot}10^{-4}$ mol·L^{-1} (2.0 mg·mL^{-1}) PHEMA-b-PGlcNAcEMA solution. 10 µL of 20 µg·mL^{-1} GS-II in PBS buffer solution was added into the polymer solution. The mixture of two solutions was then incubated for 10 min and the binding reaction was observed by TEM measurement. As shown in Figure 8.7, the micelle sizes are distributed uniformly and their structures are almost the same spheric micelles as shown in Figure 8.4. However, Figure 8.7a presents large agglomerates of micelles. Many micelles are shown inside of agglomerates and they are composed of almost the same micelle sizes of 30 nm to 40 nm in diameter. These large agglomerates may result from the lectins bound on the glycopolymer of micelle surfaces. To prove this, an access of GlcNAc solution was added to these glycopolymer micelles and lectin mixture.

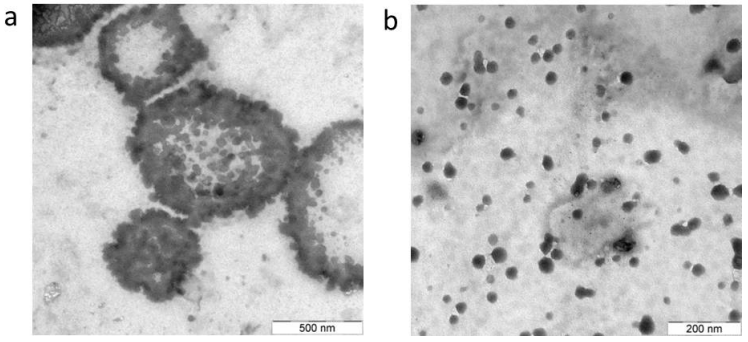

Figure 8.7: TEM micrographs of the $3.2{\cdot}10^{-4}$ mol·L^{-1} (2.0 mg·mL^{-1}) PHEMA-b-PGlcNAcEMA solution after addition of 10 µL of 20 µg·mL^{-1} GS-II in PBS buffer solution.

200 mM of the end concentration of GlcNAc was used for this competitive inhibition measurement and the mixed solution was incubated for 10 min. Then, the solution was pipetted on the grid surface for the TEM measurement. Figure 8.8 shows spheric micelles of diblock glycopolymers. Theses TEM images present no agglomerates as shown in Figure

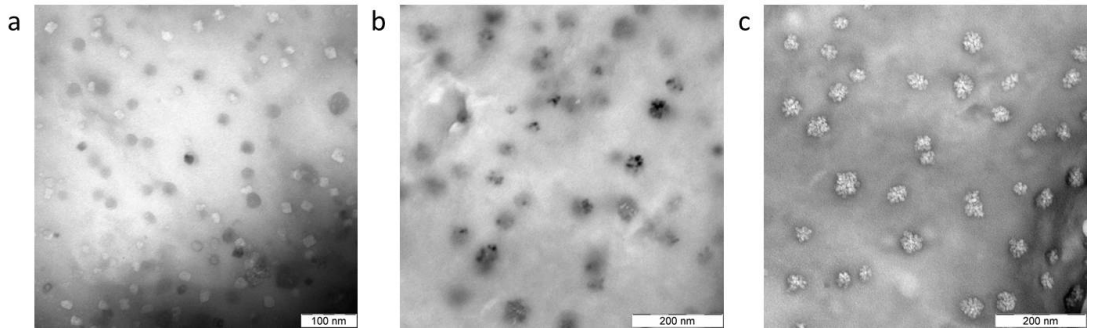

Figure 8.8: TEM micrographs of GS-II binding PHEMA-b-PGlcNAcEMA after addition of an excess of GlcNAc solution.

8.7. Figure 8.8a and b show the monodisperse micelle shapes of the diblock glycopolymer. In Figure 8.8c, the micelles reveal uniform flower-like structures and their sizes vary from 40 nm to 50 nm. The large protuberances on the surfaces may indicate the hydrophilic glycopolymer blocks of PHEMA-b-PGlcNAcEMA. Unfortunately, we cannot exactly confirm this because there is no evidence to prove this argument and no similar structure are shown before the addition of the GlcNAc solution to the lectin-glycopolymer mixtures. However, it may validate again that the free GlcNAcs can hinder the binding of micelles with the lectins.

The lectin binding activity of glycomicelles was also investigated by AFM. The preparation procedure for sample solutions was the same compared to the TEM measurement. The same concentrations of solutions were used. The polymer and polymer with GS-II solutions were spin-coated separately on silicon wafers to get thin layers of polymer particles. The silicon wafer was prepared freshly by plasma treatment (0.2 mbar, 2 min, 18W, PDC-32 G, Harrick) before its application. In general, the movement of an AFM probe over a sphere causes a broadening of features in the image. The exact particle sizes cannot be determined here, but the relative size distributions can be compared between the samples. As shown in Figure 8.9, AFM images indicate monodisperse and very fine spherical particles on the silicon wafers. The two images on the top (8.9a and 8.9b) show the height images of glycomicelles before and after lectin binding assay. The results show obvious differences in the size of the particles. The particles have a monodisperse size distribution. The micelles with GS-II lectins present little larger particles (b), whereas the glycomicelles alone have particle sizes between 30 to 70 nm in diameter. The phase images at the bottom also indicate a significant difference in size between the two samples. Thus, the lectin added glycomicelles tend from relatively larger structures and this confirms again the same result as the TEM measurement.

A cryo-scanning electron microscopy (Cryo-SEM) analysis was also performed to obtain more detailed information on the glycomicellization in water. The measurement was performed on a HITACHI S-4800 FESEM operated at 1-2 kV with a 10 μA current. Samples

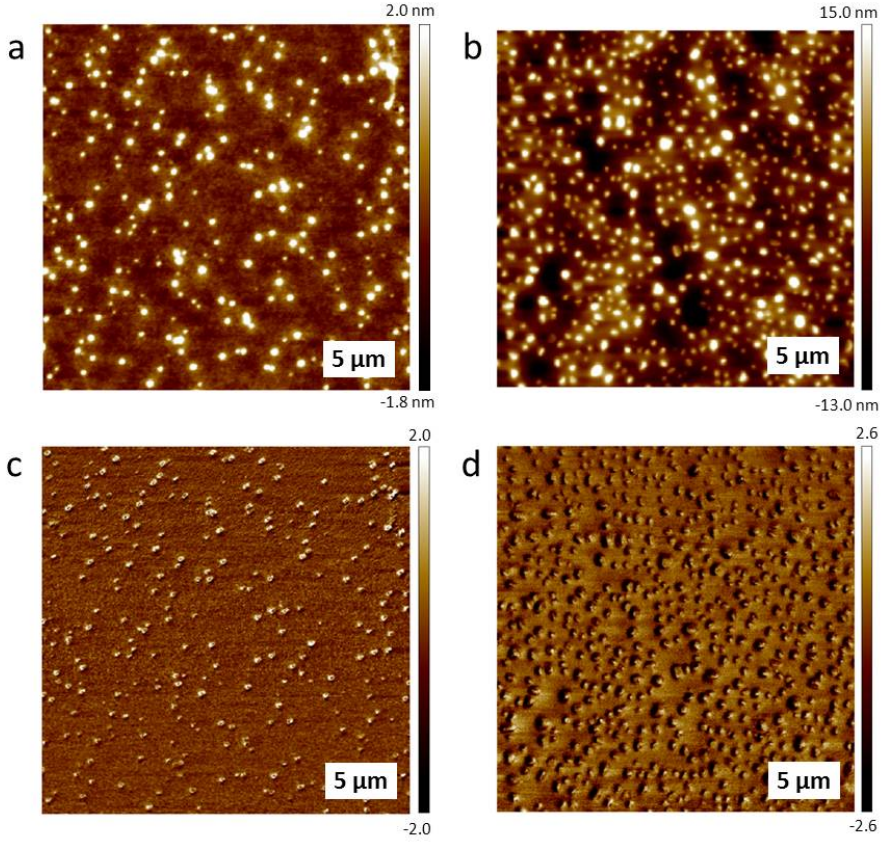

Figure 8.9: AFM height (top) and phase (bottom) images of PHEMA-b-PGlcNAcEMA glycopolymers before (a,c) and after (b,d) GS-II addition.

for cryo-SEM were prepared by flash freezing a droplet. Then, a fresh surface was created by breaking the frozen droplet and the thin layer of water was sublimated. A concentration of $3.2 \cdot 10^{-4}$ mol·L^{-1} (2.0 mg·mL^{-1}) of the diblock glycopolymer were used for the measurement. The particle sizes are distributed almost uniformly between 30 nm and 130 nm in diameter (Figure 8.10a). They are relatively larger than the particle sizes found by the other microscopic methods. However, the micelles become smaller after the sublimation of the thin water layer around the surface (Figure 8.10b). The cryo-SEM measurement verifies the micellization of PHEMA-b-PGEMA polymers in water clearly.

The polymer solution with the same concentration was analyzed by FESEM technique. For the sample preparation, the polymer solution was coated on a silicon wafer by spin-coating. The silicon wafer was treated freshly by plasma at 0.2 mbar for 2 min before applying for the spin-coater. The thin layers of samples were air-dried under ambient conditions. The dried polymers on the silicon wafer are shown in Figure 8.11. White spots at the micrographs are assumed to be the hydrophobic PHEMA core of the glycopolymer micelles. Their sizes are approximately 10 nm in diameter. The splits are the typical drying effect of polymers on the surface. Although the core structures of glycomicelles can be estimated from these FESEM images, it is difficult to predict their scale because these

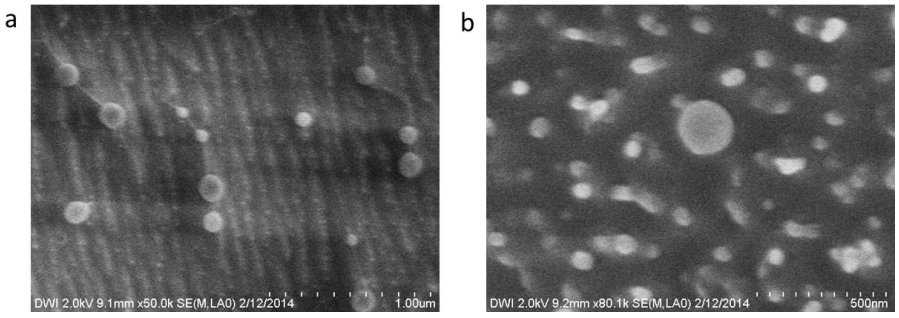

Figure 8.10: Cryo-SEM micrographs of PHEMA-b-PGlcNAcEMA glycopolymers before (a) and after (b) water sublimation.

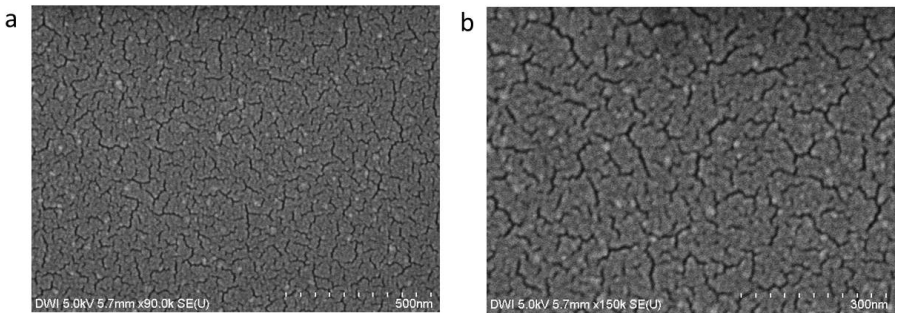

Figure 8.11: FESEM micrographs of PHEMA-b-PGlcNAcEMA glycopolymers.

structures result from dried micelles. Therefore, it is necessary to investigate the micelle size in detail. For this purpose, diblock glycopolymers in water were analyzed by DLS and FCS techniques. These measurements were performed by Stefan Walta from the Institute of Physical Chemistry II, RWTH Aachen University.

Figure 8.12 plots the hydrodynamic radius (R_h) of particles over molar concentration of PHEMA-b-PGlcNAcEMA from the DLS measurement. The R_h of the block glycopolymer was measured in water as well as HEPES puffer solution. The hydrodynamic radius reveals a very small difference comparing the two solutions. The particle radius is reduced with the increasing sample concentration in both solutions. This can be explained by swelling of the polymer micelles at low concentrations because of the water swellable PHEMA backbone. In contrast, the PHEMA backbone of glycopolymers has no enough place to swell at high concentrations of micelles. For example, the particle size at the concentration of $5.0{\cdot}10^{-4}$ mol$\cdot$L^{-1} amounts around 17.4 nm $\pm$ 0.1 nm in radius. This result agrees very well with that from the previous microscopic measurements. For the FCS measurement, fluorescence labelled GS-II was used for the binding assay between sugar and glycopolymer. The GS-II has three fluorescence binding sites and four glycan binding sites. The lectin size is 6.6 nm $\pm$ 0.2 nm in radius. After binding with glycopolymers, the particle size changes to 18.6 nm $\pm$ 0.4 nm in radius. This result agrees quite well with that of the former microscopic measurements. The GS-II inhibition and the competitive inhibition with GlcNAc were carried out to monitor its binding activity to glycomicelles. The influence

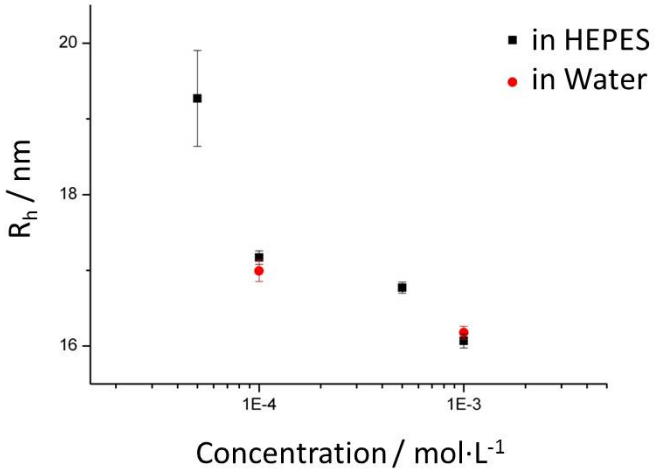

Figure 8.12: Graph of particle radius (R_h) over molar concentration of diblock glycopolymers.

of spherical diblock glycopolymers on the lectin recognition process was also examined by FCS measurement. The detailed results and discussions from DLS and FCS are submitted for publication in Chemical Communications.

The further modification properties of sugar pendants of glycopolymers were tested by the incubation of glycopolymers in enzyme solution. 9 mg of 1.5 mg·mL^{-1} glycopolymer solution was used for the enzymatic synthesis and the experimental procedure was the same as described in Chapter 2.1.4. After synthesis, the polymer solution was filtered to remove the enzyme using a 30 kDa filtration tube. Then, the solution was dropped onto a carbon-coated copper grid for a TEM measurement. The acquired micrographs are shown in Figure 8.13. The particle sizes are distributed polydispersely. However, the particles build still spherical structures and show hollow interiors like PHEMA-b-PGlcNAcEMA. Actually, it is absolutely necessary to study further whether these PHEMA-b-LacNAc particles are really the diblock glycopolymers with LacNAc pendants and have the ability to bind lectins. In the coarse of this thesis, only the possibility of further sugar modification of glycopolymer micelles could be demonstrated.

8.3 Conclusion

Here, a PHEMA-b-PGlcNAcEMA diblock glycopolymer was synthesized and its self-assembled structure in water was observed using different microscopic measurements such as AFM, TEM, in situ TEM, FESEM, and cryo-SEM. Although PHEMA-b-PGlcNAcEMA is composed of two hydrophilic polymers, the resulted diblock glycopolymers have shown

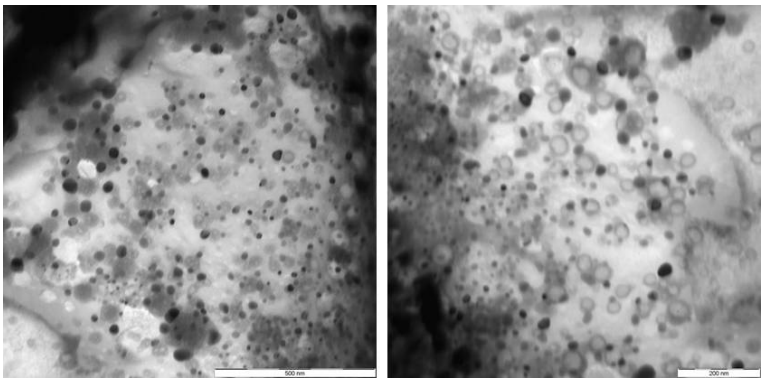

Figure 8.13: TEM micrographs of PHEMA-b-PLacNAcEMA.

monodisperse micelle particles in water. After the addition of $CuBr_2$ in the glycomicelle solution, the particles revealed more defined core-shell structures. They showed a high tendency to build large aggregates. As next, the polysaccharide-like characteristics of glycopolymers such as the lectin binding ability was investigated. TEM and AFM images indicated that the glycomicelles are capable of recognizing and binding the lectins. Then, the micelle size was measured by DLS and their lectin binding activity was observed additionally by FCS. The size of micelles was decreasing with increasing particle concentration. For example, the particle sizes lie around 17.4 nm $\pm$ 0.1 nm in radius at a concentration of $5.0{\cdot}10^{-4}$ mol$\cdot$L^{-1}. The FCS measurement confirmed the ability of glycopolymers to bind lectin. This result agreed very well with the microscopic observations. At the end, we have shown the feasibility of the direct enzymatic elongation of sugar pendants. In conclusion, the diblock copolymer from water swellable PHEMA and very hydrophilic GlcNAcEMA forms micelle structure, and the resulting glycomicelles are able to bind to lectin. Therefore, they are promising candidates for drug delivery systems and biomedical diagnostics.

9. Summary

This thesis dealt with a novel fabrication of polymer brushes and lap-on-a-chip devices which were based on glycoconjugates with lectin binding ability. Glycopolymers are consisting of synthetic polymers with pendant saccharides. Their unique property such as sugar specific protein binding is well known. In general, the binding efficiency between the monomeric sugar and the sugar binding protein lectin is too weak to be detectable. However, the binding reaction can be significantly enhanced by multivalent presentation in the form of glycopolymers. Here, the glycopolymers have been prepared by "grafting from" method not only on solid substrates but also by controlled polymerization yielding diblock glycopolymers. Atom transfer radical polymerization (ATRP) was used for the fabrication of glycopolymers as well-controlled polymerization technique. Most reactions in this work were performed in moderate conditions such as room temperature and water as solvent. Several applications using glycopolymers were explored to manufacture practically useful "lab-on-a-chip" devices.

In order to synthesize glycopolymer brushes, the glycomonomer 2-O-(*N*-acetyl-β-D-glucosamine)ethyl methacrylate (GlcNAcEMA) was synthesized by the modified König-Knorr reaction. Using this glycomonomer, a new multivalent glycopolymer platform for lectin recognition was fabricated. This new platform was manufactured by combining well-controlled ATRP reactions of glycomonomers with highly specific glycosylation reactions. The fabrication of multivalent glycopolymers consisting of poly(GlcNAcEMA) was succeeded by additional biocatalytic elongation of the glycans directly on the silicon substrate. This sugar modification was carried out by specific glycosylation using recombinant glycosyltransferases. The bioactivity of the surface grafted glycans was investigated by fluorescence linked lectin assay (FLLA). Due to the multivalency of glycan ligands, the glycopolymer brushes showed very selective, specific and strong interactions with lectins. The multi-arrays of the glycopolymer brushes have shown a great potential for applications as screening devices of specific lectins.

Recently, there is growing interest in surface gradient which contain gradually varied components along one or more given directions. We described two different forms of glycopolymer gradients. As first, a molecular gradient of the poly(2-hydroxyethyl methacrylate) (PHEMA) backbone of PGlcNAcEMA and an orthogonal pendant sugar gradient were prepared. The synthesis was conducted by dip-coating and biocatalytic elongation. The

molecular gradient of glycopolymers was made by SI-ATRP from the silicon surface. The surface was characterized by the enzyme linked lectin assay technique and an AFM measurement. The binding intensity of lectin on the surface was proportional to the length of glycopolymer brushes. The glycan gradients have revealed a highly specific lectin binding ability. As second, an ATRP initiator gradient was prepared on the silicon surface and then the GlcNAcEMA polymerized from this initiator modified surface. The resulting surface has shown different surface structures in comparison with the glycopolymer gradient brushes. However, the fluorescence microscopic measurements have confirmed again this gradient surface possessed the specific lectin binding ability.

As next, the wide applications of glycopolymer brushes were described in combination with electrochemical impedance spectroscopy (EIS) to realize an impedimetric glyco-biosensor (IGB). The GlcNAcEMA was polymerized directly from gold electrodes of EIS chips by SI-ATRP. Then, the fabricated IGB was analyzed by common surface characterization methods as well as EIS technique. The resulting surface has shown very sensitive and reproducible results. The combination of chemical polymer synthesis with electrochemical devices led to a successful fabrication of a novel glycopolymer platform with protein selective surfaces. In addition to impedance measurement based IGB, a plasmonic flow-through glyco-biosensor (PFGB) and real-time polymerization monitoring device using surface acoustic wave (SAW) were described in detail. PFGB possesses a strong benefit by using an inexpensive polycarbonate membrane, while SAW measures the mass viscosity and the conductivity with high sensitivity. In usual, these three techniques were driven by microfluidic systems. Therefore, they have unique advantages such as handling of small sample sizes, saving reagents, the enhanced efficiency of the assays, and the reduction of cross-contamination. In particular, IGB and PFGB have revealed their ability as alternative biosensors to commercially available SPR. Thus, the microfluidic glycopolymer biosensors are potentially usable for new simplified diagnostic tools to detect cancer-related lectins in blood serum.

Glycopolymers have been also applied for the synthesis of core-shell microspheres. As first, silica particles were used as solid substrate. After initiator modification, GlcNAcEMA was polymerized. As a result, the particles showed core-shell structures, but large agglomeration of particles was observed which might be caused from inter-particle coupling. As second, the glycomonomer GlcNAcEMA was polymerized using PHEMA as the macroinitiator. The resulting diblock glycopolymer PHEMA-b-PGlcNAcEMA was investigated by microscopic methods, DLS and FCS measurements. PHEMA is a well known polymer characterized by its water-swellable property. However, PHEMA cannot be fully dissolved in water because of its hydrophilic functional groups. Although the glycopolymer PGlcNAcEMA is distinguished only by the sugar pendants from PHEMA, the produced diblock glycopolymers revealed core-shell microsphere formation. This result indicates that the sugar pendants of the glycopolymers have much higher hydrophilicity in comparison with

PHEMA. The diverse microscopic observations have presented with the micelle structure of the PHEMA-b-PGlcNAcEMA diblock copolymer. The size of the particles was estimated around 32 nm in diameter and it agreed quite well with the results of DLS and FCS measurements. The lectin binding property of these polymers was also demonstrated by microscopic and FCS measurement.

In conclusion, the synthesized GlcNAcEMA has shown high potential applications for the fabrication of diverse glycochips and glyco-particles. The prepared glycopolymers including brushes and micelles possessed a specific lectin binding property. The introduced novel platforms are expected to be used in many fields of chemistry, biology, diagnostics, and biomedicine as powerful synthetic materials.

9. Zusammenfassung

Saccharide sind die am häufigsten vorkommenden bioorganischen Verbindungen. Die Wechselwirkung zwischen einem Glykan und einem Protein ist in natürlichen Systemen zu schwach, um detektiert werden zu können. Deshalb ermöglicht ein sogenanntes Glykopolymer einen erhöhten Zucker-Protein Wechselwirkungsgrad durch eine multivalente Präsentation von Saccharidgruppen. Als Glykopolymer wird im Allgemeinen ein künstliches Polymer mit Zuckerseitenketten bezeichnet. Im Rahmen dieser Doktorarbeit wurden Glykopolymere auf Oberflächen hergestellt, indem ein Glykomonomer auf verschiedene Substrate polymerisiert wurde. Für die gerichtete Polymerisation wurde Atom Transfer Radikal Polymerisation (ATRP) verwendet. Das eingesetzte Glykomonomer 2-O-(*N*-Acetyl-D-glucosamin)ethyl methacrylat (GlcNAcEMA) wurde durch eine neue Methode eigens synthetisiert und auf ATRP-Initiator modifizierten Festoberflächen wie z. B. Siliziumwafern, Gold gesputterten Wafern sowie Silica-Partikeln polymerisiert.

Polymerbürsten sind dicht gepfropfte Copolymere, so dass die einzelnen Polymerketten sich von dem Substrat weg strecken müssen. Die vorliegende Arbeit behandelt die Synthese von Polymerbürsten und die nachfolgende Charakterisierung der Polymerbürsten. Hierfür wurde die „Grafting from“ Polymerisation und die spezifische Glykosylierungsreaktion angewendet. Zum Vergleich mit dem Glykopolymer PGlcNAcEMA wurde 2-O-Ethyl methacrylat (HEMA) ohne Zuckereinheiten ebenfalls auf der Siliziumoberfläche polymerisiert. Die Oberflächencharakterisierung der Bürsten wurde mit verschiedenen chemischen und biologischen Analyseverfahren durchgeführt. Mit zunehmender Polymerisationszeit wurde eine steigende Schichtdicke von Polymeren auf der Oberfläche beobachtet. Die Protein Bindungsaktivität der hergestellten Polymeroberflächen wurde durch Fluoreszenzmarkierte Lektine bestimmt. Lektine sind komplexe (Glyko)proteine, die spezifisch an Glykanstrukturen binden können. Während Oberflächen mit PHEMA Bürsten eine starke Lektin abweisende Eigenschaft aufwiesen, zeigte die PGlcNAcEMA aufgepfropfte Oberfläche eine sehr spezifische Lektin-Bindungsaktivität. Mit Hilfe enzymatischer Reaktionen können die Zucker des Glykopolymers modifiziert werden. Somit kann eine neue Oberflächenstruktur hergestellt werden, die durch ein anderes Lektin erkannt werden kann. Des Weiteren wurde die Reaktion der Glykanmodifizierung direkt auf der Glykopolymer beschichteten Oberfläche durchgeführt. Nach Zuckermodifikation hat die Glykopolymeroberfläche sehr spezifische Lektin-Bindungseigenschaften gezeigt. Demnach konnte

man die Glykopolymer Bürsten durch die multivalente Präsentation des Zuckers sehr gut beobachten.

In letzter Zeit wächst das Interesse an Oberflächengradienten, welche als Oberflächen mit sich kontinuierlich verändernden Eigenschaften in einer oder mehrerern Richtungen angesehen werden. Nach der erfolgreichen Glykochip-Herstellung wurden Bürstenoberflächen mit zwei Arten von Gradienten hergestellt: 1. Gradient von Polymerschichtdicke und 2. Gradient im aufgepfropftem Polymerabstand. Der Polymerschichtdickengradient erfolgte durch die Polymerisation von GlcNAcEMA auf einer Initiator Monolage. Für die gleichmäßige Variierung des GlcNAcEMA wurde ein eigens hergestellter Dip-Coater verwendet. Die Glykane wurden senkrecht zum PGlcNAcEMA Gradient durch enzymatische Glykosylierung weiter modifiziert. Dadurch wurde eine Bürstenoberfläche mit zwei Substratgradienten hergestellt. Diese Glykopolymerbürsten haben wiederum eine sehr spezifische Lektin-Bindungsaktivität gezeigt. Für die Herstellung des Gradienten des Polymerabstands wurde Initiator unter Zuhilfenahme eines Dip-Coaters auf der Oberfläche immobilisiert und anschließend Glykomonomer hierauf polymerisiert. Obwohl der durch Initiator hergestellte Abstandsgradient im Vergleich zum Schichtdickengradient sehr unterschiedliche Oberflächenstrukturen erzeugt hat, haben beide Gradienten Glykochips selektiv und spezifisch Lektin bindende Eigenschaften gezeigt.

Als nächster Schritt wurde die Fertigung von Glycopolymerbürsten vom Siliziumoberflächen auf Goldelektroden übertragen. Hier wurden die chemischen und biologischen Synthesemethoden mit elektrochemischer Impedanzspektroskopie (EIS), lokalisierter Oberflächenpasmonenresonanzspektroskopie (LSPR) oder auch der akustischen Oberflächenwellen (SAW) Technik kombiniert. Die optimalen Bedingungen für die Polymerisation auf Gold Elektroden wurden durch Vorversuche auf glatten Goldsubstraten ermittelt. Zum Beispiel wurde die Gold-Oberfläche für die Bereitstellung der Initiator Schicht mit dem Initiator bis[2-(2'-Bromisobutyryloxy)ethyl]disulfid über Nacht behandelt. Die Polymerisation erfolgte direkt danach bei Raumtemperatur. Nach Polymerisation erwies sich die mit Polymerbürsten modifizierte Oberfläche extrem stabil gegen verschiedene Stressbedingungen wie z. B. Handhabung in der Luft oder Behandlung mit organischen Lösemitteln. Bei den Chips für die Herstellung impedimetrischer Glykopolymer Biosensoren (IGB) und Plasmon Fluidik Glykopolymer Biosensoren (PFGB) wurden die Goldoberflächen zuerst mit Polymerbürsten beschichtet und dann auf dem jeweiligen Messsytem passend montiert. Die beiden Chips zeigten sowohl ein gut kontrolliertes PGlcNAcEMA Wachstum auf ihren Goldelektroden als auch eine Lektin-spezifische Bindungseigenschaft. Die Lektin Bindung an Glykopolymer beschichteten Chips wurde durch EIS und LSPR Methoden untersucht. Die elektrischen Messergebnisse von IGB stimmten mit den Ergebnissen der Plasmonenresonanz (PFGB) überein. Im Fall von für SAW Messungen hergestellten Goldelektroden wurde die Vorgehensweise etwas abgeändert. Hierbei wurde eine komplett automatisierte Polymerisationsplattform erstellt und der Polymerisationsprozess online

überwachtet. Im Allgemeinen kann der SAW Technik basierte Chip sowohl Massen- als auch Konduktivitätsänderungen sehr sensitiv messen, während PFGV einen großen Vorteil wie niedrige Herstellungskosten durch den Einsatz der preiswerten Polycarbonatmembranen hat. Zusammenfassend konnte eine anregende Technologiestrategie durch die Kombination von verschiedenen Standardtechniken entwickelt werden. Insbesondere wurde ein Mikrofluidik System in die verwendeten drei Techniken eingeführt. Dadurch konnte die Anzahl an Messproben erhöht und Substraten, der Substratverbrauch reduziert, die Assay-Effizienz erhöht und auch die Kontaminationsgefahr gesenkt werden.

Schließlich wurde die Herstellung von selbstassemblierten Kern-Schale-Partikeln vorgestellt. Die Kern-Schale-Partikel können mittels zwei verschiedene Methoden hergestellt werden. Zunächst wurde die Oberflächen initiierte Polymerisation auf Silica Nanopartikeln durchgeführt. TEM Aufnahmen verdeutlichen eine erfolgreiche Polymerisation. Allerdings haben die Polymer beschichteten Partikel eine große Tendenz zur Agglomeration gezeigt. Als nächstes wurde ein neuartiges Diblockcopolymer synthetisiert, welches aus PHEMA und GlcNAc konjugierten PHEMA besteht. Obwohl sich die beiden Blöcke nur in GlcNAc Zuckereinheiten unterscheiden, hat das PHEMA-b-PGlcNAcEMA Diblock Glykopolymer in Wasser eine sehr klare Mizellen-Struktur gebildet. Die mizellare Anordnung ist auf die amphiphilen Diblockcopolymere zurückzuführen, die in Wasser selbstorganisierende Mizellenstrukturen bilden können. Da PHEMA ein bekanntes Wasser quellbares und nicht wasserlösliches Polymer ist, bildet der PHEMA Block den hydrophoben Innenteil und der sehr hydrophile PGlcNAcEMA Block die Schale. Die Größen dieser Mikrosphären wurden durch den Zugabe von Lektinen etwas vergrößert und durch GlcNAc-Überschuss wieder verkleinert. Somit ist die Lektin Bindungsfähigkeit der Glykomizellen ganz klar festgestellt worden. Die Partikelgröße um 32 nm im Durchmesser wurde durch die verschiedenen mikroskopischen Messungen, DLS und FCS Messungen mehrfach nachgewiesen.

Zusammenfassend wurde das Glykomonomer GlcNAc synthetisiert und auf verschiedene Substrate polymerisiert. Des Weiteren wurden interdisziplinäre Perspektiven durch die Kombination von mehreren Technikenaus verschiedenden Fachbereichen (z. B. Chemie, Biologie, und Elektrotechnik) aufgezeigt. Die Glykopolymer immobilisierten Oberflächen haben hoch spezifische Lektin-Bindungseigenschaften gezeigt. Infolgedessen können diese neuartigen Plattformen als leistungsstarke synthetische Materialien in vielen Bereichen wie z. B. Biosensoren, Diagnostik, und Biomedizin angewendet werden.

Acknowledgement

First of all, I would like to gratefully appreciate Prof. Dr. Alexander Böker for his inspirational supervision, understanding, and supporting during my doctoral works.

I would like to gratefully acknowledge Prof. Dr. Lothar Elling for his guidance in the development of my research work and useful discussions with him.

In addition, I would like to say a big thanks to R. R. Rosencrantz for the excellent cooperation and to kindly thank to Dr. U. Schnakenberg, J. Lazar, V. H. Nguyen and S. Walta for the nice collaboration.

I would also like to gratefully acknowledge Dr. U. Glebe for the corrections of this work and my colleagues for creating such a nice work atmosphere.

Finally, I would especially thank my family for the love and support which I have gotten over the years. In particular, I would like to thank to my parents for their encouragement, quite patience and faith in me.

Bibliography

[1] Heinrich Hühnerfuss. *Basics in carbohydrate chemistry*, chapter 1, pages 1–28. Pan Stanford Publishing Pte. Ltd., Singapore, 2011.

[2] Mariano Ortega-Munoz, Julia Morales-Sanfrutos, Francisco Perez-Balderas, Fernando Hernandez-Mateo, M. a Dolores Giron-Gonzalez, Natalia Sevillano-Tripero, Rafael Salto-Gonzalez, and Francisco Santoyo-Gonzalez. Click multivalent neoglycoconjugates as synthetic activators in cell adhesion and stimulation of monocyte/machrophage cell lines. *Organic & Biomolecular Chemistry*, 5(14):2291–2301, 2007.

[3] Orietta León, Alexandra Muñoz-Bonilla, Vanesa Bordegé, Manuel Sánchez-Chaves, and Marta Fernández-García. Amphiphilic block glycopolymers via atom transfer radical polymerization: Synthesis, self-assembly and biomolecular recognition. *Journal of Polymer Science Part A: Polymer Chemistry*, 49(12):2627–2635, 2011.

[4] IUPAC. Iupac goldbook. `http://goldbook.iupac.org/`, 2014. [Online; accessed 12-December-2014].

[5] J M Rini. Lectin structure. *Annual Review of Biophysics and Biomolecular Structure*, 24(1):551–577, 1995.

[6] Y. C. Lee and R. T. Lee. Carbohydrate-protein interactions: Basis of glycobiology. *Accounts of Chemical Research*, 28(8):321–327, 1995.

[7] ReikoT Lee and YuanC Lee. Affinity enhancement by multivalent lectin–carbohydrate interaction. *Glycoconjugate Journal*, 17(7-9):543–551, 2000.

[8] J. J. Lundquist and E. J. Toone. The cluster glycoside effect. *Chemical reviews*, 102(2):555–578, 2002. Review,Research Support, U.S. Gov't, P.H.S.

[9] Vimary Vázquez-Dorbatt, Juneyoung Lee, En-Wei Lin, and Heather D. Maynard. Synthesis of glycopolymers by controlled radical polymerization techniques and their applications. *ChemBioChem*, 13(17):2478–2487, 2012.

[10] S. R. Simon Ting, Gaojian Chen, and Martina H. Stenzel. Synthesis of glycopolymers and their multivalent recognitions with lectins. *Polymer Chemistry*, 1(9):1392–1412, 2010.

[11] Irvin E. Liener, Nathan Sharon, and Irwin J. Goldstein. *The Lectins: Properties, Functions, and Applications in Biology and Medicine*. Academic Press INC. (London) LTD., 1986.

[12] Harold Rüdiger and Hans-J. Gabius. Plant lectins: Occurrence, biochemistry, functions and applications. *Glycoconjugate Journal*, 18(8):589–613, 2001.

[13] Hans-Joachim Gabius. Animal lectins. *European Journal of Biochemistry*, 243(3):543–576, 1997.

[14] Herbert Kaltner and Hans-J. Gabius. *Animal Lectins: from Initial Description to Elaborated Structural and Functional Classification*, volume 491 of *Advances in Experimental Medicine and Biology*, chapter 6, pages 79–94. Springer US, 2001.

[15] W. Tempel, S. Tschampel, and R. J. Woods. The xenograft antigen bound to griffonia simplicifolia lectin 1-b(4). x-ray crystal structure of the complex and molecular dynamics characterization of the binding site. *The Journal of Biological Chemistry*, 277(8):6615–21, 2002.

[16] K. Turton, R. Natesh, N. Thiyagarajan, J. A. Chaddock, and K. R. Acharya. Crystal structures of erythrina cristagalli lectin with bound n-linked oligosaccharide and lactose. *Glycobiology*, 14(10):923–9, 2004.

[17] William I. Weis and Kurt Drickamer. Structural basis of lectin-carbohydrate recognition. *Annual Review of Biochemistry*, 65(1):441–473, 1996.

[18] K. Saraboji, M. Hakansson, S. Genheden, C. Diehl, J. Qvist, U. Weininger, U. J. Nilsson, H. Leffler, U. Ryde, M. Akke, and D. T. Logan. The carbohydrate-binding site in galectin-3 is preorganized to recognize a sugarlike framework of oxygens: ultra-high-resolution structures and water dynamics. *Biochemistry*, 51(1):296–306, 2012.

[19] C. Diehl, O. Engstrom, T. Delaine, M. Hakansson, S. Genheden, K. Modig, H. Leffler, U. Ryde, U. J. Nilsson, and M. Akke. Protein flexibility and conformational entropy in ligand design targeting the carbohydrate recognition domain of galectin-3. *Journal of the American Chemical Society*, 132(41):14577–89, 2010.

[20] Ali Ghadban and Luca Albertin. Synthesis of glycopolymer architectures by

reversible-deactivation radical polymerization. *Polymers*, 5(2):431–526, 2013.

[21] C. Remzi Becer. The glycopolymer code: Synthesis of glycopolymers and multivalent carbohydrate–lectin interactions. *Macromolecular Rapid Communications*, 33(9):742–752, 2012.

[22] Brigitte Voit and Dietmar Appelhans. Glycopolymers of various architectures—more than mimicking nature. *Macromolecular Chemistry and Physics*, 211(7):727–735, 2010.

[23] Nicolas Smiljanic, Vincent Moreau, Duplex Yockot, Juan M. Benito, José M. García Fernández, and Florence Djedaïni-Pilard. Supramolecular control of oligosaccharide–protein interactions: Switchable and tunable ligands for concanavalin a based on β-cyclodextrin. *Angewandte Chemie International Edition*, 45(33), 2006.

[24] Sebastian G. Spain, Matthew I. Gibson, and Neil R. Cameron. Recent advances in the synthesis of well-defined glycopolymers. *Journal of Polymer Science Part A: Polymer Chemistry*, 45(11):2059–2072, 2007.

[25] Vincent Ladmiral, Emma Melia, and David M. Haddleton. Synthetic glycopolymers: an overview. *European Polymer Journal*, 40(3):431–449, 2004.

[26] S. R. Simon Ting, Eun Hee Min, Pierre Escalé, Maud Save, Laurent Billon, and Martina H. Stenzel. Lectin recognizable biomaterials synthesized via nitroxide-mediated polymerization of a methacryloyl galactose monomer. *Macromolecules*, 42(24):9422–9434, 2009.

[27] Chang-Ming Dong, Keith M. Faucher, and Elliot L. Chaikof. Synthesis and properties of biomimetic poly(l-glutamate)-b-poly(2-acryloyloxyethyllactoside)-b-poly(l-glutamate) triblock copolymers. *Journal of Polymer Science Part A: Polymer Chemistry*, 42(22):5754–5765, 2004.

[28] Heide Götz, Eva Harth, Stefan M. Schiller, Curtis W. Frank, Wolfgang Knoll, and Craig J. Hawker. Synthesis of lipo-glycopolymer amphiphiles by nitroxide-mediated living free-radical polymerization. *Journal of Polymer Science Part A: Polymer Chemistry*, 40(20):3379–3391, 2002.

[29] Kohji Ohno, Yoshinobu Tsujii, Takeaki Miyamoto, Takeshi Fukuda, Mitsuaki Goto, Kazukiyo Kobayashi, and Toshihiro Akaike. Synthesis of a well-defined glycopolymer by nitroxide-controlled free radical polymerization. *Macromolecules*, 31(4):1064–1069, 1998.

[30] André Pfaff, Vaishali S. Shinde, Yan Lu, Alexander Wittemann, Matthias Ballauff, and Axel H. E. Müller. Glycopolymer-grafted polystyrene nanospheres. *Macromolecular Bioscience*, 11(2):199–210, 2011.

[31] Ludovic Dupayage, Maud Save, Edith Dellacherie, Cecile Nouvel, and Jean-Luc Six. Pmma-grafted dextran glycopolymers by atom transfer radical polymerization. *Journal of Polymer Science Part A: Polymer Chemistry*, 46(23):7606–7620, 2008.

[32] Vimary Vázquez-Dorbatt and Heather D. Maynard. Biotinylated glycopolymers synthesized by atom transfer radical polymerization. *Biomacromolecules*, 7(8):2297–2302, 2006.

[33] Cyrille Boyer and Thomas P. Davis. One- pot synthesis and biofunctionalization of glycopolymersviaraft polymerization and thiol-ene reactions. *Chemical Communications*, (40):6029–6031, 2009.

[34] Samuel Pearson, Nathan Allen, and Martina H. Stenzel. Core-shell particles with glycopolymer shell and polynucleoside core via raft: From micelles to rods. *Journal of Polymer Science Part A: Polymer Chemistry*, 47(6):1706–1723, 2009.

[35] Guillaume Gody, Paul Boullanger, Catherine Ladavière, Marie-Thérèse Charreyre, and Thierry Delair. Biotin α-end-functionalized gradient glycopolymers synthesized by raft copolymerization. *Macromolecular Rapid Communications*, 29(6):511–519, 2008.

[36] Ling Zhang, Julien Bernard, Thomas P. Davis, Christopher Barner-Kowollik, and Martina H. Stenzel. Acid-degradable core-crosslinked micelles prepared from thermosensitive glycopolymers synthesized via raft polymerization. *Macromolecular Rapid Communications*, 29(2):123–129, 2008.

[37] Julien Bernard, Xiaojuan Hao, Thomas P. Davis, Christopher Barner-Kowollik, and Martina H. Stenzel. Synthesis of various glycopolymer architectures via raft polymerization: From block copolymers to stars. *Biomacromolecules*, 7(1):232–238, 2005.

[38] Jeremiah A. Johnson, Ying Y. Lu, Alan O. Burts, Yeon-Hee Lim, M. G. Finn, Jeffrey T. Koberstein, Nicholas J. Turro, David A. Tirrell, and Robert H. Grubbs. Core-clickable peg-branch-azide bivalent-bottle-brush polymers by romp: Grafting-through and clicking-to. *Journal of the American Chemical Society*, 133(3):559–566, 2010.

[39] Zhou Li, Ke Zhang, Jun Ma, Chong Cheng, and Karen L. Wooley. Facile syntheses of cylindrical molecular brushes by a sequential raft and romp "grafting-through"

methodology. *Journal of Polymer Science Part A: Polymer Chemistry*, 47(20):5557–5563, 2009.

[40] Hosei Shinoda and Krzysztof Matyjaszewski. Structural control of poly(methyl methacrylate)-g-poly(lactic acid) graft copolymers by atom transfer radical polymerization (atrp). *Macromolecules*, 34(18):6243–6248, 2001.

[41] Reda Fleet, Eric T. A. van den Dungen, and Bert Klumperman. Novel glycopolymer brushes via atrp: 1. synthesis and characterization. *Macromolecular Chemistry and Physics*, 212(20):2191–2208, 2011.

[42] Bernadette Charleux, Franck D'Agosto, and Guillaume Delaittre. *Preparation of Hybrid Latex Particles and Core-Shell Particles Through the Use of Controlled Radical Polymerization Techniques in Aqueous Media*. Springer Heidelberg Dordrecht London New York, 2010. doi:10.1007/978-3-642-16060-8.

[43] Mitsuru Kato, Masami Kamigaito, Mitsuo Sawamoto, and Toshinobu Higashimura. Polymerization of methyl methacrylate with the carbon tetrachloride/dichlorotris- (triphenylphosphine)ruthenium(ii)/methylaluminum bis(2,6-di-tert-butylphenoxide) initiating system: Possibility of living radical polymerization. *Macromolecules*, 28(5):1721–1723, 1995.

[44] Jin-Shan Wang and Krzysztof Matyjaszewski. Controlled/"living" radical polymerization. atom transfer radical polymerization in the presence of transition-metal complexes. *Journal of the American Chemical Society*, 117(20):5614–5615, 1995.

[45] Krzysztof Matyjaszewski. Atom transfer radical polymerization (atrp): Current status and future perspectives. *Macromolecules*, 45(10):4015–4039, 2012.

[46] Krzystof Matyjaszewski. the matyjaszewski polymer group. `http://www.cmu.edu/maty/index.html`, 2014. [Online; accessed 17-December-2014].

[47] Nicolay V. Tsarevsky, Brent S. Sumerlin, and Chemistry Royal Society of. *Fundamentals of controlled/living radical polymerization*. RSC Pub., Cambridge, 2013. (Great Britain).

[48] Joseph Jagur-Grodzinski. *Living and controlled polymerization : synthesis, characterization, and properties of the respective polymers and copolymers*. Nova Science Publishers, New York, 2006.

[49] N. Nogueira, O. Conde, M. Miñones, J. M. Trillo, and J. Miñones Jr. Characterization of poly(2-hydroxyethyl methacrylate) (phema) contact lens using the langmuir

monolayer technique. *Journal of Colloid and Interface Science*, 385(1):202–210, 2012.

[50] Carole Maldonado-Codina and Nathan Efron. Dynamic wettability of phema-based hydrogel contact lenses. *Ophthalmic and Physiological Optics*, 26(4):408–418, 2006.

[51] Aric Opdahl, Seong H. Kim, Telly S. Koffas, Chris Marmo, and Gabor A. Somorjai. Surface mechanical properties of phema contact lenses: Viscoelastic and adhesive property changes on exposure to controlled humidity. *Journal of Biomedical Materials Research Part A*, 67A(1):350–356, 2003.

[52] Jean-Pierre Montheard, Michel Chatzopoulos, and Daniel Chappard. 2-hydroxyethyl methacrylate (hema): Chemical properties and applications in biomedical fields. *Journal of Macromolecular Science, Part C*, 32(1):1–34, 1992.

[53] Fabio di Lena and Krzysztof Matyjaszewski. Transition metal catalysts for controlled radical polymerization. *Progress in Polymer Science*, 35(8):959–1021, 2010.

[54] Wei Tang and Krzysztof Matyjaszewski. Effects of initiator structure on activation rate constants in atrp. *Macromolecules*, 40(6):1858–1863, 2007.

[55] Mike A. J. Schellekens, Frank de Wit, and Bert Klumperman. Effect of the copper counterion on the activation rate parameter in atom transfer radical polymerization. *Macromolecules*, 34(23):7961–7966, 2001.

[56] Ajaya Kumar Nanda and Krzysztof Matyjaszewski. Effect of [pmdeta]/[cu(i)] ratio, monomer, solvent, counterion, ligand, and alkyl bromide on the activation rate constants in atom transfer radical polymerization. *Macromolecules*, 36(5):1487–1493, 2003.

[57] Ajaya Kumar Nanda and Krzysztof Matyjaszewski. Effect of [bpy]/[cu(i)] ratio, solvent, counterion, and alkyl bromides on the activation rate constants in atom transfer radical polymerization. *Macromolecules*, 36(3):599–604, 2003.

[58] Wei Tang and Krzysztof Matyjaszewski. Effect of ligand structure on activation rate constants in atrp. *Macromolecules*, 39(15):4953–4959, 2006.

[59] Florian Seeliger and Krzysztof Matyjaszewski. Temperature effect on activation rate constants in atrp: New mechanistic insights into the activation process. *Macromolecules*, 42(16):6050–6055, 2009.

[60] Günter Wulff, Jürgen Schmid, and Theodor Venhoff. The synthesis of polymerizable vinyl sugars. *Macromolecular Chemistry and Physics*, 197(1):259–274, 1996.

[61] Samuel Pearson, Gaojian Chen, and Martina H. Stenzel. *Synthesis of Glycopolymers*, pages 1–118. John Wiley & Sons, Inc., 2011.

[62] Shoichi Kimura and Minoru Imoto. Synthesis of polymethacryloyl-d-glucose and its copolymers with acrylonitrile. vinyl polymerization liv. *Die Makromolekulare Chemie*, 50(1):155–160, 1961.

[63] Roy L. Whistler and James L. Goatley. Copolymerization of 1-acrylamido-1-deoxy-dhyphen;glucitol and of 1-deoxy-1-methacrylamido-d-glucitol with various vinyl monomers. *Journal of Polymer Science*, 50(153):127–132, 1961.

[64] Roy L. Whistler, Hans P. Panzer, and Hugh J. Roberts. 1-acrylamido-1-deoxy-d-glucitol, 1-deoxy-1-methacrylamido-d-glucitol and their polymerization1. *The Journal of Organic Chemistry*, 26(5):1583–1588, 1961.

[65] Kohji Ohno, Yoshinobu Tsujii, and Takeshi Fukuda. Synthesis of a well-defined glycopolymer by atom transfer radical polymerization. *Journal of Polymer Science Part A: Polymer Chemistry*, 36(14):2473–2481, 1998.

[66] Gesine Gunkel and Wilhelm T. S. Huck. Cooperative adsorption of lipoprotein phospholipids, triglycerides, and cholesteryl esters are a key factor in nonspecific adsorption from blood plasma to antifouling polymer surfaces. *Journal of the American Chemical Society*, 135(18):7047–7052, 2013.

[67] Kai Yu and Jayachandran N. Kizhakkedathu. Synthesis of functional polymer brushes containing carbohydrate residues in the pyranose form and their specific and nonspecific interactions with proteins. *Biomacromolecules*, 11(11):3073–3085, 2010.

[68] Andrew A. Brown, Neelam S. Khan, Lorenz Steinbock, and Wilhelm T. S. Huck. Synthesis of oligo(ethylene glycol) methacrylate polymer brushes. *European Polymer Journal*, 41(8):1757–1765, 2005.

[69] Sharmila Muthukrishnan, Günter Jutz, Xavier André, Hideharu Mori, and Axel H. E. Müller. Synthesis of hyperbranched glycopolymers via self-condensing atom transfer radical copolymerization of a sugar-carrying acrylate. *Macromolecules*, 38(1):9–18, 2004.

[70] Ravin Narain and Steven P. Armes. Synthesis and aqueous solution properties of

novel sugar methacrylate-based homopolymers and block copolymers. *Biomacromolecules*, 4(6):1746–1758, 2003.

[71] Muhammad Ejaz, Kohji Ohno, Yoshinobu Tsujii, and Takeshi Fukuda. Controlled grafting of a well-defined glycopolymer on a solid surface by surface-initiated atom transfer radical polymerization. *Macromolecules*, 33(8):2870–2874, 2000.

[72] Jun Li and Nianqiang Wu. *Biosensors Based on Nanomaterials and Nanodevices*. CRC Press, 2014. ISBN 978-1-4665-5151-0.

[73] Shaurya Prakash, Marie Pinti, and Bharat Bhushan. *Theory, fabrication and applications of microfluidic and nanofluidic biosensors*, volume 370. Philosophical Transactions of The Royal Scociety A, 2012.

[74] Joseph D. Taylor, K. Scott Phillips, and Quan Cheng. Microfluidic fabrication of addressable tethered lipid bilayer arrays and optimization using spr with silane-derivatized nanoglassy substrates. *Lab on a Chip*, 7(7):927–930, 2007.

[75] Elisabeth Galopin, Maxime Beaugeois, Bernard Pinchemel, Jean-Christophe Camart, Mohamed Bouazaoui, and Vincent Thomy. Spr biosensing coupled to a digital microfluidic microstreaming system. *Biosensors and Bioelectronics*, 23(5):746–750, 2007.

[76] Hye Jin Lee, Terry T. Goodrich, and Robert M. Corn. Spr imaging measurements of 1-d and 2-d dna microarrays created from microfluidic channels on gold thin films. *Analytical Chemistry*, 73(22):5525–5531, 2001.

[77] Bingcheng Lin. *Biosensors in Microfluidic Chips*, volume 304, chapter 5, pages 117–152. Springer, 2011. doi:10.1007/128-2011-143.

[78] John T. S. Irvine, Derek C. Sinclair, and Anthony R. West. Electroceramics: Characterization by impedance spectroscopy. *Advanced Materials*, 2(3):132–138, 1990.

[79] Eugenii Katz and Itamar Willner. Probing biomolecular interactions at conductive and semiconductive surfaces by impedance spectroscopy: Routes to impedimetric immunosensors, dna-sensors, and enzyme biosensors. *Electroanalysis*, 15(11):913–947, 2003.

[80] Mariele M. Pedroso, Ailton M. Watanabe, Maria Cristina Roque-Barreira, Paulo R. Bueno, and Ronaldo C. Faria. Quartz crystal microbalance monitoring the real-time binding of lectin with carbohydrate with high and low molecular mass. *Microchemical Journal*, 89(2):153–158, 2008.

[81] Kateryna Lebed, Andrzej J. Kulik, László Forró, and Małgorzata Lekka. Lectin–carbohydrate affinity measured using a quartz crystal microbalance. *Journal of Colloid and Interface Science*, 299(1):41–48, 2006.

[82] J. M. Goddard and J. H. Hotchkiss. Polymer surface modification for the attachment of bioactive compounds. *Progress in Polymer Science*, 32(7):698–725, 2007.

[83] Seunghwan Lee and Janos Vörös. An aqueous-based surface modification of poly(dimethylsiloxane) with poly(ethylene glycol) to prevent biofouling. *Langmuir*, 21(25):11957–11962, 2005.

[84] Hongyan Bi, Sheng Meng, Yan Li, Kai Guo, Yupeng Chen, Jilie Kong, Pengyuan Yang, Wei Zhong, and Baohong Liu. Deposition of peg onto pmma microchannel surface to minimize nonspecific adsorption. *Lab on a Chip*, 6(6):769–775, 2006.

[85] Shaurya Prakash, Timothy M. Long, John C. Selby, Jeffrey S. Moore, and Mark A. Shannon. "click" modification of silica surfaces and glass microfluidic channels. *Analytical Chemistry*, 79(4):1661–1667, 2006.

[86] Janine Mok, Michael N. Mindrinos, Ronald W. Davis, and Mehdi Javanmard. Digital microfluidic assay for protein detection. *Proceedings of the National Academy of Sciences*, 111(6):2110–2115, 2014.

[87] Zhao Chen, M. Thuo Martin, and Liu Xinyu. A microfluidic paper-based electrochemical biosensor array for multiplexed detection of metabolic biomarkers. *Science and Technology of Advanced Materials*, 14(5):054402, 2013.

[88] Seokheun Choi and Junseok Chae. A microfluidic biosensor based on competitive protein adsorption for thyroglobulin detection. *Biosensors & bioelectronics*, 25(1):118–123, 2009.

[89] Thorsten L. Anders. *Synthesis of new difunctional couplers and 2-acetamido-2-deoxy-β-D-glucoside derivatives for the preparation of biologic active sP(EO-stat-PO) hydrogel-coatings.* PhD thesis, 2012.

[90] Wilhelm Königs and Eduard Knorr. Über einige derivate des traubenzuckers und der galactose. *Berichte der deutschen chemischen Gesellschaft*, 34(1):957–981, 1901.

[91] A. van Blaaderen and A. Vrij. Synthesis and characterization of monodisperse colloidal organo-silica spheres. *Journal of Colloid and Interface Science*, 156(1):1–18, 1993.

[92] Thomas G. Waddell, Donald E. Leyden, and Mary T. DeBello. The nature of organosilane to silica-surface bonding. *Journal of the American Chemical Society*, 103(18):5303–5307, 1981.

[93] B. Sauerzapfe, D. J. Namdjou, T. Schumacher, N. Linden, K. Křenek, V. Křen, and L. Elling. Characterization of recombinant fusion constructs of human β1,4-galactosyltransferase 1 and the lipase pre-propeptide from staphylococcus hyicus. *Journal of Molecular Catalysis B: Enzymatic*, 50(2–4):128–140, 2008.

[94] S. M. Logan, E. Altman, O. Mykytczuk, J. R. Brisson, V. Chandan, M. J. Schur, F. St Michael, A. Masson, S. Leclerc, K. Hiratsuka, N. Smirnova, J. Li, Y. Wu, and W. W. Wakarchuk. Novel biosynthetic functions of lipopolysaccharide rfaj homologs from helicobacter pylori. *Glycobiology*, 15(7):721–33, 2005.

[95] Claudia Rech, Ruben R. Rosencrantz, Karel Křenek, Helena Pelantová, Pavla Bojarová, Christiane E. Römer, Franz-Georg Hanisch, Vladimír Křen, and Lothar Elling. Combinatorial one-pot synthesis of poly-n-acetyllactosamine oligosaccharides with leloir-glycosyltransferases. *Advanced Synthesis & Catalysis*, 353(13):2492–2500, 2011.

[96] B. Sauerzapfe, K. Krenek, J. Schmiedel, W. W. Wakarchuk, H. Pelantova, V. Kren, and L. Elling. Chemo-enzymatic synthesis of poly-*n*-acetyllactosamine (poly-lacnac) structures and their characterization for cgl2-galectin-mediated binding of ecm glycoproteins to biomaterial surfaces. *Glycoconjugate Journal*, 26(2):141–59, 2009.

[97] G. Binnig, C. F. Quate, and Ch Gerber. Atomic force microscope. *Physical Review Letters*, 56(9):930–933, 1986. PRL.

[98] Peter Hinterdorfer and Yves F. Dufrene. Detection and localization of single molecular recognition events using atomic force microscopy. *Nat Meth*, 3(5):347–355, 2006. 10.1038/nmeth871.

[99] Daniel J. Muller and Yves F. Dufrene. Atomic force microscopy as a multifunctional molecular toolbox in nanobiotechnology. *Nat Nano*, 3(5):261–269, 2008. 10.1038/nnano.2008.100.

[100] Julie A. Last, Paul Russell, Paul F. Nealey, and Christopher J. Murphy. The applications of atomic force microscopy to vision science. *Investigative Ophthalmology & Visual Science*, 51(12):6083–6094, 2010.

[101] Nuno C. Santos and Miguel A. R. B. Castanho. An overview of the biophysical

applications of atomic force microscopy. *Biophysical Chemistry*, 107(2):133–149, 2004.

[102] M. Knoll and E. Ruska. Das elektronenmikroskop. *Zeitschrift für Physik*, 78(5-6):318–339, 1932.

[103] F. M. Ross. Growth processes and phase transformations studied in situ transmission electron microscopy. *IBM Journal of Research and Development*, 44(4):489–501, 2000.

[104] David B. Williams and C. Barry Carter. *The Transmission Electron Microscope*, chapter 1, pages 3–22. Springer US, 2009.

[105] R. F. Egerton. *Physical Principles of Electron Microscopy*. Springer US, 2005.

[106] Rudolf Reichelt. *Scanning Electron Microscopy*. Springer New York, 2007.

[107] P. J. McMarr, K. Vedam, and J. Narayan. Spectroscopic ellipsometry: A new tool for nondestructive depth profiling and characterization of interfaces. *Journal of Applied Physics*, 59(3):694–701, 1986.

[108] Walter M. Duncan and Steven A. Henck. Insitu spectral ellipsometry for real-time measurement and control. *Applied Surface Science*, 63(1–4):9–16, 1993.

[109] P. Drude. Ueber die gesetze der reflexion und brechung des lichtes an der grenze absorbirender krystalle. *Annalen der Physik*, 268(12):584–625, 1887.

[110] H. G. Tompkins and E. A. Irene. *Handbook of ellipsometry*. Springer-Verlag GmbH & Co. KG, 2005.

[111] K. Vedam. Spectroscopic ellipsometry: a historical overview. *Thin Solid Films*, 313–314(0):1–9, 1998.

[112] Hans Elwing. Protein absorption and ellipsometry in biomaterial research. *Biomaterials*, 19(4–5):397–406, 1998.

[113] Fredrik Tiberg. Physical characterization of non-ionic surfactant layers adsorbed at hydrophilic and hydrophobic solid surfaces by time-resolved ellipsometry. *Journal of the Chemical Society, Faraday Transactions*, 92(4):531–538, 1996.

[114] H. Fujiwara. *Spectroscopic ellipsometry*. Wiley, 2007.

[115] Thomas Young. An essay on the cohesion of fluids. *Philosophical Transactions of the Royal Society of London*, 95:65–87, 1805.

[116] T. T. Chau, W. J. Bruckard, P. T. L. Koh, and A. V. Nguyen. A review of factors that affect contact angle and implications for flotation practice. *Advances in Colloid and Interface Science*, 150(2):106–115, 2009.

[117] P. C. Zielke. *Experimentelle Untersuchung der Bewegung von Tropfen auf Festkörperoberflächen mit einem Gradienten der Benetzbarkeit.* PhD thesis.

[118] Yuehua Yuan and T. Randall Lee. *Contact Angle and Wetting Properties*, volume 51 of *Springer Series in Surface Sciences*, chapter 1, pages 3–34. Springer Berlin Heidelberg, 2013.

[119] Robert N. Wenzel. Resistance of solid surfaces to wetting by water. *Industrial & Engineering Chemistry*, 28(8):988–994, 1936.

[120] A. B. D. Cassie and S. Baxter. Wettability of porous surfaces. *Transactions of the Faraday Society*, 40(0):546–551, 1944.

[121] Xue-Mei Li, David Reinhoudt, and Mercedes Crego-Calama. What do we need for a superhydrophobic surface? a review on the recent progress in the preparation of superhydrophobic surfaces. *Chemical Society Reviews*, 36(8):1350–1368, 2007.

[122] Roman S. Voronov, Dimitrios V. Papavassiliou, and Lloyd L. Lee. Review of fluid slip over superhydrophobic surfaces and its dependence on the contact angle. *Industrial & Engineering Chemistry Research*, 47(8):2455–2477, 2008.

[123] Rositsa Karamanska, Jonathan Clarke, Ola Blixt, JamesI MacRae, JiquanQ Zhang, PaulR Crocker, Nicolas Laurent, Adam Wright, SabineL Flitsch, DavidA Russell, and RobertA Field. Surface plasmon resonance imaging for real-time, label-free analysis of protein interactions with carbohydrate microarrays. *Glycoconjugate Journal*, 25(1):69–74, 2008.

[124] Ku-Lung Hsu, Jeffrey C. Gildersleeve, and Lara K. Mahal. A simple strategy for the creation of a recombinant lectin microarray. *Molecular BioSystems*, 4(6):654–662, 2008.

[125] Songming Chen, Tom LaRoche, Darren Hamelinck, Derek Bergsma, Dean Brenner, Diane Simeone, Randall E. Brand, and Brian B. Haab. Multiplexed analysis of glycan variation on native proteins captured by antibody microarrays. *Nat Meth*, 4(5):437–444, 2007. 10.1038/nmeth1035.

[126] Shen Hu and David T. Wong. Lectin microarray. *Proteomics. Clinical applications*, 3(2):148–154, 2009. 21132067[pmid] Proteomics Clin Appl.

[127] Rakefet Rosenfeld, Haim Bangio, Gerrit J. Gerwig, Revital Rosenberg, Ronny Aloni, Yossi Cohen, Yehudit Amor, Inbar Plaschkes, Johannis P. Kamerling, and Ruth Ben-Yakar Maya. A lectin array-based methodology for the analysis of protein glycosylation. *Journal of Biochemical and Biophysical Methods*, 70(3):415–426, 2007.

[128] M. Duk, E. Lisowska, J. H. Wu, and A. M. Wu. The biotin/avidin-mediated microtiter plate lectin assay with the use of chemically modified glycoprotein ligand. *Analytical Biochemistry*, 221(2):266–272, 1994.

[129] AlbertM Wu, JuneH Wu, Ming-Sung Tsai, Zhangung Yang, Nathan Sharon, and Anthony Herp. Differential affinities of erythrina cristagalli lectin (ecl) toward monosaccharides and polyvalent mammalian structural units. *Glycoconjugate Journal*, 24(9):591–604, 2007.

[130] June H. Wu, Tanuja Singh, Anthony Herp, and Albert M. Wu. Carbohydrate recognition factors of the lectin domains present in the ricinus communis toxic protein (ricin). *Biochimie*, 88(2):201–217, 2006.

[131] Roisin Thompson, Aileen Creavin, Michael O'Connell, Brendan O'Connor, and Paul Clarke. Optimization of the enzyme-linked lectin assay for enhanced glycoprotein and glycoconjugate analysis. *Analytical Biochemistry*, 413(2):114–122, 2011.

[132] J. Philip McCoy Jr, James Varani, and Irwin J. Goldstein. Enzyme-linked lectin assay (ella): Ii. detection of carbohydrate groups on the surface of unfixed cells. *Experimental Cell Research*, 151(1):96–103, 1984.

[133] Francisco Fabregat-Santiago, Juan Bisquert, Germà Garcia-Belmonte, Gerrit Boschloo, and Anders Hagfeldt. Influence of electrolyte in transport and recombination in dye-sensitized solar cells studied by impedance spectroscopy. *Solar Energy Materials and Solar Cells*, 87(1–4):117–131, 2005.

[134] Harry O. Finklea, Daniel A. Snider, John Fedyk, Eyal Sabatani, Yael Gafni, and Israel Rubinstein. Characterization of octadecanethiol-coated gold electrodes as microarray electrodes by cyclic voltammetry and ac impedance spectroscopy. *Langmuir*, 9(12):3660–3667, 1993.

[135] Shalini Gupta, Peter K. Kilpatrick, Elizabeth Melvin, and Orlin D. Velev. On-chip latex agglutination immunoassay readout by electrochemical impedance spectroscopy. *Lab on a Chip*, 12(21):4279–4286, 2012.

[136] R. K. Mendes, D. C. M. Ferreira, R. F. Carvalhal, L. A. Peroni, D. R. Stach-Machado, and L. T. Kubota. Development of an electrochemical immunosensor for phakopsora pachyrhizi detection in the early diagnosis of soybean rust. *Journal of the Brazilian Chemical Society*, 20:795–801, 2009.

[137] Mark E. Orazem and Tribollet Bernard. *Electrochemical Impedance Spectroscopy*. Wiley, 2008.

[138] Chuanmin Ruan, Liju Yang, and Yanbin Li. Immunobiosensor chips for detection of escherichia coli o157:h7 using electrochemical impedance spectroscopy. *Analytical Chemistry*, 74(18):4814–4820, 2002.

[139] Rahul R. Shah, David Merreceyes, Marc Husemann, Ian Rees, Nicholas L. Abbott, Craig J. Hawker, and James L. Hedrick. Using atom transfer radical polymerization to amplify monolayers of initiators patterned by microcontact printing into polymer brushes for pattern transfer. *Macromolecules*, 33(2):597–605, 2000.

[140] Matthew A. Cooper. Optical biosensors in drug discovery. *Nat Rev Drug Discov*, 1(7):515–528, 2002. 10.1038/nrd838.

[141] Abdennour Abbas, Matthew J. Linman, and Quan Cheng. New trends in instrumental design for surface plasmon resonance-based biosensors. *Biosensors and Bioelectronics*, 26(5):1815–1824, 2011.

[142] FARID E. AHMED, JOHN E. WILEY, DOUGLAS A. WEIDNER, CHRIS BONNERUP, and HELVECIO MOTA. Surface plasmon resonance (spr) spectrometry as a tool to analyze nucleic acid–protein interactions in crude cellular extracts. *Cancer Genomics - Proteomics*, 7(6):303–309, 2010.

[143] Amanda J. Haes, W. Paige Hall, Lei Chang, William L. Klein, and Richard P. Van Duyne. A localized surface plasmon resonance biosensor: First steps toward an assay for alzheimer's disease. *Nano Letters*, 4(6):1029–1034, 2004.

[144] Katherine A. Willets and Richard P. Van Duyne. Localized surface plasmon resonance spectroscopy and sensing. *Annual Review of Physical Chemistry*, 58(1):267–297, 2007.

[145] Buchenauer Andreas, Bialon Magdalena, Segun Daniel, Püttmann Christiane, Stein Christoph, Barth Stefan, and Schnakenberg Uwe. Plasmonic flow-through biosensor using a polymeric substrate. *Journal of Micromechanics and Microengineering*, 24(3):034001, 2014.

[146] Lord Rayleigh. On waves propagated along the plane surface of an elastic solid. *Proceedings of the London Mathematical Society*, s1-17(1):4–11, 1885.

[147] Leslie Y. Yeo and James R. Friend. Surface acoustic wave microfluidics. *Annual Review of Fluid Mechanics*, 46(1):379–406, 2014.

[148] Xiaoyun Ding, Peng Li, Sz-Chin Steven Lin, Zackary S. Stratton, Nitesh Nama, Feng Guo, Daniel Slotcavage, Xiaole Mao, Jinjie Shi, Francesco Costanzo, and Tony Jun Huang. Surface acoustic wave microfluidics. *Lab on a Chip*, 13(18):3626–3649, 2013.

[149] Kerstin Länge, BastianE Rapp, and Michael Rapp. Surface acoustic wave biosensors: a review. *Analytical and Bioanalytical Chemistry*, 391(5):1509–1519, 2008.

[150] Anca Mateescu, Jianding Ye, Ravin Narain, and Maria Vamvakaki. Synthesis and characterization of novel glycosurfaces by atrp. *Soft Matter*, 5(8):1621–1629, 2009.

[151] Q. Yang, M. X. Hu, Z. W. Dai, J. Tian, and Z. K. Xu. Fabrication of glycosylated surface on polymer membrane by uv-induced graft polymerization for lectin recognition. *Langmuir*, 22(22):9345–9, 2006.

[152] Qiang Zhang, Lu Su, Jennifer Collins, Guosong Chen, Russell Wallis, Daniel A. Mitchell, David M. Haddleton, and C. Remzi Becer. Dendritic cell lectin-targeting sentinel-like unimolecular glycoconjugates to release an anti-hiv drug. *Journal of the American Chemical Society*, 136(11):4325–4332, 2014.

[153] James B. Konopka. N-acetylglucosamine functions in cell signaling. *Scientifica*, 2012:489208, 2012. 23350039[pmid] Scientifica (Cairo).

[154] Shamoon Naseem, Salvatore M. Parrino, Dane M. Buenten, and James B. Konopka. Novel roles for glcnac in cell signaling. *Communicative & Integrative Biology*, 5(2):156–159, 2012.

[155] T. Vallant, H. Brunner, U. Mayer, H. Hoffmann, T. Leitner, R. Resch, and G. Friedbacher. Formation of self-assembled octadecylsiloxane monolayers on mica and silicon surfaces studied by atomic force microscopy and infrared spectroscopy. *The Journal of Physical Chemistry B*, 102(37):7190–7197, 1998.

[156] Jeffrey Pyun, Tomasz Kowalewski, and Krzysztof Matyjaszewski. Synthesis of polymer brushes using atom transfer radical polymerization. *Macromolecular Rapid Communications*, 24(18):1043–1059, 2003.

[157] Marc Husseman, Eva E. Malmström, Molly McNamara, Mathew Mate, David Mecer-

reyes, Didier G. Benoit, James L. Hedrick, Paul Mansky, E. Huang, Thomas P. Russell, and Craig J. Hawker. Controlled synthesis of polymer brushes by "living" free radical polymerization techniques. *Macromolecules*, 32(5):1424–1431, 1999.

[158] Krzysztof Matyjaszewski, Peter J. Miller, Nisha Shukla, Boonchuan Immaraporn, Andrew Gelman, Barry B. Luokala, Tiberiu M. Siclovan, Guido Kickelbick, Thomas Vallant, Helmuth Hoffmann, and Tadeusz Pakula. Polymers at interfaces: Using atom transfer radical polymerization in the controlled growth of homopolymers and block copolymers from silicon surfaces in the absence of untethered sacrificial initiator. *Macromolecules*, 32(26):8716–8724, 1999.

[159] Nicolay V. Tsarevsky, Tomislav Pintauer, and Krzysztof Matyjaszewski. Deactivation efficiency and degree of control over polymerization in atrp in protic solvents. *Macromolecules*, 37(26):9768–9778, 2004.

[160] IrwinJ Goldstein. Lectins fromgriffonia simplicifolia seeds. *Journal of Biosciences*, 5(1):65–71, 1983.

[161] AlbertM Wu, JuneH Wu, Ming-Sung Tsai, Zhangung Yang, Nathan Sharon, and Anthony Herp. Differential affinities of erythrina cristagalli lectin (ecl) toward monosaccharides and polyvalent mammalian structural units. *Glycoconjugate Journal*, 24(9):591–604, 2007.

[162] Christiane E. Kupper, Ruben R. Rosencrantz, Birgit Henßen, Helena Pelantová, Stephan Thönes, Anna Drozdová, Vladimir Kř̃en, and Lothar Elling. Chemoenzymatic modification of poly-n-acetyllactosamine (lacnac) oligomers and n,n-diacetyllactosamine (lacdinac) based on galactose oxidase treatment. *Beilstein Journal of Organic Chemistry*, 8:712–725, 2012.

[163] Hyunji Park, Ruben R. Rosencrantz, Lothar Elling, and Alexander Böker. Glycopolymer brushes for specific lectin binding by controlled multivalent presentation of N-Acetyllactosamine glycan oligomers. *Macromolecular Rapid Communications*, 36:45–54, 2015.

[164] Xiankun Lin, Qiang He, and Junbai Li. Complex polymer brush gradients based on nanolithography and surface-initiated polymerization. *Chemical Society Reviews*, 41(9):3584–3593, 2012.

[165] Jan Genzer and Rajendra R. Bhat. Surface-bound soft matter gradients. *Langmuir*, 24(6):2294–2317, 2008.

[166] Rajendra R. Bhat, Bryce N. Chaney, Jon Rowley, Andrea Liebmenn-Vinson, and Jan

Genzer. Tailoring cell adhesion using surface-grafted polymer gradient assemblies. *Advanced Materials*, 17(23):2802–2807, 2005.

[167] Ying Mei, Tao Wu, Chang Xu, Kurt J. Langenbach, John T. Elliott, Bryan D. Vogt, Kathryn L. Beers, Eric J. Amis, and Newell R. Washburn. Tuning cell adhesion on gradient poly(2-hydroxyethyl methacrylate)-grafted surfaces. *Langmuir*, 21(26):12309–12314, 2005.

[168] Rajendra R. Bhat, Michael R. Tomlinson, and Jan Genzer. Orthogonal surface-grafted polymer gradients: A versatile combinatorial platform. *Journal of Polymer Science Part B: Polymer Physics*, 43(23):3384–3394, 2005.

[169] RajendraR Bhat, MichaelR Tomlinson, Tao Wu, and Jan Genzer. *Surface-Grafted Polymer Gradients: Formation, Characterization, and Applications*, volume 198 of *Advances in Polymer Science*, chapter 60, pages 51–124. Springer Berlin Heidelberg, 2006.

[170] Wenxi Huang, Skanth, Gregory L. Baker, and Merlin L. Bruening. Surface-initiated thermal radical polymerization on gold. *Langmuir*, 17(5):1731–1736, 2001.

[171] George M. Whitesides and Paul E. Laibinis. Wet chemical approaches to the characterization of organic surfaces: self-assembled monolayers, wetting, and the physical-organic chemistry of the solid-liquid interface. *Langmuir*, 6(1):87–96, 1990.

[172] D. S. Karpovich and G. J. Blanchard. Direct measurement of the adsorption kinetics of alkanethiolate self-assembled monolayers on a microcrystalline gold surface. *Langmuir*, 10(9):3315–3322, 1994.

[173] Jianqiang Meng, Jing Yuan, Yinlin Kang, Yufeng Zhang, and Qiyun Du. Surface glycosylation of polysulfone membrane towards a novel complexing membrane for boron removal. *Journal of Colloid and Interface Science*, 368(1):197–207, 2012.

[174] Kai Yu, A. Louise Creagh, Charles A. Haynes, and Jayachandran N. Kizhakkedathu. Lectin interactions on surface-grafted glycostructures: Influence of the spatial distribution of carbohydrates on the binding kinetics and rupture forces. *Analytical Chemistry*, 85(16):7786–7793, 2013.

[175] Sarah-Jane Richards and Matthew I. Gibson. Optimization of the polymer coating for glycosylated gold nanoparticle biosensors to ensure stability and rapid optical readouts. *ACS Macro Letters*, 3(10):1004–1008, 2014.

[176] Zhichao Pei, Henrik Anderson, Teodor Aastrup, and Olof Ramström. Study of real-

time lectin–carbohydrate interactions on the surface of a quartz crystal microbalance. *Biosensors and Bioelectronics*, 21(1):60–66, 2005.

[177] Xueming Li, Yuxin Pei, Ruina Zhang, Qi Shuai, Feng Wang, Teodor Aastrup, and Zhichao Pei. A suspension-cell biosensor for real-time determination of binding kinetics of protein-carbohydrate interactions on cancer cell surfaces. *Chemical Communications*, 49(85):9908–9910, 2013.

[178] Nicole J Jaffrezic-Renault, Nedjla Zehani, Sergei V Dzyadevych, and Rochdi Kherrat. Sensitive impedimetric biosensor for direct detection of diazinon based on lipases. *Frontiers in Chemistry*, 2, 2014.

[179] Jo V. Rushworth, Asif Ahmed, Heledd H. Griffiths, Niall M. Pollock, Nigel M. Hooper, and Paul A. Millner. A label-free electrical impedimetric biosensor for the specific detection of alzheimer's amyloid-beta oligomers. *Biosensors and Bioelectronics*, 56(0):83–90, 2014.

[180] Liju Yang and Anthony Guiseppi-Elie. *Impedimetric Biosensors for Nano- and Microfluidics*, chapter 686, pages 811–823. Springer US, 2008.

[181] Bechir Mrabet, Minh Ngoc Nguyen, Aymen Majbri, Samia Mahouche, Mireille Turmine, Amina Bakhrouf, and Mohamed M. Chehimi. Anti-fouling poly(2-hydoxyethyl methacrylate) surface coatings with specific bacteria recognition capabilities. *Surface Science*, 603(16):2422–2429, 2009.

[182] Mirela Zamfir, Cesar Rodriguez-Emmenegger, Stella Bauer, Leonie Barner, Axel Rosenhahn, and Christopher Barner-Kowollik. Controlled growth of protein resistant phema brushes via s-raft polymerization. *Journal of Materials Chemistry B*, 1(44):6027–6034, 2013.

[183] George M. Whitesides. The origins and the future of microfluidics. *Nature*, 442(7101):368–373, 2006. 10.1038/nature05058.

[184] Catherine Rivet, Hyewon Lee, Alison Hirsch, Sharon Hamilton, and Hang Lu. Microfluidics for medical diagnostics and biosensors. *Chemical Engineering Science*, 66(7):1490–1507, 2011.

[185] Andrew M. Davis and Simon Ward. *The Handbook of Medicinal Chemistry*. RSC Smart Materials. Royal Society of Chemistry, 2014. ISBN:9781849736251.

[186] F. Ted Limpoco and Ryan C. Bailey. Real-time monitoring of surface-initiated atom transfer radical polymerization using silicon photonic microring resonators: Impli-

cations for combinatorial screening of polymer brush growth conditions. *Journal of the American Chemical Society*, 133(38):14864–14867, 2011.

[187] Raphael Barbey, Laurent Lavanant, Dusko Paripovic, Nicolas Schüwer, Caroline Sugnaux, Stefano Tugulu, and Harm-Anton Klok. Polymer brushes via surface-initiated controlled radical polymerization: Synthesis, characterization, properties, and applications. *Chemical Reviews*, 109(11):5437–5527, 2009.

[188] Wayne F. Reed. *Automated Continuous Online Monitoring of Polymerization Reactions (ACOMP) and Related Techniques*. John Wiley & Sons, Ltd, 2006.

[189] Bindushree Radhakrishnan, Rajesh Ranjan, and William J. Brittain. Surface initiated polymerizations from silica nanoparticles. *Soft Matter*, 2(5):386–396, 2006.

[190] Werner Stöber, Arthur Fink, and Ernst Bohn. Controlled growth of monodisperse silica spheres in the micron size range. *Journal of Colloid and Interface Science*, 26(1):62–69, 1968.

[191] A. Van Blaaderen, J. Van Geest, and A. Vrij. Monodisperse colloidal silica spheres from tetraalkoxysilanes: Particle formation and growth mechanism. *Journal of Colloid and Interface Science*, 154(2):481–501, 1992.

[192] Yan Wang, Xi Zhang, Jinliang Yan, Yan Xiao, and Meidong Lang. Surface modification of hydroxyapatite with poly(methyl methacrylate) via surface-initiated atrp. *Applied Surface Science*, 257(14):6233–6238, 2011.

[193] Kohji Ohno, Takashi Morinaga, Kyoungmoo Koh, Yoshinobu Tsujii, and Takeshi Fukuda. Synthesis of monodisperse silica particles coated with well-defined, high-density polymer brushes by surface-initiated atom transfer radical polymerization. *Macromolecules*, 38(6):2137–2142, 2005.

[194] Timothy von Werne and Timothy E. Patten. Atom transfer radical polymerization from nanoparticles: A tool for the preparation of well-defined hybrid nanostructures and for understanding the chemistry of controlled/"living" radical polymerizations from surfaces. *Journal of the American Chemical Society*, 123(31):7497–7505, 2001.

[195] Hongchen Dong, Manzhou Zhu, Jeong Ae Yoon, Haifeng Gao, Rongchao Jin, and Krzysztof Matyjaszewski. One-pot synthesis of robust core/shell gold nanoparticles. *Journal of the American Chemical Society*, 130(39):12852–12853, 2008.

[196] Tian-Ying Guo, Ping Liu, Jing-Wei Zhu, Mou-Dao Song, and Bang-Hua Zhang.

Well-defined lactose-containing polymer grafted onto silica particles. *Biomacromolecules*, 7(4):1196–1202, 2006.

[197] André Pfaff, Anja Schallon, Thomas M. Ruhland, Alexander P. Majewski, Holger Schmalz, Ruth Freitag, and Axel H. E. Müller. Magnetic and fluorescent glycopolymer hybrid nanoparticles for intranuclear optical imaging. *Biomacromolecules*, 12(10):3805–3811, 2011.

[198] Qiang Zhang and DavidM Haddleton. *Synthetic Glycopolymers: Some Recent Developments*, volume 262 of *Advances in Polymer Science*, chapter 254, pages 39–59. Springer International Publishing, 2013.

[199] Kenji Yamada, Masahiko Minoda, and Takeaki Miyamoto. Controlled synthesis of amphiphilic block copolymers with pendant n-acetyl-d-glucosamine residues by living cationic polymerization and their interaction with wga lectin. *Macromolecules*, 32(11):3553–3558, 1999.

[200] Qiang Zhang, Jennifer Collins, Athina Anastasaki, Russell Wallis, Daniel A. Mitchell, C. Remzi Becer, and David M. Haddleton. Sequence-controlled multi-block glycopolymers to inhibit dc-sign-gp120 binding. *Angewandte Chemie*, 125(16):4531–4535, 2013.